CEPREMAP
CENTRE POUR LA RECHERCHE ECONOMIQUE ET SES APPLICATIONS

Document de travail (Docweb) n°2602

Climate Trade Costs: Extreme Weather, Transportation, and Supply Chains — RIEF Best Paper Prize 2026

Hubert MASSONI

July 2026

Coûts commerciaux climatiques : événements météorologiques extrêmes, transport et chaînes d'approvisionnement[1]

Hubert MASSONI[2]

Résumé : Les infrastructures de transport sont vulnérables aux événements météorologiques extrêmes. Cette vulnérabilité est particulièrement marquée dans les ports maritimes, où les cyclones tropicaux interrompent fréquemment les opérations et contraignent les entreprises à s'adapter aux perturbations du transport. Je quantifie ces réponses en appariant des données d'expédition maritime à haute fréquence aux trajectoires de cyclones tropicaux. L'exposition aux cyclones tropicaux perturbe temporairement l'activité portuaire (1–2 semaines), incitant les entreprises à réorienter leurs expéditions vers des ports alternatifs (1–4 mois), mais ce mécanisme d'adaptation est insuffisant pour prévenir un déclin persistant du commerce inter-entreprises. Afin d'évaluer les implications en équilibre général de ces perturbations météorologiques, je développe un modèle quantitatif de réseaux de production spatiaux avec choix de routes endogène. Les coûts de transport au niveau portuaire augmentent avec le trafic (congestion) et le risque cyclonique, et diminuent avec la capacité portuaire (économies d'échelle). En étudiant les risques climatiques futurs pesant sur le réseau de transport, je montre que les effets sur le bien-être sont principalement distributifs : les forces de congestion dans les ports absorbent l'essentiel du choc climatique en équilibre général, tandis que la réorientation des routes par les entreprises a une efficacité limitée. Pour traduire ces résultats en recommandations de politique économique, je dérive des statistiques suffisantes analytiques permettant d'évaluer et de cibler les investissements portuaires futurs à l'aune du changement climatique. Les règles d'allocation qui ignorent le risque météorologique et les réponses adaptatives des entreprises redistribuent les investissements entre les ports, avec des conséquences distributives.

Mots-clés : Commerce international ; transport ; événements météorologiques extrêmes ; changement climatique ; infrastructures portuaires ; réseaux de production

Climate Trade Costs: Extreme Weather, Transportation, and Supply Chains

Abstract: Transportation infrastructure is vulnerable to extreme weather events. Vulnerability is prominent at maritime ports, where tropical cyclones frequently

[1]I am grateful to Emanuele Campiglio and Bruno Conte for their guidance and support. This paper benefited from conversations with Jeanne Astier, Clare Balboni, Johannes Boehm, Mathieu Couttenier, Pierre Coster, Alejandro Graziano, Vasily Korovkin, Isabelle Méjean, David Nagy, Giacomo Oppocher, Gianluca Orefice, Filippo Pavanello, Giulia Romani, Filippo Santi, Vincenzo Scrutinio, Edouard Schaal, Tommaso Sonno, Catherine Thomas, Guglielmo Zappalà, and from the comments of numerous seminar and conference participants. I am grateful to Alireza Naghavi for kindly sharing data.

[2]University of Bologna, Department of Economics, hubert.massoni2@unibo.it

halt operations and force firms to adapt to transportation disruptions. I quantify these responses by linking high-frequency maritime shipment data to tropical cyclone tracks. Exposure to tropical cyclones temporarily disrupts port activities (1–2 weeks), prompting firms to reroute shipments to alternative ports (1–4 months), but this adaptation mechanism is insufficient to prevent persistent declines in firm-to-firm trade. To evaluate the general-equilibrium implications of these weather disruptions, I develop a quantitative model of spatial production networks with endogenous routing. Port-level transportation costs increase with traffic (congestion) and cyclone risk, and decrease with port capacity (scale). Investigating future climate hazards to the transportation network, I find that welfare effects are primarily distributional; congestion forces at ports account for most of the general-equilibrium absorption of the climate shock, while firm-level rerouting has limited effectiveness. To translate evidence into policy, I derive analytical sufficient statistics for evaluating and targeting future port investments in light of climate change. Allocation rules that ignore weather risk and firms' adaptive responses redistribute investment across ports, with distributional consequences.

Keywords : International trade; transportation; extreme weather; climate change; port infrastructure; production networks

JEL Codes: F18, R41, Q54, H54

1 Introduction

Transportation infrastructure is the backbone of international trade and attracts large investments to improve efficiency and resilience. Yet, infrastructure is particularly vulnerable to extreme weather. Maritime ports – channeling more than 80% of global trade volumes – exemplify this risk through their exposure to storm surge, high winds, and flooding. Weather hazards threaten not only the physical infrastructure of ports but also the trade flows that depend on them.[1] Escalating climate risk raises concerns about the resilience of transportation networks, and the trade they carry.

Weather-related disruptions expose firms to shipping bottlenecks, delays, and uncertainty (Blaum et al., 2024). Firms can reduce exposure to disrupted ports by diverting away from risky infrastructure or from suppliers that rely on it. However, these private responses can also amplify disruptions by inducing congestion spillovers along alternative routes (Allen and Arkolakis, 2022; Brancaccio et al., 2024). Accounting for such endogenous rerouting is crucial for evaluating returns to port investment, given that transportation costs have general equilibrium effects on the spatial distribution of economic activity (Allen et al., 2025; Redding and Turner, 2015).

This paper studies firms' adaptation margins to transport-related climate risks and their impacts on the economy. First, using shipment-level maritime trade data linked to port operations and tropical cyclone exposure, I show that weather shocks disrupt port activity and prompt firm-level rerouting, but that this adaptation mechanism is insufficient to prevent persistent supply-chain disruptions. Second, to quantify the general-equilibrium impacts of future climate risks to port infrastructure, I develop a model of spatial production networks that captures routing decisions and the congestion spillovers they induce across transportation networks. Third, to evaluate public investment in ports, I develop an analytical sufficient-statistics framework that links port improvements to welfare while accounting for firms' responses and weather risk.

I measure firms' responses to transportation shocks by combining Brazilian administrative maritime trade data (bills of lading) with detailed micro-spatial information on tropical cyclones and daily global port operations. The data cover the universe of

[1] Studying 1,340 ports globally, Verschuur et al. (2023b) find that 86% of ports are exposed to more than three weather-related hazards. About one-third of this risk is attributable to tropical cyclones, exposing USD 63 billion in trade annually.

Brazilian imports from 2014 to 2023 at the shipment level. Bills of lading contain information on shipment characteristics, on each trading firm, and on the ports used to ship the goods. Tropical cyclones provide plausibly exogenous weather shocks to infer firm-level adaptation margins.[2] I investigate the effect of these weather shocks on port activity and the responses of Brazilian firms to foreign transportation disruptions – i.e., shocks to the shipment's port of origin.[3]

I exploit a stacked difference-in-differences design (Cengiz et al., 2019; Deshpande and Li, 2019) to provide novel empirical evidence on how port exposure to tropical cyclones propagates through supply chains. Using quasi-random variation in cyclone exposure across ports, I first show that tropical cyclones temporarily disrupt the operations of maritime ports, on average for 12 days around the cyclone's landfall.[4] Second, I use shipment-level data to examine private adaptation through rerouting. Leveraging variation in port exposure to cyclones across the set of ports used by a pair of firms, I find that these disruptions induce immediate rerouting away from exposed ports, before a prompt recovery. This response is more pronounced and persistent when the exposure is the first experienced by the trading relationship, lasting approximately four months. Non-containerized shipping drives this rerouting response, consistent with the greater scheduling flexibility of non-liner services. Third, aggregating shipment data at the firm-to-firm level, I show that port exposure to cyclones generates a persistent and significant decline in relationship activity throughout the post-shock window, concentrated among relationships exposed more than once and among containerized trade. The evidence indicates that rerouting is an adaptation mechanism whose effectiveness erodes: it absorbs a first port disruption, but is insufficient under repeated shocks or when liner-schedule constraints limit route substitution.

To investigate the welfare impacts of these adaptation margins in the context of climate change, I develop a static model of spatial production networks with endogenous trade costs affected by weather disruptions. Informed by the empirical evidence,

[2] Although tropical cyclones are concentrated within well-defined storm seasons and broad geographic areas, the exact location, timing, and intensity of the events remain unpredictable (Hsiang and Jina, 2014).

[3] In the sample I consider, no Brazilian port is exposed to tropical cyclones. Brazil's coastal regions lie near the equator, where sea surface temperatures are relatively stable and the Coriolis force is weak – tropical cyclones rarely form or intensify in this region.

[4] Since port authorities forecast cyclones' trajectories and intensities, port downtime can precede landfall. I use precautionary thresholds from Coast Guard authorities to inform my definition of a port-level shock. See Section 2.

the model accounts for private decisions: firms reroute trade toward safer routes in response to weather risk. However, such routing responses can affect other parts of the transportation network if congestion spillovers raise the costs of using alternative routes. In the model, firms located across regions require intermediate inputs to produce final goods. They make joint sourcing and routing decisions based on factory-gate and transportation costs to find the most cost-effective supplier and delivery route. Road transportation is allowed when regions are directly connected by land, and maritime transportation is allowed when both regions have port infrastructure. Shipping through ports entails additional transportation costs related to port traffic and weather risks, which are alleviated by port capacity.

Before closing the model globally, I illustrate the three trade-cost channels the model emphasizes – port traffic, port capacity, and cyclone risk – by estimating a model-consistent route-level trade-share regression on the Brazilian microdata linked to information on port operations and cyclone risk. I address endogeneity in port traffic and capacity using a novel set of geography-based instruments. For port traffic, I use global container throughput interacted with each port's 1950 coastal-population share – a predetermined demand shifter that scales common traffic shocks across ports while leaving local handling costs unchanged. For port capacity, I use mean terrain ruggedness around ports – a geologic supply determinant that raises inland evacuation costs and limits optimal capacity, yet remains exogenous to current trade flows.[5]

I calibrate the model at the country level for the global economy and use probabilistic projections of tropical cyclones to infer future weather risk at ports under an unmitigated climate change scenario.[6] The model quantifies the distributional impacts of these climate-related risks on maritime traffic and regional welfare. Aggregate welfare changes are limited (-0.01%), though the regional dispersion is large: the 5^{th}-percentile region loses 0.11% of real income, and the largest losses concentrate in regions whose imports depend most heavily on climate-exposed ports.[7] A scenario

[5]This exercise is motivating rather than identifying: it documents that trade shares respond in the expected direction to port traffic, port capacity, and baseline cyclone risk, but the Brazil-only sample limits external validity, and I do not map its estimates back into the global calibration. The structural parameters are instead recovered by targeting observed cross-port traffic moments.

[6]I rely on model-based quantification and counterfactual exercises to address the impacts of climate change. While the reduced-form evidence I propose captures firms' responses to individual weather events, the maritime shipments data cover only ten years and therefore do not allow observing a distributional *shift* in weather risk – a key feature of climate change.

[7]The magnitude of welfare effects from perturbations of transportation costs in spatial-network

decomposition that successively suppresses firm rerouting and the port-level congestion feedback shows that the two endogenous channels together dampen 74.3% of the direct welfare loss, but that the congestion price feedback dominates (73.3%), while firm-level rerouting accounts for only 1.0%.

Finally, I explore infrastructure policy and how future climate risks can affect infrastructure investment patterns. I propose an analytical sufficient-statistics approach to recover first-order welfare gains from port capacity improvements. I express marginal welfare gains from port capacity as a function of general-equilibrium objects, accounting for adjustments in both production and transportation networks, and port-level weather risk. The mean welfare elasticity is 1.4 basis points per one-percent capacity expansion, but marginal returns are highly skewed: the 5^{th}-percentile port has a near-zero elasticity while the 95^{th}-percentile port reaches 6.19 basis points. A closed-form channel decomposition shows that the traffic-spillover channel is negative (-13%): expanding one port pulls traffic from alternatives, redistributing congestion across the network, and systematically dampening the production-network benefits of capacity improvements. I use these welfare elasticities to construct a *heuristic* allocation rule in which each port's share of aggregate investment is proportional to its welfare return, and study how climate change shifts the rule.

To further demonstrate the use of the sufficient-statistics approach for port investment allocation, I use evidence that EU27 ports plan approximately EUR 84 billion of capacity investment by 2034 (ESPO, 2024). I distribute this budget across 79 EU ports using the heuristic allocation rule evaluated at the EU level – each port's share proportional to its EU27 welfare elasticity – and ask how much the allocation changes once one accounts for port-level climate risk. To translate spending into capacity, I map investment into port capacity using an elasticity estimated from World Bank PPI projects. The answer is primarily distributional. A climate-blind allocation costs only 0.093 basis points of aggregate EU27 welfare relative to a climate-aware allocation, but at the country level the same myopia reshuffles welfare gains materially.

Related Literature. This paper connects three strands of research. First, it relates to the growing literature on how natural disasters and extreme weather affect production networks (Barrot and Sauvagnat, 2016; Boehm et al., 2019; Carvalho et al., 2021;

models with routing is in line with the closely related literature; see Section 6.2 for a discussion.

Pankratz and Schiller, 2021; Rabano and Rosas, 2024). Both the empirical and theoretical exercises I undertake are most closely related to recent work studying firms' responses to climate risks: Balboni et al. (2024) and Castro-Vincenzi et al. (2024) document flood impacts on domestic supply chains and firms' adaptive responses, while Martinez (2024), Blaum et al. (2024), and Clark et al. (2024) explicitly address weather disruptions to transportation and their effects on firms' sourcing choices.[8] Building on the insight that firms incorporate climate risks when making sourcing decisions, I reinterpret private adaptation through the lens of transportation–linked disruptions. I foreground an additional margin – rerouting – and show how these private decisions generate congestion spillovers that justify a role for infrastructure policy.

Second, the paper contributes to the literature on transportation costs and infrastructure as determinants of economic activity. A subset of this literature studies the welfare consequences of traffic congestion (Brancaccio et al., 2020; Fajgelbaum and Schaal, 2020; Allen and Arkolakis, 2022). I draw on the framework of Allen and Arkolakis (2022) and incorporate an optimal transportation problem – where firms select bilateral least–cost routes – into a model of spatial production networks. Closely related, Ganapati et al. (2024) introduce increasing returns in maritime traffic, and Wong and Fuchs (2022) study multimodal networks. I extend this class of models by introducing infrastructure–level operating costs and capacity constraints that endogenously shape congestion (Ducruet et al., 2024; Brancaccio et al., 2024). This modeling choice delivers precise traffic predictions at the *node* level (ports), rather than at the *link* level (shipping lanes). This distinction is particularly relevant for maritime trade, where bottlenecks arise primarily at terminals (and a few chokepoints), while open–sea lanes rarely bind. In addition, the sufficient–statistics approach I develop brings climate risk into the welfare analysis of infrastructure policy (Allen et al., 2025). This approach preserves the discipline of the routing structure and delivers transparent comparative statics for future climates.

Finally, this study relates to the broader literature on the spatial consequences of climate change (Bilal and Rossi-Hansberg, 2023; Desmet and Rossi-Hansberg, 2015; Cruz and Rossi-Hansberg, 2024; Rudik et al., 2021). Rather than viewing trade frictions as

[8] Balboni et al. (2024) also consider flood–induced road disruptions and subsequent firms' responses using GPS tracker data from commercial trucks. Their quantitative framework, however, does not model disaster–driven changes in transportation costs nor the spillovers those shocks generate across the broader transport network.

merely constraining climate–induced geographic reallocation, I highlight that climate damage can propagate across space through transportation networks, generating indirect losses in otherwise less–exposed regions via rerouting and congestion. This has implications for infrastructure policy because local shocks can trigger network–wide externalities at critical nodes. Related work studies the spatial allocation of infrastructure under climate risk, including the costs of maintaining coastal cities (Desmet et al., 2021; Balboni, 2025). I propose a complementary perspective: assessments of where to expand infrastructure must internalize firms' routing responses. Rerouting can reshape the spatial propagation of local shocks by diverting trade flows, and infrastructure investments should be designed to support these adjustments while managing congestion externalities.

The rest of the paper proceeds as follows. Section 2 provides empirical evidence on firms' responses to weather-related transportation disruptions. Section 3 develops the theoretical model. Section 4 estimates a model-consistent reduced-form regression on trade-cost determinants. Section 5 brings the model to the data. Section 6 presents quantitative results under climate-change scenarios. Section 7 studies infrastructure policy. Section 8 concludes.

2 Empirical Evidence

Studying how weather shocks propagate through supply chains poses an identification challenge with two distinct layers. The first concerns the attribution of direct effects. A tropical cyclone that hits a maritime port does not confine its effects to port infrastructure alone – it simultaneously exposes the port and the foreign suppliers located in the affected area to the same shock.[9] Attributing downstream disruptions to the transportation channel therefore requires separating the port shock from the direct exposure of the trading parties themselves. The second layer concerns propagation channels. Even once the direct port effect is cleanly isolated, firms may respond through several margins: rerouting shipments to alternative ports, reducing trade intensity on existing routes, or allowing buyer–supplier relationships to lapse altogether. Each channel implies a distinct welfare cost, and disentangling them requires studying

[9]Direct disruptions to maritime routes – for instance, tropical cyclones whose tracks intersect active shipping lanes – are not studied here. The exact path taken by individual vessels is not recorded in the data: bill of lading records report origin and destination ports but not the maritime trajectory.

port operations, route choices, and firm-to-firm trade separately.

Two features of the setting I focus on address these challenges in sequence. The first is geographic. Brazil is a large, globally-connected importer whose domestic ports lie entirely outside the cyclone belt.[10] Brazilian buyers are therefore never directly exposed to cyclone shocks, which rules out destination-side contamination and restricts the attribution problem to the origin side of the supply chain. Treatment is defined exclusively on the basis of origin ports – ports used by foreign suppliers – and residual concern about direct supplier-side exposure is addressed by absorbing supplier-specific heterogeneity at each stage of the analysis. The second feature is empirical. Disentangling firm responses from infrastructure disruptions requires data that separately identify the trading parties and the transportation infrastructure used for each shipment. I exploit bill-of-lading data,[11] in which each transaction records both the buyer–supplier pair and the origin and destination ports through which the shipment transits. By merging these shipment-level records with daily port traffic data, I can study each propagation channel at its natural unit of aggregation – port operations from daily traffic data, route choices from port-to-port shipment flows, and firm-to-firm trade from buyer–supplier relationships.

A further econometric challenge arises because tropical cyclone exposure is staggered across time, ports can be treated multiple times, and treatment effects are plausibly heterogeneous across ports and relationships. Standard two-way fixed-effects estimators are biased in such settings (Borusyak et al., 2024). I address this by adopting a stacked difference-in-differences design (Cengiz et al., 2019; Deshpande and Li, 2019) that enforces clean treated–control comparisons at each event and accommodates non-absorbing treatments.

The analysis delivers three main findings. First, exposure to tropical cyclones causes a sharp and persistent disruption to port operations – an average 9% decrease in the probability of port activity – lasting approximately one to two weeks, with effects concentrated among ports subject to prolonged wind exposure. Second, firms respond by rerouting shipments away from affected ports: the probability of using an

[10]No Brazilian port in the sample is exposed to tropical cyclones over the 2014–2023 period (see Figure 2a).

[11]A bill of lading is a document issued by a carrier to acknowledge receipt or shipment of cargo. It typically contains information on the cargo's origin, destination, quantity, packaging, shipping details, and description.

affected route decreases by 12% at the time of exposure. This adjustment is largely contemporaneous – route activity recovers within one month on average – but is more pronounced and persistent when the exposure is the first experienced by the trading relationship, lasting approximately four months. Non-containerized shipping drives this rerouting response, consistent with the greater scheduling flexibility of non-liner services. Third, despite this adaptation, port exposure to cyclones generates a persistent and significant decline in firm-to-firm relationship activity throughout the post-shock window – an average 17% decrease in the probability of trading – concentrated among relationships exposed to cyclone shocks more than once and among trade in containerized goods.

2.1 Data

This subsection introduces the data used in the empirical analysis. I combine Brazilian maritime trade data with global port-level information and tropical cyclone tracks. Appendix B provides a comprehensive review of all data sources and processing.

Firm-to-firm shipments. I study firm-to-firm relationships and trading routes using bill of lading data assembled by S&P Panjiva. The dataset encompasses the universe of maritime import transactions conducted by Brazilian firms between June 2014 and December 2023. Each shipment entry includes the company names of both the Brazilian importer and the foreign exporter. Geographic details – such as street address, city, postal code, and country – are recorded for each trading party, allowing precise geocoding of shipment origins and destinations. The data also record the maritime ports of loading (origin) and unloading (destination) for each shipment, enabling the reconstruction of trading routes. For each transaction, an indicator specifies whether the goods were containerized. The dataset includes the weight, volume, and current US dollar value of each shipment. It also reports whether the trading parties owned the cargo or acted as forwarders – i.e., third parties transporting the goods.

I perform a series of steps to clean the data and remove incomplete shipment information. I refer to geolocated establishments belonging to an identified parent company as *firms*.[12] First, I remove all shipments with missing Panjiva party identifiers,

[12] To address frequent typos in company names and geographic details, I clean the name strings and assign a single firm ID to all establishments sharing the same parent company name and geolocated within a 10 km radius.

since I cannot identify the trading parties. Second, I drop from the sample all firms that are not geolocated at the city or postal code level. Third, I restrict attention to shipments where both parties are declared the real owners of the cargo, thereby excluding warehouses and transportation companies.[13] Fourth, I remove all importers not geolocated in Brazil and all exporters geolocated in Brazil. Finally, I drop all shipments transiting through ports that cannot be matched to the IMF PortWatch port universe, measuring global port-level traffic.

Throughout the empirical section, I denote Brazilian importers as *buyers* (indexed by b), foreign exporters as *suppliers* (indexed by s), and buyer–supplier pairs $\{b, s\}$ as *relationships*. Based on the geographic coordinates of establishments, I assign to each supplier and buyer their location at the subnational level, denoted n_o for the origin location and n_d for the destination location, respectively.[14] When shipments transit from a port of origin p_o to a port of destination p_d, I denote the quadruplet $\{n_o, n_d, p_o, p_d\}$ as a *route* (indexed by r). The set of routes used by relationship (b, s) is denoted $\mathcal{R}_{bs}$. The baseline sample contains 915,587 shipments from 21,387 suppliers to 16,149 buyers, across 1,147 routes. Appendix B.1 describes the sampling procedure and provides summary statistics on firm-to-firm trade. Figure 1a presents the geographic distribution of firms in the sample, and Figure 1b maps the maritime routes and ports retained in the sample.

Global port-level traffic. To measure global port-level traffic, I use daily indicators of port activity provided by IMF PortWatch. The data include daily counts of port calls and estimates of import and export volumes, disaggregated by ship type (e.g., container, dry bulk), for 1,666 global ports from 2019 to 2023.[15] I match 621 ports by name to those in the Brazilian bill of lading data and use the daily port-level aggregates of imported and exported volumes – expressed in *twenty-foot equivalent units* (TEU) – as a proxy for port traffic.[16] Port capacity K_p is measured as the 99$^{\text{th}}$ percentile of daily

[13]Although third parties are likely to influence traffic at ports through routing decisions, they are not relevant for studying firm-to-firm relationships, as the data do not link these shipments to the production-oriented firms trading the goods.

[14]I map firms to the Global Administrative Unit Layers (GAUL), a set of administrative units with global coverage created by the Food and Agriculture Organization (FAO). I use GAUL1 administrative units – the first administrative layer within a country's structure (e.g., states in the US).

[15]The port-level data (2019–2023) do not cover the entire timeframe of the Brazilian bill of lading data (2014–2023). I therefore use them to verify that tropical cyclones affect port operations (Section 2.3.1).

[16]TEU (twenty-foot equivalent unit) is a standard measure of container capacity. Data are downloaded from IMF PortWatch. The data are based on raw Automatic Identification System (AIS) data

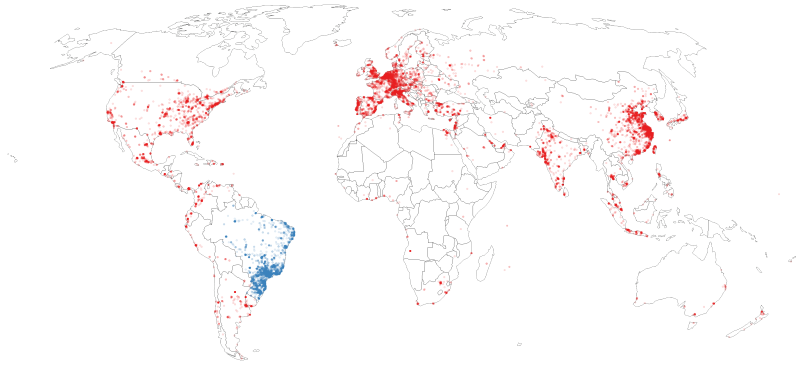

(a) Location of trading firms

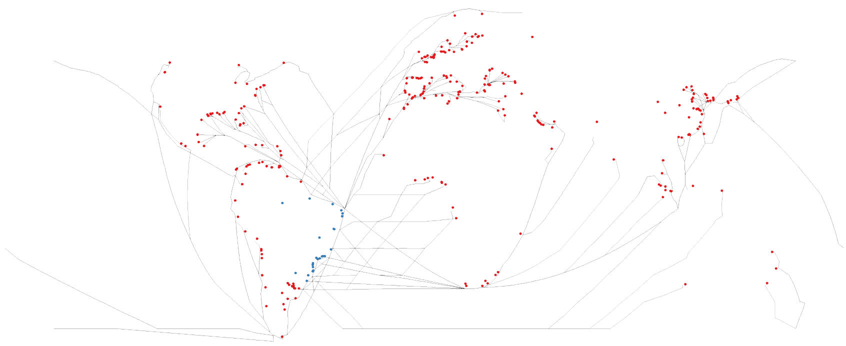

(b) Maritime routes

Notes: Panel 1a maps the locations of firms in the baseline sample. Each dot represents a firm: red dots denote foreign suppliers (n = 21,387), and blue dots denote Brazilian buyers (n = 16,149). Panel 1b maps the locations of ports and the corresponding active maritime routes in the sample. Each dot represents a port: red dots indicate foreign ports of origin (n = 286), and blue dots indicate Brazilian ports of destination (n = 24). Lines represent active routes (n = 1,147). I plot the shortest sea routes – computed using the Eurostat `SeaRoute` program – as a proxy for maritime routes, and exclude inland waterway routes.

Figure 1: Firms, Ports, and Routes

PortWatch TEU (imports + exports) over 2019–2023.

Tropical cyclone tracks. I obtain information on tropical cyclones from the IBTrACS (International Best Track Archive for Climate Stewardship) database (Knapp et al., 2010). This database provides a comprehensive record of tropical storms and cyclones since 1841. It contains detailed characteristics of storm systems' positions and intensities, with a temporal resolution of 3 hours and a spatial resolution of 0.1°. I focus on all cyclones recorded from 2014 to 2023 that were observed within 300 km of countries hosting ports in the sample. Figure 2a maps the tropical cyclone events in the sample,

from the United Nations Global Platform. Port-level daily estimates are calculated by the PortWatch team, following the methodology described in Arslanalp et al. (2021).

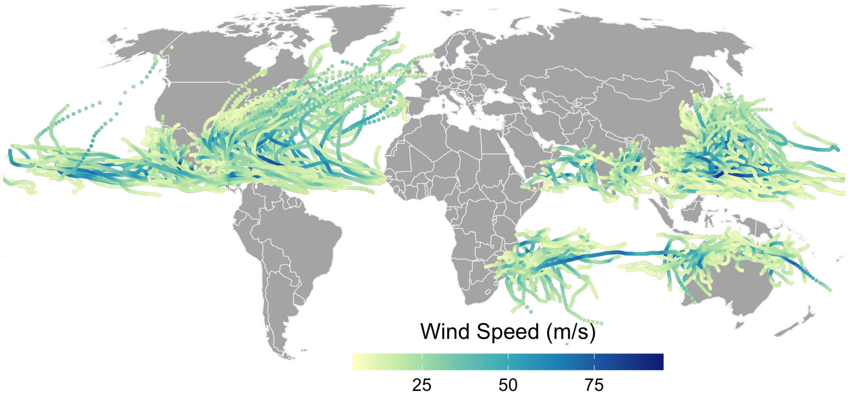

(a) Tropical Cyclones Tracks (2014-2023)

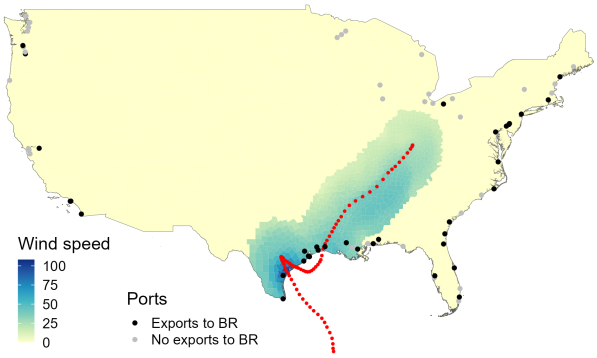

(b) Wind Speed Profile (Harvey, 2017)

Notes: Panel 2a shows the paths of all tropical cyclones recorded from 2014 to 2023 within 300 km of countries hosting ports in the sample. Wind speeds (m/s) correspond to the storm center (eye) and are reported at a 3-hour temporal resolution (IBTrACS). Panel 2b shows the maximum sustained wind speed experienced by US counties during Hurricane Harvey (23 August to 02 September 2017). The red dots represent the eye of the hurricane across its lifespan (IBTrACS). Wind speed is modeled using the method of Willoughby et al. (2006), adjusted for asymmetry using Chen (1994). Black dots indicate US ports that export to Brazil in the Brazilian bill of lading data. Grey dots represent US ports that do not export to Brazil.

Figure 2: Tropical Cyclones: Historical Tracks and Wind Speed Profiles

along with the sustained wind speeds (in meters per second) experienced along their paths. Appendix B.3 describes the data in detail and provides summary statistics on cyclone wind profiles at ports.

2.2 Empirical strategy

Measuring port exposure to cyclones. Tropical cyclones may affect the operations of maritime ports in several ways (Verschuur et al., 2023a). Port infrastructure is at risk of damage from heavy rain, floods, and intense winds. To prevent the risk of infrastructure damage upon the arrival of a tropical cyclone, ports can suspend operations – i.e., restrict vessels from entering the port, partially or completely – as a means to ensure the safety of port infrastructure and prevent vessel damage.[17] While the safety guidelines vary across ports and countries, most Coast Guard authorities restrict port operations around the threshold of 34–35 knots of expected wind speed (sustained *gale*), or approximately 18 meters per second.[18] Flynn (2023) refers to this zone of precaution as the *34-knot ship avoidance area*.

Exhaustive information on the closure of ports exposed to tropical cyclones is not easily accessible, nor is data on the actual wind speeds experienced around ports during cyclone events. I therefore proxy disruptive tropical cyclone events by modeling the wind speed experienced around port locations.[19] The input to this cyclone profile simulation method is the IBTrACS data described in Section 2.1. The output is a vector of cyclone characteristics at the port level, including the maximum sustained wind speed experienced at each port during the event. Figure 2b provides an example of the cyclone profile modeling procedure across the US for Hurricane Harvey (August 2017).

For my baseline definition of a port-level shock, I use a threshold of 18 m/s for experienced maximum wind speed. Appendix C.0.1 verifies that exposure to weaker wind speeds (between 9 and 18 m/s) does not induce port disruptions. Importantly, I use the time of the first-ever recorded information on the cyclone as the timing of the shock. This corresponds to the moment when the weather agency first detected the cyclone anomaly, thereby helping to avoid any anticipation by economic agents in a difference-in-differences setting. Table B.6 reports summary statistics on tropical cyclones.

Identification. I leverage the quasi-random timing and location of tropical cyclones to examine how (i) port operations, (ii) firm-level route choices, and (iii) firm-to-firm trade are affected by weather shocks. The empirical setting I consider poses several challenges to estimation. First, the treatment is staggered, and the treatment effect is

[17] For instance, the US Coast Guard issues *port conditions* that restrict vessel traffic upon the projected arrival of gale-force winds (greater than 34 knots). At the highest alert level (condition ZULU), the port is closed to all vessel traffic. See Appendix A for an example.

[18] The knot is a unit of speed corresponding to one nautical mile per hour. Sustained gale-force winds approximately correspond to wind speeds greater than 63 kilometers per hour, or 39 miles per hour.

[19] I use the parametric model of Willoughby et al. (2006), adjusted for asymmetry following Chen (1994)

likely heterogeneous across groups and over time. Tropical cyclones may affect ports that differ in their preparedness and recovery capacity. Moreover, treated relationships may differ in unobservable factors that influence their duration and resilience to shocks, such as relationship age or input specificity. Recent work has shown that two-way fixed-effects difference-in-difference estimators are biased in such settings (Borusyak et al., 2024). Second, the treatment is non-absorbing: ports – and therefore relationships – can be treated multiple times while recovering in between. Third, the treatment is likely continuous, depending on the magnitude of the cyclone or the degree of exposure to weather-related disruptions.[20] Fourth, to isolate the effects of cyclones on ports from those on firms, I need to control for a rich set of fixed effects.

I seek to address these concerns by using *stacked* dynamic difference-in-difference specifications, following Cengiz et al. (2019) and Deshpande and Li (2019). Conceptually, I define each time period during which at least one tropical cyclone occurs as a cyclone *event*, indexed by τ. For each event, I define a uniform event window, over which I observe the dynamics of port- and firm-level outcomes in the lead-up to and aftermath of the cyclone shock.[21] I extend this framework to allow for non-absorbing treatments. That is, I only include units that either (i) are treated *once* within the event window (clean treated) or (ii) are not treated at all during the window (clean controls). Units may be treated multiple times (i.e., they may appear in several event windows), as long as subsequent treatments fall outside the relevant window.[22] This approach allows me to control for a rich set of pre-shock unit characteristics and therefore strengthens the credibility of the common-trends assumption, while avoiding non-admissible comparisons inherent to staggered designs.[23] The identifying assumption is that, absent cyclone exposure, treated and control units would have followed parallel trends. The quasi-random timing and location of tropical cyclones – conditional on the fixed effects structure – supports this assumption, as there is no reason to expect systematic differential trends between ports that happen to lie on a cyclone's path and

[20]Ports may rely on a set of critical infrastructure to operate, such as nearby power grids or entrepôts, with differing levels of exposure to weather disasters (Verschuur et al., 2023a). Firms also exhibit varying degrees of reliance on high-risk routes for the delivery of goods.

[21]To preserve compositional balance between treated and control groups, I restrict attention to cyclone events for which outcomes are fully observed within the event window.

[22]This implies an assumption of treatment-effect stabilization, as in Dube et al. (2023).

[23]Wing et al. (2024) caution that stacked fixed-effects settings may introduce bias when averaging ATT estimates across events if the share of treated units varies. However, the authors do not yet offer an extension of their framework for non-absorbing treatments.

those that do not.

2.3 Results

In this section, I investigate the disruptions caused by port exposure to tropical cyclones at the port and firm-to-firm levels. I first show that tropical cyclones induce a short but severe disruption to port operations. I then document that firms reroute shipments to avoid affected ports. I finally show that, despite this adaptation at the route level, port exposure to cyclones generates persistent disruptions to firm-to-firm trade – concentrated among relationships exposed to cyclone shocks more than once.

2.3.1 Port-level disruptions

I first document that tropical cyclones temporarily affect the operations of ports. I construct daily measures of port activity from the IMF PortWatch data. The first outcome of interest – the extensive margin of port operations – is a binary variable that takes the value 1 if at least one vessel entered the port on day t, i.e., the port is *active*. Two additional outcomes capture the intensive margin of port operations, conditional on the port being active: the log number of vessels entering port p on day t, and the log volume (in TEU) transiting through the port.

To construct the sample, I first restrict attention to ports that I can identify in the Brazilian bill of lading data and that therefore export at least once to Brazil. I then consider an event window of 15 days before and after each cyclone event τ, where τ refers to the day on which the first observation of a cyclone track is recorded at sea. Within each event window, I subsample all ports that are either (i) exposed only once to sustained winds of at least 18 m/s, or (ii) not exposed to sustained winds from tropical cyclones. The final sample consists of 594 ports, potentially exposed to 120 cyclone events from 2019 to 2023.[24] I consider the following specification to estimate the effect of cyclones on port operations:

$$y_{p,t,\tau} = \sum_{h=-15}^{15} \beta_h \cdot \mathbb{1}\{t-\tau=h\} \cdot E_{p,\tau} + \alpha_{p,\tau} + \alpha_{t,\tau} + \varepsilon_{p,t,\tau}\ , \tag{1}$$

where $y_{p,t,\tau}$ corresponds to the outcome of interest for port p on day t around cyclone event τ. In the baseline specification, the treatment variable $E_{p,\tau}$ is binary, taking the value 1 if port p was exposed to sustained winds of at least 18 m/s at event τ. The

[24] 148 ports are treated at least once in the sample.

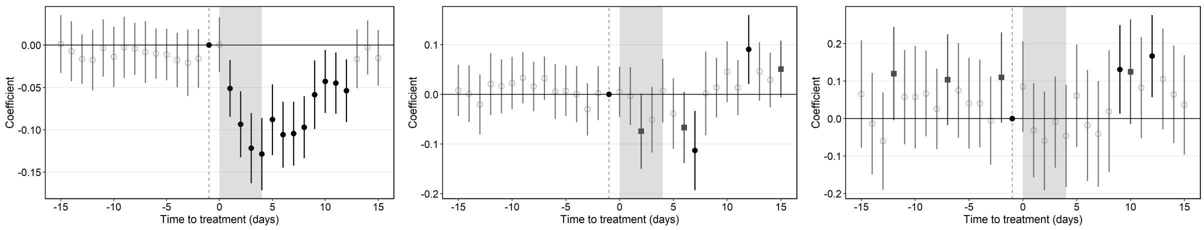

(a) Port activity (b) Log vessel count (c) Log TEU

Figure 3: The impact of exposure to cyclones on port operations

Notes: These panels plot the effect of exposure to tropical cyclones on daily port-level outcomes, as specified by Equation (1). The outcome in Panel 3a is a binary variable taking the value 1 if at least one vessel entered the port on day t (port activity), and 0 otherwise. The outcome in Panel 3b is the log number of vessels that use the port on day t, conditional on the port being active. The outcome in Panel 3c is the log volume (TEU) transiting through the port on day t, conditional on the port being active. Standard errors are clustered at the port level. The bars correspond to 95% confidence intervals. Black dots are point estimates significant at the 5% level, gray squares at the 10% level, and empty dots are non-significant at the 10% level.

regression controls for port-event and time-event fixed effects. Standard errors are clustered at the port level.

Figure 3a shows the results of estimating Equation (1) on the extensive margin of port operations, for a 15-day window before and after the shocks. The effect of port exposure to cyclones is a sharp decrease in the probability that the port is active, lasting approximately one to two weeks and gradually tapering thereafter. The effect corresponds to an average 9% decrease in the probability of port activity across the post-event window (15 days).[25] Figure 3b shows that, even when ports remain active, the number of vessels admitted to the port area may decrease, as ports reduce the intensity of operations. There is suggestive evidence that, immediately after the shock, port operations briefly *recapture* – that is, port productivity increases temporarily to reduce further shipment delays.

Heterogeneity and sensitivity. I first explore the sensitivity of the results to alternative treatment definitions. In Appendix C.0.1, I verify that exposure to weaker wind speeds (between 9 and 18 m/s) does not induce port disruptions (Figure C.1a). Continuous treatment measures – hours of exposure (Figure C.2a) and wind speed in m/s (Figure C.3a) – confirm a dose-response pattern. I also verify that stronger exposure induces larger disruptions in port activity. I estimate Equation (1) by splitting the treated group

[25]The unconditional probability of port activity in the pre-event window is 0.78. The duration of the effect is consistent with the findings of Verschuur et al. (2020). Reviewing the effect of natural disasters on port operations using vessel tracking data, they find a median disruption duration of six days.

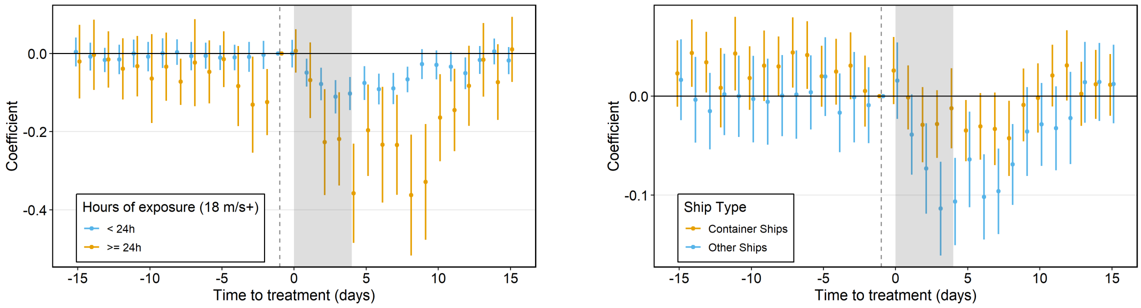

(a) Port activity (by exposure)

(b) Port activity (by ship type)

Figure 4: Heterogeneity in exposure to cyclones on port operations

Notes: These panels plot the effect of exposure to tropical cyclones on daily port-level outcomes, as specified by Equation (1). The outcome of both panels is a binary variable, taking the value 1 if at least one vessel entered the port on day t (port activity), and 0 otherwise. In Panel 4a, I estimate Equation (1) by splitting the treated group by the duration of exposure to at least 18 m/s: below and above 24 hours of exposure. In Panel 4b, I estimate Equation (1) using port–ship-type–specific outcomes: containerized vs. other ships. Standard errors are clustered at the port level. The bars correspond to 95% confidence intervals. Black dots are point estimates significant at the 5% level, gray squares are point estimates significant at the 10% level, and empty dots are point estimates non-significant at the 10% level.

by the duration of exposure to at least 18 m/s. Hours of exposure proxy for both the port's distance to the ship-avoidance area and the cyclone's intensity. Figure 4a confirms that port-level disruptions are concentrated among ports exposed for at least 24 hours to sustained wind speeds.

Second, the data allow me to distinguish between ship types. I estimate Equation (1) using port–ship-type–specific outcomes: containerized vs. other ships (e.g., bulk). Container ships (or "liner" ships) typically operate along fixed, pre-planned lines, limiting real-time route adjustments, while owners/operators of other ship types have comparatively more flexibility in scheduling (Ksciuk et al., 2023). Figure 4b shows that container ships are less responsive to port exposure to cyclones, consistent with pre-scheduled shipping.

2.3.2 Route Choice

I then examine how port exposure to cyclones affects firms' choice of shipping routes. I seek to understand whether route choice serves as a margin of adaptation after firm pairs are treated. I use monthly aggregates of the Brazilian shipment data at the buyer–supplier–route level (b, s, r), where routes r are proxied by the pair of ports through which shipments are loaded (port of origin p_o) and unloaded (port of destination p_d).[26]

[26]Formally, routes are also defined over the origin and destination regions of shipments: $\{n_o, n_d, p_o, p_d\}$. Conditional on (geolocated) firms fixed effects, route definition boils down to $\{p_o, p_d\}$.

The outcome of interest is a monthly measure of the extensive margin of route activity: a binary variable equal to 1 if there is a positive number of shipments between b and s using route r, and 0 otherwise. Route activity is conditioned on relationship–route *entry* – i.e., a route can be active for a relationship only after its first shipment on that route.[27] I also consider an intensive margin outcome – namely, the log of the number of shipments between b and s using route r, conditional on relationship–route activity.

To construct the sample, I aim to compare relationship–routes that are as similar as possible in frequency, volume, and timing of shipments.[28] I define an event window of 5 months before and 10 months after each cyclone event τ, where τ refers to the month in which the first observation of a cyclone track is recorded at sea.[29] I sample relationship–routes that trade at least once within the 5-month pre-shock window, thereby restricting attention to relationship-routes active before the shock. Relationship–routes are treated if their port of origin is exposed to tropical cyclones at event τ. Importantly, ports of destination (i.e., Brazilian ports) in the sample are not exposed to tropical cyclones (see Figure 2a), allowing me to define treatment solely on the basis of origin ports. I consider the following specification to estimate the effect of cyclone-induced port disruptions on route choice:

$$y_{bsr,t,\tau} = \sum_{h=-5}^{10} \left[\beta_h \cdot \mathbb{1}\{t - \tau = h\} \cdot E_{p_o \in r,\tau} + \delta_h X_{bsr,h,\tau} + \alpha_{h,\tau} \right] + \alpha_{bsr,\tau} + \alpha_{bs,t} + \varepsilon_{bsr,t,\tau} \,, \tag{2}$$

where $y_{bsr,t,\tau}$ corresponds to the outcome of interest for relationship–route (b, s, r) at month t around cyclone event τ. In the baseline specification, the treatment variable $E_{p_o \in r,\tau}$ is binary, equal to 1 if the port of origin p_o in route r was exposed to at least 18 m/s of sustained wind speed at event τ. The regression includes time–event, relationship–route–event, and relationship–month fixed effects. This specification restricts comparisons to route choices within relationships and within events. Control variables $X_{bsr,h,\tau}$ are time dummies interacted with pre-treatment characteristics of

[27] This avoids comparing poorly defined *potential* routes – i.e., periods before a route's first recorded shipment. If a relationship's first shipment on a route occurs within the first year of the sample, I assume the relationship–route enters in the first month of the sample.

[28] Before applying event-based sample restrictions, I remove all relationship-routes active only once throughout the sample. These 'one-timer' relationship-routes are noise and do not help identifying the dynamics of firms' responses to treatment.

[29] τ refers to a month in which at least one cyclone forms and at least one port is exposed. A cyclone event may include multiple cyclones, and ports may be exposed several times within the same event.

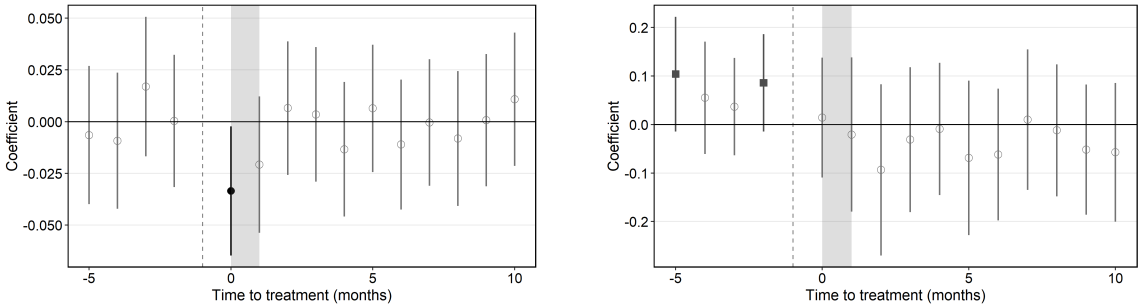

(a) Route activity

(b) Log # shipments

Figure 5: The impact of port exposure to cyclones on route choice

Notes: These panels plot the effect of port exposure to tropical cyclones on monthly firm-to-firm–route-level outcomes, as specified by Equation (2). The outcome in Panel 5a is a binary variable equal to 1 if at least one shipment is observed for the trading pair through route r in month t (active route), and 0 otherwise. The outcome in Panel 5b is the log number of shipments through route r in month t, conditional on the relationship–route being active. Regressions include relationship–month fixed effects, and control for time dummies interacted with relationship-routes' pre-treatment characteristics. Standard errors are clustered at the relationship level. The bars show 95% confidence intervals. Black dots indicate point estimates significant at the 5% level, gray squares at the 10% level, and empty dots denote estimates that are not significant at the 10% level.

each relationship–route.[30] Standard errors are clustered at the relationship level.

Figure 5a reports the estimation of Equation (2) on route activity, 5 months before and 10 months after the shock. Results indicate that port exposure to cyclones decreases trade through affected routes relative to unaffected routes only at impact, and promptly recover the use of the affected route. At the time of exposure, the effect corresponds to a 12% decrease in the probability of using the affected route.[31] Figure 5b shows that firms do not adjust shipment size when they continue trading through the affected route. Because the specification includes relationship-level fixed effects, the estimated impact of rerouting reflects an additional adjustment margin beyond any direct disruption at the firm-to-firm level. In other words, the results isolate the role of route substitution as a distinct channel of adaptation, separate from the overall continuity of trade relationships between firms.[32]

Heterogeneity and sensitivity. First, I verify that the *intensity* of treatments does not qualitatively affect the results. I estimate Equation (2), interacting the treatment indicator with two intensity measures of exposure to cyclones: the maximum sustained

[30] These include the number of shipments, the number of active months, and the month of the last shipment within the 5-month pre-treatment period.

[31] The unconditional probability of route activity in the pre-shock window is 0.43.

[32] Figures C.4a and C.4b report additional intensive margins: log weight (kg) and the number of shipments, both conditional on relationship-route activity. Both margins show similar patterns to that of shipment volume.

wind speed along the cyclone path (in m/s), and number of hours the ports experienced wind speeds of at least 18 m/s. The first measure captures the intensity of the weather event, while the second measures the exposure of ports to the critical wind speed threshold. Figures C.5a and C.5b report the results of these alternative treatments on route activity, with no significant changes in patterns. Appendix C.0.2 reports the full set of robustness checks, including additional intensive margins (Figure C.4a).

Second, the short-lived treatment effect on route choice suggests that firms adapt ex ante to the possibility of increased transportation costs due to weather shocks. Still, Equation (2) pools all treatments and does not capture heterogeneity in treatment effects based on a relationship's treatment history. I therefore decompose Equation (2) by including two treatment variables: $\mathbb{1}^{1}_{bs,\tau} \times E_{p_o \in r,\tau}$, which equals 1 if the treatment at τ is the first experienced by relationship (b,s), and $\mathbb{1}^{1<}_{bs,\tau} \times E_{p_o \in r,\tau}$, which equals 1 for any subsequent treatment. This allows me to examine whether firms learn or adapt following past events. Figure C.6a shows that the rerouting mechanism is much more pronounced for the first treatment than for subsequent ones. Route activity decreases for approximately four months following the first port exposure to a cyclone – well after port operations resume. By contrast, subsequent treatments lead to only a one-month decline in route activity, likely reflecting the mechanical effect of port closures. This suggests that firms learn from experience and quickly converge toward ex ante adaptation in response to future shocks.

Third, route choice may also be constrained by which party schedules shipments. Containerized goods are typically carried by liner ships, operated by large companies along fixed, pre-planned services. While firms can switch operators, choices may be limited by compatibility between preferred ports and the ability of those ports to service container ships. Bulk shipping, by contrast, generally offers greater flexibility in scheduling vessels and ports. To assess the importance of these constraints, I decompose Equation (2) by allowing treatment effects to differ between containerized and non-containerized shipping. I define $\mathbb{1}^{c}_{bs,r,\tau} \times E_{p_o \in r,\tau}$ to equal 1 if the relationship traded only containerized goods in the 5-month pre-treatment window, and $\mathbb{1}^{\text{non-c}}_{bs,r,\tau} \times E_{p_o \in r,\tau}$ to equal 1 if at least one shipment was non-containerized. Figure C.7a shows that non-containerized shipping accounts for most of the treatment effect, consistent with greater scheduling flexibility outside containerized services.

2.3.3 FIRM-TO-FIRM DISRUPTIONS

I finally turn to the effect of port exposure to cyclones on firm-to-firm trade. I am mainly interested in the extensive margin of firm-to-firm trade – that is, in supply chain composition. I use monthly aggregates of the Brazilian shipment data at the buyer–supplier level (b, s). My first outcome of interest is a monthly measure of relationship activity, defined as a binary variable equal to 1 if a positive number of shipments occurs within the relationship (b, s) in month t, and 0 otherwise. Relationship activity is conditioned on the entry of both the buyer and the supplier, respectively defined as the month of the first recorded shipment received by b or sent by s.[33] I also consider an intensive-margin outcome, defined as the log of number of shipments between b and s, conditional on relationship activity.

The sample is constructed analogously to that in Section 2.3.2, though selection criteria are defined at the relationship (b, s) level. Treated relationships are those that used at least one exposed *port of origin* during the pre-shock window. I consider the following specification to estimate the effect of cyclone-induced port disruptions on firm-to-firm trade:

$$y_{bs,t,\tau} = \sum_{h=-5}^{10} \left[\beta_h \cdot \mathbb{1}\{t - \tau = h\} \cdot E_{p_o \in \mathcal{R}^{\tau}_{bs},\tau} + \delta_h X_{bs,h,\tau} + \alpha_{h,\tau} \right] + \alpha_{bs,\tau} + \alpha_{b,t} + \alpha_{s,t} + \varepsilon_{bs,t,\tau}\,, \tag{3}$$

where $y_{bs,t,\tau}$ denotes the outcome of interest for buyer–supplier relationship (b, s) in month t around cyclone event τ. In the baseline specification, the treatment variable $E_{p_o \in \mathcal{R}^{\tau}_{bs},\tau}$ is binary, equal to 1 if at least one port of origin p_o used by the relationship (i.e., in the set of routes $\mathcal{R}^{\tau}_{bs}$) was exposed to sustained wind speeds of at least 18 m/s during event τ.[34] The regression includes buyer–month and supplier–month fixed effects, which absorb buyer- and supplier-specific shocks. This is important for isolating the effect of cyclones on the ports used by relationships while controlling for potential direct effects on suppliers themselves. Control variables $X_{bs,h,\tau}$ are time dummies in-

[33] Here, I follow Balboni et al. (2024). As for route activity, this avoids comparisons between poorly defined *potential* relationships – i.e., before the first recorded activity of the trading parties. When the first recorded shipment is observed within the first year of the sample, I assume that the firm enters during the first period of the sample.

[34] The set of routes $\mathcal{R}^{\tau}_{bs}$ is time-dependent, as it is defined using the pre-shock window.

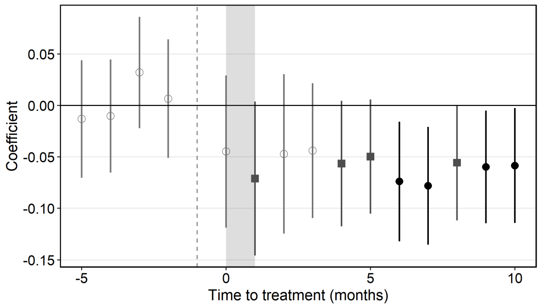

(a) Relationship activity

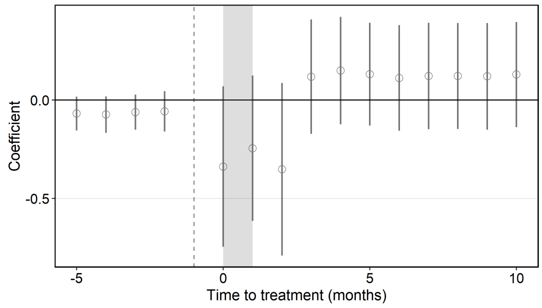

(b) Log # shipments

Figure 6: The impact of port exposure to cyclones on firm-to-firm relationship

Notes: These panels plot the effect of port exposure to tropical cyclones on monthly firm-to-firm-level outcomes, as specified by Equation (3). The outcome in Panel 6a is a binary variable equal to 1 if at least one shipment is observed for the trading pair in month t (active relationship), and 0 otherwise. The outcome in Panel 6b is the log number of shipments for the relationship, conditional on the relationship being active. Regressions include buyer–time and supplier–time fixed effects, and control for time dummies interacted with relationships' pre-treatment characteristics. Standard errors are clustered at the buyer level. The bars denote 95% confidence intervals. Black dots indicate point estimates significant at the 5% level, gray squares at the 10% level, and empty dots denote non-significant estimates at the 10% level.

teracted with pre-treatment characteristics of each relationship.[35] Standard errors are clustered at the buyer level.

Figure 6a reports the estimation of Equation (3) on relationship activity, 5 months before and 10 months after the shock. Results indicate that port exposure to cyclones generates a significant and persistent reduction in relationship activity throughout the post-shock window. The effect corresponds to an average 17% decrease in the probability of trading for treated relationships compared to untreated relationships across the post-shock window (10 months).[36] Figure 6b suggests that firms do not significantly adjust shipment intensity when they continue trading. Overall, these results indicate that port disruptions translate into lasting supply-chain recomposition – a finding that stands in contrast to the short-lived adjustment observed at the route level.

Heterogeneity and sensitivity. First, I investigate whether the intensity of exposure to treatment alters the results. I estimate Equation (3), interacting the treatment indicator with the share of pre-treatment trade (measured by the number of shipments) using routes exposed to cyclones. Figures C.9a and C.9b show no pattern changes when considering such continuous treatment. Appendix C.0.3 reports additional intensive

[35] As with relationship–routes, these include the number of shipments, the number of active months, and the month of the last shipment within the 5-month pre-treatment period, specified at the buyer–supplier level.

[36] The unconditional probability of relationship activity in the pre-shock window is 0.42.

margins and the full set of heterogeneity decompositions.

Second, I investigate the same heterogeneity dimensions as in Section 2.3.2, i.e., along the treatment history and by containerization status of shipments. Figure C.10a reveals a sharp asymmetry between first and subsequent treatments. Relationships treated for the first time show no significant disruption in activity – consistent with the rerouting documented in Section 2.3.2 providing an effective buffer on first exposure. Relationships exposed more than once, by contrast, exhibit persistent and significant reductions in activity throughout the entire post-shock window, suggesting that the adaptive capacity afforded by route substitution does not extend to repeated shocks.[37] Figure C.11a further shows that containerized relationships bear a more consistent and persistent disruption than non-containerized ones – in line with the constraints on rerouting documented at the route level.

The reduced-form evidence is silent on two dimensions that matter for welfare. First, it does not capture the congestion costs imposed on untreated relationships when treated firms reroute through alternative ports. Second, the event-study design identifies firms' responses to individual cyclone events, not their responses to a permanent shift in the distribution of weather risk. The next two sections develop a structural framework to address both.

3 Theory

The reduced-form evidence left two questions beyond its reach: the general-equilibrium congestion externality that rerouting creates at untreated ports, and the welfare response to a permanent distributional shift in port-level weather risk. This section develops a model that addresses both.

In this section, I develop a theory of spatial production network formation with endogenous trade costs and weather shocks to trade infrastructure. The model is built to rationalize the three features of the data that Section 2 documented: (i) tropical cyclones disrupt the operations of maritime ports, (ii) firms respond to these disruptions by rerouting shipments through less exposed ports, and (iii) the disruptions nonetheless pass through to firm-to-firm trade.

[37] This asymmetry could partly reflect survivorship: relationships observed at second treatment are those that did not dissolve after the first shock, a selected sample that may differ in durability or switching costs.

To capture the empirical evidence on the impacts of trade infrastructure exposure to weather disasters on global supply chains, I assume that, in a production network environment similar to Oberfield (2018), firms make joint sourcing and routing decisions based on suppliers' factory-gate costs and transportation costs.[38] Transportation costs are endogenous to traffic congestion, as in Allen and Arkolakis (2022), and for maritime routes include the costs of using port infrastructure, which is potentially affected by weather disasters. Firms are perfectly informed about the underlying distribution of weather-related risks to port infrastructure.

The model delivers predictions that are not testable in the reduced-form empirical evidence in Section 2. First, the model incorporates traffic congestion, which is likely to affect transportation costs in the long run. Section 2.3 shows that firms adapt to weather shocks by redirecting trade through alternative routes. If traffic congestion increases the cost of using these alternatives, such adaptation may, in turn, distort the bilateral components of sourcing shares and affect the aggregate impact of infrastructure exposure to weather disasters. Second, while the empirical results describe reactions to single weather events, they do not address a local shift in the *distribution* of events – i.e., a shift in port-level climate conditions. The model accommodates such a counterfactual by assuming that a shift in the distribution of weather disasters is akin to a sequence of realized events through which firms update their information about the probability distribution of extreme weather events.[39]

Environment. The economy consists of a discrete set $\mathcal{N}$ of regions (indexed by n or n'), each populated by a unit measure of firms, $M_n = 1 \; \forall n \in \mathcal{N}$, and an exogenous measure of households $L_n \in \{L_n\}_{n \in \mathcal{N}} \equiv \mathcal{L}$. Each region is endowed with a fundamental productivity $a_n \in \{a_n\}_{n \in \mathcal{N}} \equiv \mathcal{A}$. Some regions contain port infrastructure, which enables trade across regions that are not directly connected by land.[40] The set of ports is denoted $\mathcal{P}$. Both regions and ports are connected through a *transportation network*, i.e., a set of bilateral trade frictions incurred when shipping directly from one location (a

[38] I draw from the model of endogenous production network formation under idiosyncratic and aggregate weather-disaster risks presented in Balboni et al. (2024). Chen et al. (2023) proposes a related model in which technology compatibility between firms shapes the marginal costs of inputs. I extend this class of models to include a geography, endogenous trade costs, and transportation-related weather risks.

[39] Although static, the model can also describe the immediate aftermath of a weather disaster and therefore accommodate the dynamic – but short-lived – disruptions described in Section 2.3.

[40] Regions may contain multiple ports.

region or a port) to another. The transportation network depends on both endogenous variables (traffic) and exogenous ones (distance and capacity). Regions are distant from each other, with a bilateral measure of distance $\epsilon_{nn'} \in \{\epsilon_{nn'}\}_{n,n' \in \mathcal{N}^2} \equiv \mathcal{D}$. Each port has a capacity $K_p \in \{K_p\}_{p \in \mathcal{P}} \equiv \mathcal{K}$ (e.g., port berths). Regions are connected via a countable set of routes $\mathcal{R}$, which allow for trade in intermediate inputs.

Households. Households in region n inelastically supply labor l_i to local firms and consume a bundle of differentiated final goods supplied by local firms:

$$q_n = \left(\int_{i \in M_n} q_i^{\frac{\sigma-1}{\sigma}} di \right)^{\frac{\sigma}{\sigma-1}}, \tag{4}$$

where q_i is the quantity of final goods supplied by firm $i \in M_n$, and $\sigma > 1$ is the elasticity of substitution across varieties of final goods in region n. I assume no trade in final goods and no migration across regions.[41] Households face the budget constraint:

$$\int_{i \in M_n} q_i p_i \, di = w_n + \Pi_n, \tag{5}$$

where p_i is the price charged by firm i for final goods, w_n is the wage rate in region n, and Π_n denotes per-capita profits rebated from firms to households in region n.

Firms. Firms produce by combining local labor with perfectly substitutable intermediate inputs supplied by other firms along different routes. Each firm faces a mass of potential suppliers located in all regions (including its own) and a set of delivery routes. A specific combination of labor, input, and delivery route yields a *technique* of production, defined over a supplier–buyer match ϕ and a delivery route r:

$$y_i(\phi, r) = \chi \, a_{n(i)} \, l_i^{1-\alpha} \big(z(\phi) x_i(\phi, r) \big)^{\alpha}, \tag{6}$$

where l_i is the amount of labor used by firm i, $x_i(\phi, r)$ is the amount of intermediate inputs supplied through route r, $z(\phi)$ is the match-specific input-augmenting productivity, and $a_{n(i)}$ is the productivity shifter of region $n(i)$.[42]

Firms choose the technique that yields the minimum marginal cost of production, at which they sell their goods to other firms – i.e., buyers have full bargaining power

[41] These are restrictive assumptions, but they map directly to the evidence presented in Section 2.3, and to the fact that the bill of lading data only include firm-related transactions. A consequence is that the model rules out the imported-consumer-goods welfare channel standard in multi-country trade models, so the welfare effects reported in Section 6 operate exclusively through intermediate-input trade.

[42] χ is a normalizing constant equal to $\alpha^{-\alpha}(1-\alpha)^{-(1-\alpha)}$.

(Oberfield, 2018). When selling final goods to local households, firms engage in monopolistic competition. Trade in intermediate inputs is subject to route-specific iceberg costs: for each unit required in production, $\tau_{n(j)n(i)}(r) \geq 1$ units must be shipped from supplier region $n(j)$ to buyer region $n(i)$ along route r. The factory-gate marginal cost of production using technique (ϕ, r) is therefore:

$$c_i(\phi, r) = \frac{w_{n(i)}^{1-\alpha}}{a_{n(i)}} \left(\tau_{n(j)n(i)}(r) \frac{c_j(\phi)}{z(\phi)} \right)^{\alpha}, \tag{7}$$

where $c_j(\phi)$ is the marginal cost of inputs from supplier j. I assume the following distributional form to obtain a tractable characterization of the equilibrium:

Assumption 1. *For any firm i in region n, the number of potential suppliers $j \in M_{n'}$ from which i can draw a match with productivity $z > \bar{z}$ follows a Poisson distribution with mean $a_{n'}\bar{z}^{-\xi}$, where $a_{n'}$ is the fundamental productivity of firms in region n'.*

Assumption 1 describes the distribution of match-specific productivity among the techniques available to a firm in region n. The parameter ξ governs the tail behavior of the distribution of productivity draws (Oberfield, 2018; Chen et al., 2023; Balboni et al., 2024). A higher value of ξ implies more similarity across draws, making buyers more willing to substitute toward alternative suppliers when route-level or factory-gate costs increase.

Shipping. Firms from region n can ship to any other region.[43] However, shipments may be indirect, as some regions are not directly connected (e.g., by a direct road or a maritime route). Shipping routes are composed of a countable set $\mathcal{B}_r$ of legs, with $|\mathcal{B}_r| - 1$ stops from origin n ($k = 1$) to destination n' ($k = |\mathcal{B}_r|$). Each stop may be a port or a region. Each stop involves leg-specific iceberg transportation costs between locations, as well as port-level transportation costs. For a route r connecting n to n' through $|\mathcal{B}_r|$ legs, including $|\mathcal{P}_r|$ ports, the transportation costs are given by:

$$\tau_{n(j)n(i)}(r) = \prod_{k=1}^{|\mathcal{B}_r|} d_{r_{k-1}, r_k} \prod_{m=1}^{|\mathcal{P}_r|} t_{p(r)_m}. \tag{8}$$

For domestic sourcing ($n = n'$), I assume that $\mathcal{R}_{nn}$ consists of a single direct route

[43] With a slight abuse of terminology, *shipping* encompasses both road and maritime transportation. In this setting, transportation mode choice (e.g., road vs. maritime) is implied by route choice, with an elasticity equal to the dispersion of match-specific productivity ξ governing firm-to-firm matching (Fuchs and Wong, 2024).

with no shipping legs ($|\mathcal{B}_r| = 0$) and no port infrastructure ($|\mathcal{P}_r| = 0$), so that $\mathcal{R}_{nn} = \{\tau_{nn}(r_{\text{direct}})\} = 1$. This reflects the assumption that domestic suppliers deliver to domestic buyers without using the international transportation network. Following Ganapati et al. (2024), I allow transportation costs to depend on both endogenous and exogenous variables:

$$d_{r_{k-1},r_k} = d\big(\epsilon_{r_{k-1},r_k}\big), \quad t_{p(r)_m} = t(\Xi, K_{p(r)_m}) \times \theta_{p(r)_m}, \tag{9}$$

where ϵ_{r_{k-1},r_k} denotes exogenous transportation costs (i.e., distance), Ξ is a matrix of traffic flows, $K_{p(r)_m}$ denotes port-level infrastructure capacity, and $\theta_{p(r)_m}$ denotes port-level weather-related wedges, with the following assumption:

ASSUMPTION 2. *Port-level wedges are randomly drawn from a Pareto distribution with c.d.f.* $F_{p(r)}(\theta) = 1 - \theta^{-\psi_{p(r)}}$ *for* $\theta_{p(r)} \geq 1$.

Assumption 2 describes the distribution of port-level wedges. With a higher shape parameter $\psi_{p(r)}$, firms will on average draw lower transportation cost wedges, as the tail of the distribution becomes thinner. This assumption ensures that transportation costs in Equation (8) remain tractable. The set of shape parameters $\{\psi_p\}_{p\in\mathcal{P}}$ governing these weather-related wedges – i.e., climate trade costs – is denoted Ψ and summarizes the port-level tropical cyclone climate.

Sourcing and routing decisions. I first characterize the distribution of factory-gate costs:

PROPOSITION 1. *Under Assumption 1, the marginal cost of firms in* $M_{n'}$ *follows a Weibull distribution:*

$$P\big(c_i(\phi, r) > c\big) = \exp\left[-\left(a_{n'} w_{n'}^{\alpha-1}\right)^{\frac{\xi}{\alpha}} \left(\sum_n a_n\, \bar{c}_n^{-\xi} \sum_{r\in\mathcal{R}_{nn'}} \prod_{k=1}^{|\mathcal{B}_r|} d_{r_{k-1},r_k}^{-\xi} \prod_{m=1}^{|\mathcal{P}_r|} \bar{t}_{p(r)_m}^{-\xi}\right) c^{\frac{\xi}{\alpha}}\right], \tag{10}$$

$$\textit{where} \quad \bar{c}_n^{-\xi} = a_n^{\xi} w_n^{(\alpha-1)\xi} \left(\sum_{\tilde{n}} a_{\tilde{n}}\, \bar{c}_{\tilde{n}}^{-\xi} \sum_{r\in\mathcal{R}_{\tilde{n}n}} \prod_{k=1}^{|\mathcal{B}_r|} d_{r_{k-1},r_k}^{-\xi} \prod_{m=1}^{|\mathcal{P}_r|} \bar{t}_{p(r)_m}^{-\xi}\right)^{\alpha} \Gamma(1-\alpha), \tag{11}$$

$$\textit{and} \quad \bar{t}_{p(r)_m}^{-\xi} = t\big(\Xi, K_{p(r)_m}\big)^{-\xi} \frac{\psi_{p(r)_m}}{\psi_{p(r)_m} + \xi}. \tag{12}$$

Proof. See Appendix D.1.

This result follows from the fact that, if the *effective* price of inputs for suppliers in all origin regions and delivering through any route follows a Weibull distribution, then the distribution of factory-gate prices for all firms i in destination n' also follows a Weibull distribution.[44] The production-network structure affects the distribution of marginal costs through the factory-gate costs of upstream suppliers, as shown in Equation (11), which specifies downstream cost indices as a fixed point. Transportation costs depart from related models of production-network formation (Chen et al., 2023; Balboni et al., 2024) by explicitly incorporating the set of links and transportation infrastructure that compose routes. I characterize the joint sourcing and routing decisions of firms as a corollary to Proposition 1.

COROLLARY 1. *The probability that firm i in n' sources from route r connecting n to n' is:*

$$\pi_{i,r} = \frac{a_n\, \bar{c}_n^{-\xi} \prod_{k=1}^{|\mathcal{B}_r|} d_{r_{k-1},r_k}^{-\xi} \prod_{m=1}^{|\mathcal{P}_r|} \bar{t}_{p(r)_m}^{-\xi}}{\sum_{\tilde{n}} a_{\tilde{n}}\, \bar{c}_{\tilde{n}}^{-\xi} \sum_{r\in\mathcal{R}_{\tilde{n}n'}} \prod_{k=1}^{|\mathcal{B}_r|} d_{r_{k-1},r_k}^{-\xi} \prod_{m=1}^{|\mathcal{P}_r|} \bar{t}_{p(r)_m}^{-\xi}}. \tag{13}$$

Proof. See Appendix D.1.

Equation (13) represents the unconditional probability of choosing route r to source goods. Given that route r links destination n' to origin n, Equation (13) jointly specifies the sourcing region and the delivery route. Because this probability is independent of firm i characteristics, $\pi_{i,r}$ is also the share of *expenditures* of region n' on region n through route r. Aggregating the sourcing–routing shares across routes yields region-to-region bilateral trade shares, as shown in Corollary 2:

COROLLARY 2. *The bilateral trade share between n' and n is:*

$$\pi_{nn'} = \frac{a_n\, \bar{c}_n^{-\xi}\, \tau_{nn'}^{-\xi}}{\sum_{\tilde{n}} a_{\tilde{n}}\, \bar{c}_{\tilde{n}}^{-\xi}\, \tau_{\tilde{n}n'}^{-\xi}}, \tag{14}$$

$$\textit{where} \quad \tau_{nn'} = \left(\sum_{r\in\mathcal{R}_{nn'}} \left(\prod_{k=1}^{|\mathcal{B}_r|} d_{r_{k-1},r_k}^{-\xi} \right) \left(\prod_{m=1}^{|\mathcal{P}_r|} \bar{t}_{p(r)_m}^{-\xi} \right) \right)^{-\frac{1}{\xi}}. \tag{15}$$

Proof. See Appendix D.1.

Equation (14) resembles the gravity structure of traditional trade models (Anderson and van Wincoop, 2003), with the addition of production network–affected marginal-

[44] I define the effective price of inputs delivered by supplier j through route r as

$$\lambda_j(\phi, r) = \frac{c_j}{z(\phi)} \prod_{k=1}^{|\mathcal{B}_r|} d_{r_{k-1},r_k} \prod_{m=1}^{|\mathcal{P}_r|} t_{p(r)_m}.$$

cost indices $\bar{c}_n$ and endogenous transportation costs. Equation (15) captures the departure from trade models with endogenous routing (Allen and Arkolakis, 2022; Ganapati et al., 2024; Fuchs and Wong, 2024) by explicitly incorporating infrastructure-level costs. For domestic transactions ($n = n'$), I impose $\tau_{nn} = 1$, a direct consequence of $\mathcal{R}_{nn} = \{\tau_{nn}(r_{\text{direct}})\} = 1$.

Equilibrium transportation costs. Define the auxiliary matrix of bilateral transportation resistance Δ as a $(|\mathcal{N}| + |\mathcal{P}|) \times (|\mathcal{N}| + |\mathcal{P}|)$ matrix. Each of the first $|\mathcal{N}|$ rows and columns of Δ corresponds to a region, while each of the last $|\mathcal{P}|$ rows and columns corresponds to a port. Denoting both regions and ports as *locations*, indexed by l or l', the (l, l') entry $\delta_{ll'}$ of Δ is zero if l and l' are not directly connected (denoted $l \not\sim l'$). If the two locations are connected and l' is a port, then $\delta_{ll'} = d_{ll'}^{-\xi}\, \bar{t}_{l'}^{-\xi}$; if the two locations are connected and l' is not a port, then $\delta_{ll'} = d_{ll'}^{-\xi}$. It follows that the region-to-region transportation costs are given by the Leontief inverse of the auxiliary matrix Δ:[45]

$$\tau_{nn'}^{-\xi} = \begin{cases} 1 & \text{if } n = n', \\ \left[(I - \Delta)^{-1}\right]_{nn'} & \text{if } n \neq n'. \end{cases} \tag{16}$$

The conditional probability that a good passes through port p, given origin n and destination n', is:

$$\Theta_{p|nn'} = \left(\frac{\tau_{np}\, \tau_{pn'}}{\tau_{nn'}} \right)^{-\xi}. \tag{17}$$

Using these port-level conditional probabilities, I characterize traffic as the total value of goods that transit through ports:[46]

$$\Xi_p = \sum_{n} \sum_{n' \neq n} \Theta_{p|nn'}\, X_{nn'}. \tag{18}$$

where $X_{nn'}$ is the total trade value from n to n'. Equation (9) implies that port traffic affects transportation costs – a form of externality that firms do not internalize

[45] As in Allen and Arkolakis (2022) and Ducruet et al. (2024) self-loops are excluded from the resistance matrix (i.e., $\delta_{ll} = 0$ for all locations l), ensuring that each term in the geometric series $I + \Delta + \Delta^2 + \cdots$ corresponds to a distinct shipping route rather than a path that revisits the same location consecutively. The Leontief inverse $(I - \Delta)^{-1}$ is well-defined when the spectral radius of Δ is below one. For $n \neq n'$, $\left[(I - \Delta)^{-1}\right]_{nn'}$ sums over all paths connecting n to n' through the transportation network. For $n = n'$, $\left[(I - \Delta)^{-1}\right]_{nn} = 1 + [\Delta^2]_{nn} + \cdots > 1$ reflects round-trip paths departing from and returning to n. Since $\mathcal{R}_{nn} = \{r_{\text{direct}}\}$ with $\tau_{nn}(r_{\text{direct}}) = 1$, round-trip paths are not part of the domestic route set, so I set $\tau_{nn}^{-\xi} = 1$ rather than $\left[(I - \Delta)^{-1}\right]_{nn}$.

[46] Here again, I follow Allen and Arkolakis (2022) and Ducruet et al. (2024). The conditional probability $\Theta_{p|nn'}$ is defined for $n \neq n'$. Domestic flows ($n = n'$) are excluded from the traffic sum: since $\mathcal{R}_{nn} = \{r_{\text{direct}}\}$ with $|\mathcal{P}_r| = 0$, domestic transactions do not transit through port infrastructure.

when making sourcing–routing decisions. I formalize this idea with the following parametrization of bilateral and port-level transportation frictions:

$$d_{nn'}^{-\xi} = \kappa_d \cdot \epsilon_{nn'}^{\lambda_1} \quad , \quad \bar{t}_p^{-\xi} = \kappa_p \cdot \Xi_p^{\lambda_2} \cdot K_p^{\lambda_3} \cdot \frac{\psi_p}{\psi_p + \xi}, \tag{19}$$

where λ_1 is the elasticity of link-level costs to distance, λ_2 is the elasticity of port-level costs to port traffic, and λ_3 is the elasticity of port-level costs to port capacity. The shifters $\kappa_d > 0$ and $\kappa_p > 0$ scale the resistance matrix Δ: κ_d sets the baseline cost of shipping across a link of given distance, and κ_p sets the baseline cost of transiting through a port of given capacity, traffic and climate.[47] In the empirical parametrization of Sections 4–6, the Pareto climate term $\psi_p/(\psi_p + \xi)$ is replaced by a reduced-form power function of observed wind speed (Equation 21).

Closing the model. Appendix D.2 completes the description of the model environment. The model closes with a goods market–clearing condition, which requires that trade in intermediate inputs be balanced.

Equilibrium. The economy is characterized by a set of parameters $\{\sigma, \alpha, \xi, \lambda_1, \lambda_2, \lambda_3\}$, a geography $\mathcal{G} = \{\mathcal{N}, \mathcal{P}, \mathcal{L}, \mathcal{M}, \mathcal{A}, \mathcal{D}, \mathcal{K}, \Psi\}$, and a distribution of wages and factory-gate prices $\{w_n, \bar{c}_n\}_{n \in \mathcal{N}}$, such that markets clear and the transportation network is in equilibrium. Appendix D.3 formally defines the general equilibrium of the model with traffic congestion and provides the system of equations that characterize it. The model admits an exact-hat-algebra formulation, described in Appendix F.3, which I use to solve for counterfactual equilibria, using the algorithm described in Appendix F.4.

Welfare. The welfare outcome used throughout the quantitative analysis in Section 6 is region-level real income, which admits a closed-form expression in the primitives of the model.

PROPOSITION 2. *Region-level welfare in this economy, measured as real income, is given by*

$$V_n = L_n w_n \left[a_n w_n^{\alpha - 1} \left(\sum_{n'} a_{n'} \bar{c}_{n'}^{-\xi} \tau_{n'n}^{-\xi} \right)^{\frac{\alpha}{\xi}} \right]^{\sigma - 1} \Gamma \left(1 - \frac{\alpha(\sigma - 1)}{\xi} \right). \tag{20}$$

Proof. See Appendix D.1.

[47] From Proposition 1, Assumption 2, and the definition of port-level trade costs in Equation (9), $\bar{t}_p^{-\xi} = t(\Xi, K_p)^{-\xi} \frac{\psi_p}{\psi_p + \xi}$. I parametrize $t(\Xi, K_p)^{-\xi} = \kappa_p \Xi_p^{\lambda_2} K_p^{\lambda_3}$.

The welfare expression combines three forces: wages earned from inelastic labor supply, a region-specific market access term $\sum_{n'} a_{n'}\bar{c}_{n'}^{-\xi}\tau_{n'n}^{-\xi}$ that aggregates the factory-gate costs of all potential suppliers weighted by their bilateral transportation costs, and the local productivity shifter a_n. Both the wage term and the market access term are endogenous to the transportation network, and therefore respond to any shock on port-level trade costs. In exact-hat-algebra counterfactuals the local productivity shifter a_n drops out of the ratio $\hat{V}_n$, so only the endogenous responses of $\{w_n, \bar{c}_n, \tau_{n'n}\}$ drive the welfare change.

4 Reduced-form evidence on trade-cost determinants

Before closing the model globally, I illustrate the three trade-cost channels the model emphasises – port traffic, port capacity, and cyclone risk – on the Brazilian bill-of-lading data of Section 2. The regression of this section is motivating rather than identifying: the Brazil-only sample limits external validity, and I do not map its estimates back into the global calibration.

Before presenting the estimation, I specify the reduced-form link between the model's climate channel and observed data. In taking the Pareto climate term of Equation (19) to the data, I replace $\psi_p/(\psi_p + \xi)$ with a power function of observed wind speed:

$$\bar{t}_p^{-\xi} = \kappa_p \cdot \Xi_p^{\lambda_2} \cdot K_p^{\lambda_3} \cdot (1 + CycloneRisk_p)^{\lambda_w}, \tag{21}$$

where $CycloneRisk_p$ is the expected annual wind speed (m/s) within 50 km of port p constructed from the STORM tropical-cyclone hazard model (Appendix B.4), and $\lambda_w \leq 0$ is the climate elasticity of port-level trade costs. This parametrization preserves the theoretical role of the Pareto term – higher cyclone exposure raises port costs – while allowing the climate channel to be estimated directly from observed wind-speed variation. Sections 4–6 and the appendices use this form throughout.

4.1 Data

This subsection introduces the data entering the reduced-form regression of Section 4.2. Construction details and summary statistics are delegated to Appendix E.1.

Brazilian bills of lading. I use the S&P Panjiva bills of lading for maritime imports entering Brazil to build a route-month panel at the supplier-country $\times$ port-of-lading $\times$ port-of-unlading level. I start from the same raw dataset as Section 2 (Appendix B.1) but apply a substantially different sample-construction procedure: I keep only shipments whose ports of lading and unlading can both be matched to a PortWatch identifier, I drop the establishment-level geolocalisation used in Section 2, and I restrict the sample to 2019–2023 to align with the PortWatch traffic series. Shipments are then aggregated at the route-month level.[48] The full procedure is documented in Appendix E.1.

Global port traffic and capacity. I use the IMF PortWatch daily port-activity series (2019–2023) to measure port traffic and port capacity at the port of lading. Monthly port traffic is the monthly sum of daily port-level TEU throughput; port capacity is the time-invariant 99$^{\text{th}}$ percentile of daily TEU over the sample. The raw series and the PortWatch–Panjiva port crosswalk are described in Appendix B.2.

Tropical cyclone climate. Cyclone risk at each port is measured using the STORM tropical-cyclone hazard dataset (Bloemendaal et al., 2020a,b), which simulates 10,000 years of synthetic storm tracks to estimate wind hazards at approximately 10 km resolution. STORM provides gridded return-period rasters of maximum sustained wind speed (m/s) for a present-day climate (1980–2015) and a future climate consistent with Representative Concentration Pathway 8.5 (RCP8.5) / Shared Socioeconomic Pathway 5 (SSP5) (2015–2050), the latter based on the mean of four climate model simulations. For each scenario, I compute expected annual wind speed by weighting the return-period rasters by their annual probability, and extract the port-level mean within a 50km buffer around each port (Figure B.1a). The baseline and RCP8.5 expected wind speeds serve as port fundamentals in both the estimation of transportation costs (Section 4.2) and the climate-change counterfactuals (Section 6.1). Appendix B.4 provides full construction details.

Instruments for port traffic and capacity. The 2SLS specifications instrument port traffic with adjusted global container throughput interacted with each port's 1950 coastal-population share (from the HYDE 3.3 historical gridded population within a 100km

[48] Unlike the Section 2 cleaning pipeline, which drops non-vessel-operating carriers and freight forwarders to retain only real cargo owners, here I keep both forwarders and real cargo owners. The route-month aggregation does not require identifying the underlying buyer, and retaining forwarder shipments improves coverage of the route panel.

buffer; Appendix B.5), and port capacity with the mean Terrain Ruggedness Index within a 20km buffer of each port (Appendix B.5).

4.2 Empirical strategy and results

I run a reduced-form analogue of the route-level bilateral trade share derived in Corollary 1 to document how route-level trade responds to port traffic, port capacity, and cyclone risk:

$$\begin{aligned}\log(\pi^{volume}_{n_d,r,t}) &= \alpha_{n_o,t} + \alpha_{n_d,t} + \alpha_{p_d,t} + \alpha_1 \log(Distance_r) + \alpha_2 \log(\Xi^{TEU}_{p_o,t}) \\ &\quad + \alpha_3 \log(K^{TEU}_{p_o}) + \alpha_4 \log(1 + CycloneRisk_{p_o}) + \varepsilon_{n_d,r,t}.\end{aligned} \tag{22}$$

The left-hand side $\pi^{volume}_{n_d,r,t}$ is the monthly share of shipment volume (TEU) that destination n_d sources through route r, constructed from the route-month Panjiva panel of Section 4.1 (Appendix E.1).[49] Routes are approximated as the quadruplet $\{n_o, n_d, p_o, p_d\}$, where p_o and p_d are the ports of origin and destination. Route distance is the least-cost land–sea distance from supplier origin to buyer destination passing through p_o and p_d. Port traffic is the monthly total TEU transiting through p_o; port capacity is the 99$^{\text{th}}$ percentile of daily TEU at p_o over 2019–2023. Cyclone risk is the STORM baseline expected wind speed within a 50km buffer of p_o.[50] Supplier-country-by-month and port-of-destination-by-month fixed effects absorb the general-equilibrium origin and destination terms in Equation (13).

Regressing route-level bilateral trade shares on port traffic and port capacity is vulnerable to simultaneity: both regressors are equilibrium-derived outcomes in the market for port throughput, so unobserved shocks that shift demand or supply curves also enter the error term. I address these endogeneity concerns by estimating Equation (22) with two-stage least squares (2SLS) and two orthogonal curve-shifters. Port traffic is instrumented with global container throughput interacted with each port's 1950 coastal-population share – a predetermined demand shifter that scales worldwide traffic variations across ports while leaving local handling costs unchanged. Capacity is

[49] I use volume rather than value as the main outcome because the volume field offers the highest coverage in the raw Panjiva data, with 70.9% of raw shipment volume retained in the route-month aggregation, against 65.6% for value, 42.6% for weight, and 76.2% for the count of shipments. Estimates obtained on the alternative outcome definitions are reported in Appendix Table E.1.

[50] In the data, $CycloneRisk_p$ is the baseline expected wind speed within 50km of port p (in m/s; Appendix B.4); I enter it in logs as $\log(1 + CycloneRisk_p)$ to accommodate ports with no baseline cyclone activity. Under the parametrization of Equation (21), α_4 is the reduced-form analogue of $-\lambda_w/\xi$.

Table 1: Estimation of transportation costs

	$\pi^{volume}_{n_d,r,t}$	
	(1)	(2)
Log Port Origin Traffic	0.55	-1.79
	(0.02)	(0.14)
Log Port Origin Capacity	-0.47	2.24
	(0.03)	(0.17)
Log Distance (sea)	-0.39	-0.09
	(0.01)	(0.02)
Log Distance (land)	-0.93	-0.89
	(0.01)	(0.01)
Log Cyclone Risk	0.05	-0.02
	(0.01)	(0.01)
Observations	98,039	98,039
Adjusted R^2	0.30	0.21
Wald-F, Log Port Origin Traffic		14,116.91
Wald-F, Log Port Origin Capacity		14,260.68
n_o-month fixed effects	✓	✓
p_d-month fixed effects	✓	✓

Notes: This table presents the results of the estimation of transportation costs, as specified by Equation 22. The outcome is the log monthly share of shipment volume (TEU) that destination location n_d (Brazil) sources through route r. Port Origin Traffic refers to monthly estimates of total TEU volumes transiting through ports of origin of shipments. Port Origin Capacity refers to the 99^{th} percentile of daily TEU volume at ports. Distance refers to the total route distance (over land or sea). Cyclone Risk refers to the expected windspeed at ports, as reported in the STORM data. Column (1) reports the OLS estimation, while Column (2) reports the 2SLS estimation. Robust standard errors are clustered at the $\{n_o, p_o, p_d\}$-month level.

instrumented with mean terrain ruggedness within 20km of the port, a geologic supply determinant that raises inland evacuation costs and therefore limits optimal port capacity, while remaining exogenous to current trade flows. Appendix E.1 details the construction of the instruments.

Table 1 reports the results. Conditional on port capacity, a 1% increase in port traffic reduces route-level bilateral trade shares by 1.79%. Assuming a trade elasticity of $\xi = 8$ (Allen and Arkolakis, 2022), this implies a 0.22% increase in port-level trade costs.[51] Conversely, a 1% increase in port capacity decreases port-level trade costs by 0.28%, indicating the presence of scale economies.[52] Furthermore, a 1% increase in

[51]By comparison, Allen and Arkolakis (2022) find an elasticity of traffic flow (per lane) with respect to transportation cost of 0.09 in the US highway system.

[52]Given the high observed correlation between port-level traffic and capacity, this finding is consistent with Ganapati et al. (2024), who document scale economies in the maritime network, although they do not disentangle traffic from capacity.

cyclone risk lowers route-level bilateral trade shares by 0.02% – corresponding to approximately 0.003% increase in transportation costs. The three estimated channels line up with the signs the theory predicts. These Brazil-sample magnitudes are reported for illustration and are not carried into the global calibration of Section 5.3, which recovers the transportation-cost elasticities from a global port-traffic moment. I return to the theoretical and literature-based justification for the sign restrictions imposed on that calibration in Section 5.3.

5 Bringing the model to the data

The counterfactual exercises of Section 6 require a version of the model of Section 3 that reproduces the early-twenty-first-century global economy. This section describes how I close the model to the data. Because the counterfactuals are solved in exact hat algebra (Section 6.1), the vector of fundamental productivities $\{a_n\}$ need not be recovered: the calibration only has to pin down the objects that enter the equilibrium system in relative changes.

The remaining model objects come in three groups, each handled differently. The three deep elasticities of the theory – the final-goods substitution σ, the intermediate-input share α, and the trade elasticity ξ – are taken from the literature: they are well-identified in adjacent work on trade and production networks, and these elasticities cannot be identified from the single port-traffic moment the internal calibration targets. The data inputs – countries, ports, distances, bilateral trade shares, population, wages, port capacity, and port-level wind-speed exposure – are built from raw sources (Section 5.1) and restricted to a tractable geographic sample (Section 5.2). The remaining transportation-cost parameters $\{\kappa_d, \kappa_p, \lambda_1, \lambda_2, \lambda_3, \lambda_w\}$ are recovered by an internal calibration that targets observed port traffic (Section 5.3).

5.1 Data

Appendix F.1 provides comprehensive construction details and summary statistics for all data sources used in the calibration.

Countries and ports. The geographic backbone is the set of Natural Earth admin-0 polygons (10-scale, ISO3 code), which provide a stable national partition of the globe and centroid coordinates for every country. Ports are drawn from the 1,666 locations of the IMF PortWatch daily-activity series and matched to admin-0 polygons by their PortWatch ISO3 field. Together, admin-0 polygons and PortWatch ports define the nodes of the model's transportation graph. Construction details are in Appendix F.1.1.

Land and sea distances. Transportation costs in the model scale with distances on three types of links: country-to-country (land), port-to-country (land), and port-to-port (sea). I measure country-to-country distances as great-circle distances between admin-0 centroids, masked so that only first-order polygon neighbours are connected. Port-to-country distances are great-circle distances from each port to every country centroid, retained only for ports that lie inside the country. Port-to-port sea distances come from the Eurostat `SeaRoute` shortest-path program, which returns the shortest maritime path between any two ports in the PortWatch set. The three blocks stack into the economy-wide distance matrix D of size $(|\mathcal{N}| + |\mathcal{P}|) \times (|\mathcal{N}| + |\mathcal{P}|)$. Appendix B.5 provides details.

Vessel voyages and network sparsification. The `SeaRoute` program returns a shortest-path distance for every ordered pair of PortWatch ports, but the overwhelming majority of those pairs carry no actual vessel traffic. I therefore use empirical transit probabilities built from Global Fishing Watch 2017 AIS vessel voyages (Kroodsma et al., 2018; Global Fishing Watch, 2024) to sparsify the port-to-port block: at each origin port, I keep the smallest set of destinations whose cumulative transit probability reaches 0.90, cap the in-degree at 2,000 links, and trim the remaining sea distances at the 95$^{\text{th}}$ percentile (Appendix B.5).[53]

Bilateral trade flows. Bilateral trade flows $X_{nn'}$ between countries come from the International Trade and Production Database for Estimation (ITPD-E), release 1.1 (Borchert et al., 2022). I use the 2019 cross-section, which reports bilateral trade values in millions of current US dollars, and aggregate across all sectors within each ordered country pair, $X_{nn'} = \sum_s X^s_{nn'}$. Bilateral trade shares are recovered by column normalization, $\pi_{nn'} = X_{nn'} / \sum_{\tilde{n}} X_{\tilde{n}n'}$. These shares are the π matrix used throughout the calibration. Appendix F.1.1 documents the aggregation procedure.

[53]Sparsification is needed for two reasons. First, a dense matrix with an entry for every pair of ports assigns positive resistance to routes that are never used in practice, which biases the model's routing probabilities towards commercially irrelevant corridors. Second, the resulting resistance matrix has to stay inside a feasibility region for the fixed-point algorithm that solves the model's equilibrium; the cut-offs above are rule-based rather than sample-outcome-based, and are chosen so that the feasibility condition holds comfortably throughout the calibration.

Population and GDP per capita. The model requires country population L_n and an empirical counterpart of country wages. I build both from the 1° gridded estimates of Rossi-Hansberg and Zhang (2025), averaged over 2012–2020 and aggregated to admin-0 polygons – summing grid cells for population and taking the area-weighted mean for GDP per capita. Population enters the model directly; GDP per capita serves as the starting point for the balanced-trade wage vector recovered in Section 5.3. Appendix B.5 describes the gridded source.

Port capacity and climate exposure. Finally, each port carries three port-specific inputs. Port capacity K_p is the 99^{th} percentile of daily PortWatch TEU (imports + exports) over 2019–2023, a short-run throughput ceiling observable in the data. Observed port traffic Ξ_p^{data} – the calibration target moment of Section 5.3 – is the yearly total TEU at each port averaged over the same period. Port-level cyclone exposure $CycloneRisk_p$ is the STORM baseline expected wind speed within a 50 km buffer of each port (Appendix B.4), and its RCP8.5 counterpart supplies the climate shock used in the counterfactuals of Section 6. Port-level PortWatch series are described in Appendix B.2; the STORM climate construction is in Appendix B.4.

5.2 Geography sample

Although the theory of Section 3 admits sub-national regions, I close the model at the country level: each admin-0 polygon is one region, and its ports are modelled as distinct nodes attached to that region. Not all of the raw data can be plugged directly into the model. Some countries and ports have no measured economic activity and would introduce either degenerate shares or noise; more importantly, the algorithm that solves the baseline equilibrium requires that every country be reachable from every other country through some sequence of land and sea legs, so the location graph must be topologically connected. I apply three filters in sequence, from the coarsest to the tightest.

Active locations. I first drop countries with zero population or zero GDP per capita in the Rossi-Hansberg and Zhang (2025) raster, countries absent from the ITPD-E trade matrix (for which the trade-share row is empty), and PortWatch ports whose 99^{th}-percentile daily TEU is zero. These three filters remove a thin tail in each dimension.

Top-of-traffic coverage. I then keep only the ports whose cumulative share of 2019–

2023 total TEU reaches 95%, starting from the largest. This step is motivated purely by tractability: the long tail of very small ports inflates the dimension of the model's resistance matrix without contributing meaningfully to the calibration target or to bilateral trade volumes.

Largest connected component. Finally, I restrict the sample to the largest connected component of the resulting location graph, which drops a handful of isolated island countries and stranded ports. The three filters jointly leave $N = 150$ countries and $P = 502$ ports. This subsample accounts for approximately 80.5% of global port traffic in TEU volume and 70.2% of global port calls over 2019–2023 (Figure F.1).

5.3 Calibration

With the final sample in hand, I now recover the parameters the model needs to reproduce the baseline equilibrium. Three deep elasticities are fixed to values from the literature, country wages are adjusted so that the ITPD-E trade-share matrix satisfies the model's balanced-trade identity, and the transportation-cost parameters are recovered internally by targeting observed port traffic. The full algorithm is laid out in Appendix F.2.

Literature parameters. I set $\sigma = 2$ following Castro-Vincenzi (2024), $\alpha = 0.8$ following Balboni et al. (2024), and $\xi = 8$ following Allen and Arkolakis (2022). Because the internal calibration below targets a single moment per port, these elasticities cannot be identified separately within the model; taking them from adjacent work on trade and production networks frees the degrees of freedom available to the transportation-cost parameters.

Balanced-trade wages. The GDP-per-capita vector I build from Rossi–Hansberg is not, in general, consistent with the ITPD-E trade-share matrix π: ITPD-E records non-zero trade deficits, while the model is static and assumes balanced trade. I therefore recover a wage vector w that satisfies the balanced-trade identity $wL = \pi^\top wL$ on the final N-country sample, as the left eigenvector of π associated with eigenvalue 1.[54] The resulting vector deviates from ITPD-E production by 25.7% on average (production-weighted), reflecting the size of ITPD-E trade imbalances, and is the w vector used in

[54] I obtain it by iterating the Picard map $wL^{\text{new}} = \pi^\top wL^{\text{old}}$ from the ITPD-E production vector $Y_n = \sum_{n'} X_{nn'}$ as starting point, and pin down the scale by rescaling $\sum_n w_n L_n$ to match total ITPD-E production.

everything that follows.

Transportation-cost parameters. The parameters $\{\kappa_d, \kappa_p, \lambda_1^{\text{land}}, \lambda_1^{\text{sea}}, \lambda_2, \lambda_3, \lambda_w\}$ of the empirical transportation-cost parametrization (Equation 21) govern how transportation costs in the model scale with distance, port traffic, port capacity, and wind-speed exposure.[55] I recover them by requiring that the model-implied distribution of port traffic match its empirical counterpart as closely as possible. Formally, I minimize the mean squared log deviation

$$\mathcal{L}(\theta) = \frac{1}{|\mathcal{P}|} \sum_{p \in \mathcal{P}} \left[\log \tilde{\Xi}_p^{\text{eq}}(\theta) - \log \tilde{\Xi}_p^{\text{data}} \right]^2, \tag{23}$$

where $\tilde{\Xi}_p^{\text{eq}}(\theta)$ and $\tilde{\Xi}_p^{\text{data}}$ are the model-implied and observed port traffic, each normalized by their cross-port mean so that the absolute scale is not separately identified from κ_p. Because the objective is non-convex, I first run a coarse grid search over the parameter space and then refine the best point by local optimization.

The calibration imposes three sign restrictions on the transportation-cost elasticities: $\lambda_2 \leq 0$ (port traffic raises costs), $\lambda_3 \geq 0$ (port capacity reduces costs), and $\lambda_w \leq 0$ (higher baseline expected wind speed raises costs). Each follows from the model's microfoundation and from independent evidence outside this paper. The traffic restriction $\lambda_2 \leq 0$ is the congestion externality of Allen and Arkolakis (2022) and the multimodal routing model of Fuchs and Wong (2024), in which traffic raises the marginal cost of using a link and firms do not internalise the externality. The capacity restriction $\lambda_3 \geq 0$ is the scale-economies channel of Ganapati et al. (2024), which attributes unit-cost declines at larger maritime hubs to port and vessel size. The wind-speed restriction $\lambda_w \leq 0$ follows from the causal effects of tropical-cyclone disruptions on port throughput documented in Section 2. The reduced-form estimates of Section 4 are consistent with all three restrictions.

Calibrated values and fit. Table 2 reports the calibrated values. At the optimum, the model-implied port traffic correlates $\rho = 0.58$ with the targeted moment (Appendix Figure F.2). Because port traffic is the calibration target, this correlation is a goodness-of-fit diagnostic rather than external validation: it confirms that the solver roughly

[55] I split the distance elasticity λ_1 into a land component λ_1^{land} and a sea component λ_1^{sea}, applied respectively to the country–country and port–port blocks of the distance matrix: land and sea transport have sufficiently different cost structures that forcing a single elasticity on the two would noticeably worsen the calibration fit.

Table 2: Calibration of parameters and data inputs

	Description	Source / Procedure
Panel A: Parameters from the literature		
$\sigma = 2$	Final-goods CES	Castro-Vincenzi (2024)
$\alpha = 0.8$	Intermediate-input share	Balboni et al. (2024)
$\xi = 8$	Trade elasticity	Allen and Arkolakis (2022)
Panel B: Internally calibrated parameters		
$\kappa_d = 0.286$	Distance cost shifter	Appendix F.2
$\kappa_p = 1.046$	Port cost shifter	Appendix F.2
$\lambda_1^{\text{land}} = -0.26$	Distance elasticity, land legs	Appendix F.2
$\lambda_1^{\text{sea}} = -0.11$	Distance elasticity, sea legs	Appendix F.2
$\lambda_2 = -0.42$	Traffic elasticity	Appendix F.2
$\lambda_3 = 1.37$	Capacity elasticity	Appendix F.2
$\lambda_w = -0.03$	Wind-speed elasticity	Appendix F.2
Panel C: Data inputs		
$\mathcal{N}$	150 countries	Natural Earth admin-0; 5.2
$\mathcal{P}$	502 ports	IMF PortWatch; 5.2
L	Country population	Rossi-Hansberg and Zhang (2025); 5.1
w	Country wages	Balanced-trade fixed point; 5.3
π	Bilateral trade shares	ITPD-E 2019 (Borchert et al., 2022); 5.1
D	Distance matrix	Eurostat SeaRoute & great-circle; 5.1
K	Port capacity	IMF PortWatch; 5.1
$CycloneRisk$	Port-level climate	STORM baseline; 5.1

reproduces the cross-port dispersion in traffic given the free parameters of Panel B of Table 2. The exact-hat-algebra pipeline has the further property that the baseline equilibrium reproduces observed bilateral trade shares π and country wage bills wL by construction, so no separate untargeted fit is reported here.

6 Quantitative results

This section quantifies how climate change at ports propagates through global supply chains under an unmitigated emissions scenario (RCP8.5), and the mitigating role of two adaptation margins built into the model: firms rerouting trade through less exposed ports, and the endogenous response of port-level trade costs to traffic. I first describe how the counterfactual is computed (Section 6.1), present the baseline RCP8.5 equilibrium and its cross-region heterogeneity (Section 6.2), and isolate the contribution of each adaptation channel through a pair of restricted counterfactuals (Section 6.3). Throughout this section port capacities K_p are held at their baseline calibrated values; the investigation of the role of port capacity under the climate shock is taken up in Section 7.

6.1 Counterfactual methodology

I solve for counterfactual equilibria in exact hat algebra, following Dekle et al. (2007, 2008) and Caliendo and Parro (2015). Writing the general-equilibrium system of Section 3 in relative changes ($\hat{x} \equiv x'/x$), the counterfactual equilibrium is characterized entirely by objects that are observable or calibrated at baseline – the wage bill $\{w_n L_n\}$, the bilateral trade-share matrix $\{\pi_{nn'}\}$, the port-traffic vector $\{\Xi_p\}$, the resistance matrix $\mathbf{\Delta}$ that encodes the transportation network, and the structural elasticities. Given these inputs and the exogenous port-level wind-speed shock, I solve for the counterfactual vectors of wages $\{\hat{w}_n\}$, factory-gate costs $\{\hat{c}_n^{-\xi}\}$, and port traffic $\{\hat{\Xi}_p\}$ as a fixed point. Regional welfare changes $\{\hat{V}_n\}$ then follow in closed form.

The exact hat algebra of this model departs from the standard Dekle et al. (2007) template in two respects. First, port-level trade costs are endogenous: they respond to traffic through the congestion elasticity λ_2, and traffic in turn depends on bilateral trade flows, which depend on bilateral costs. This circularity creates an additional fixed-point layer in which the algorithm must iterate jointly on the traffic vector and the resistance matrix. Second, bilateral trade costs $\tau_{nn'}^{-\xi}$ are aggregated from port-level costs through the resistance matrix $\mathbf{\Delta}$, a nonlinear aggregation that does not admit a hatted representation: computing $\hat{\tau}_{nn'}^{-\xi}$ requires reconstructing the counterfactual resistance matrix in levels rather than expressing it as a function of other hatted variables. The full derivation of the hatted system is detailed in Appendix F.3, and the numerical algorithm in Appendix F.4.

The climate shock. The exogenous shock is the change in expected wind speed at each port implied by the STORM climate-model ensemble under RCP8.5 relative to the baseline climate. Structurally, the climate component of port-level trade costs enters through the windspeed parametrization of Equation (21), where $\lambda_w < 0$ is the calibrated climate elasticity (Table 2). The RCP8.5 wind-speed field therefore translates directly into a vector of port-cost shifters. Figure 7 maps the global change in expected wind speed from tropical cyclones across the two climates. The raw baseline and RCP8.5 fields are reported in Appendix B.4, Figures B.1a and B.1b.

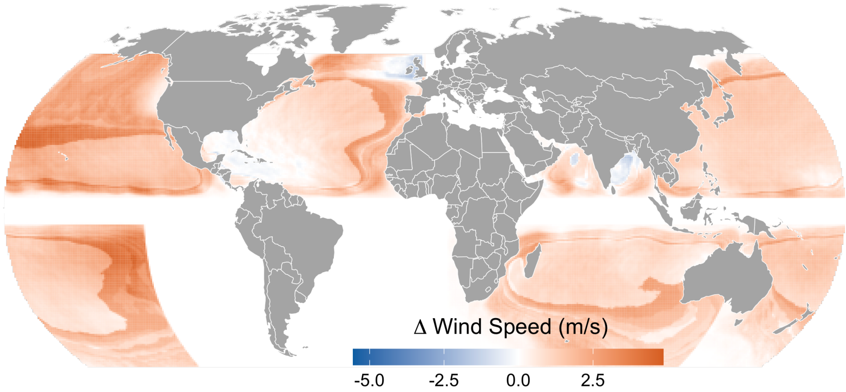

Figure 7: Δ Tropical Cyclone Wind Speed (RCP8.5)

Notes: The map shows the change in expected wind speed induced by tropical cyclones, comparing the present-day scenario (1980–2015) with the RCP8.5 future scenario (2015–2050). Estimates are based on 10,000 years of synthetic storm tracks from the STORM model, with wind speeds weighted by the inverse of their return periods. Figures B.1a and B.1b in Appendix B.4 report the raw data.

6.2 Baseline RCP8.5 results

I first report the full-model RCP8.5 counterfactual, in which firms reroute optimally and port-level trade costs respond endogenously to traffic. Throughout, aggregate welfare is the GDP-weighted mean of regional welfare changes $\hat{V}_n - 1$, and aggregate port traffic is the total-traffic-weighted mean of port-level changes in $\hat{\Xi}_p - 1$. Under this counterfactual, aggregate welfare changes by approximately -0.01%, and aggregate port traffic by -0.50%. Figure 8 maps both outcomes. At the 5$^{\text{th}}$ percentile of the regional welfare distribution, welfare falls by about 0.11%; at the 95$^{\text{th}}$ percentile, welfare is virtually unchanged. Port traffic is similarly dispersed: the 5$^{\text{th}}$ percentile port loses 1.45% of its traffic, while the 95$^{\text{th}}$ percentile port gains 0.18%.

These aggregate magnitudes are small in absolute terms, and deserve to be read in context. Three observations place them. First, the input shock is itself modest at most ports. Across the 502 calibration ports, the mean change in expected wind speed between baseline and RCP8.5 is 0.53 m/s and the median is 0.14 m/s, with 59.6% of ports seeing an increase in expected windspeed and a 95$^{\text{th}}$-percentile shift of 1.70 m/s against a maximum of 2.99 m/s (Figure 7). The bulk of world trade flows through ports outside the tropical-cyclone belt and is unaffected at first order; the shock is concentrated on a minority of exposed hubs rather than spread uniformly across the network. Second, the translation from wind-speed shift to port costs is dampened by the small calibrated λ_w: conditional on port traffic, port-level trade costs rise by 0.58%

on average (median 0.40%). Bilateral trade shares respond smoothly to perturbations of this scale, and most importing countries can substitute along the sourcing-routing margin.

Third, the resulting magnitudes are consistent with the range that the closest quantitative literature reports for marginal cost-wedge perturbations of spatial-network models. These exercises typically consider infrastructure improvements rather than climate shocks, but the perturbation enters the equilibrium system in the same way – a marginal shift in link- or node-level trade costs – so the welfare responses they characterize provide a natural benchmark. Closest in setting, Ganapati et al. (2024) study the global container-shipping network with endogenous routing through entrepôt hubs: a 1% transport-cost reduction at one country generates global welfare gains ranging from less than 1 to about 8 basis points depending on the country's centrality in the network, and their non-marginal counterfactuals (a 5% Brexit trade-cost increase, the opening of the Arctic passage) produce aggregate welfare effects of -9.2 and $+6.4$ basis points, respectively. Closer to this section's congestion-at-nodes mechanism, Fuchs and Wong (2024) find that a 1% transshipment-cost reduction at each of 228 U.S. intermodal terminals raises real GDP by 0.002–0.020% per terminal; larger effects (a welfare loss of roughly 1.4%) arise only under the extreme counterfactual of removing rail-network access entirely. Allen and Arkolakis (2022) evaluate link-level 1% iceberg-cost reductions on the U.S. Interstate Highway System and report per-link welfare elasticities ranging from 0.00005 to 0.003. The RCP8.5 wind-speed shift is itself a marginal perturbation of the port cost structure, and the aggregate magnitudes reported here (aggregate welfare of -0.01% and a 5^{th}-percentile regional loss of 0.11%) are of a comparable order of magnitude. These results capture the welfare cost of the specific channels the model admits – port-level trade costs, congestion, and routing – under a permanent shift in port-level wind exposure. They do not claim to bound the full economic cost of climate change: the model holds fixed all other margins through which weather affects the economy, including direct damages to firms and households.

The losses in Panel (a) of Figure 8 are unevenly distributed, and the largest of them concentrate not in regions that host climate-exposed ports themselves, but in regions whose imports flow disproportionately *through* such ports. To make this point precise,

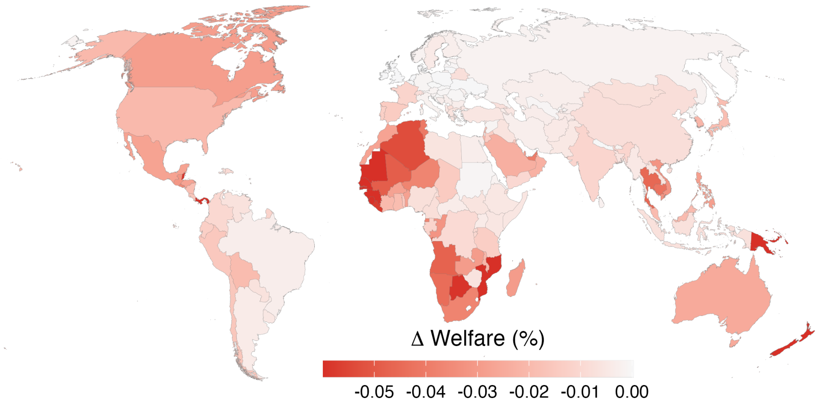

(a) Δ Welfare (%)

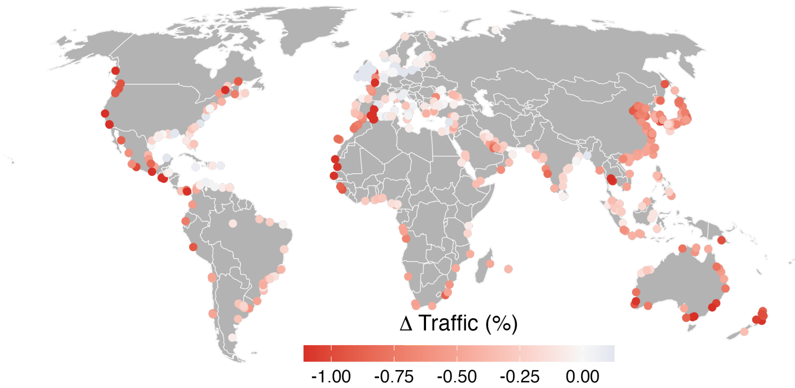

(b) Δ Port traffic (%)

Figure 8: Regional welfare and port traffic – RCP8.5 counterfactual

Notes: Panel (a) reports the percentage change in region-level welfare (real income, Proposition 2) between the calibrated baseline and the full-model RCP8.5 counterfactual, in which firms reroute optimally and port-level trade costs respond endogenously to traffic. Panel (b) reports the percentage change in port-level traffic over the same two equilibria. Color scales are truncated at the 5$^{\text{th}}$ and 95$^{\text{th}}$ percentiles. The restricted-scenario counterparts (fixed routing and fixed congestion) are reported in Appendix F.5.

let s_{np} denote the share of region n's imports that transits port p – obtained by aggregating port-passage probabilities from the Leontief inverse of the resistance matrix over origins, weighted by baseline bilateral trade shares – with superscripts (0) and (1) for baseline and RCP8.5 values of $CycloneRisk_p$ respectively. Region n's import-weighted exposure to port climate $E_n = \sum_p s_{np}\, CycloneRisk_p$ admits the additive decomposition

$$E_n^{(1)} - E_n^{(0)} = \underbrace{\sum_p s_{np}^{(0)} \left(CycloneRisk_p^{(1)} - CycloneRisk_p^{(0)}\right)}_{\text{climate component}} + \underbrace{\sum_p \left(s_{np}^{(1)} - s_{np}^{(0)}\right) CycloneRisk_p^{(1)}}_{\text{rerouting component}}. \tag{24}$$

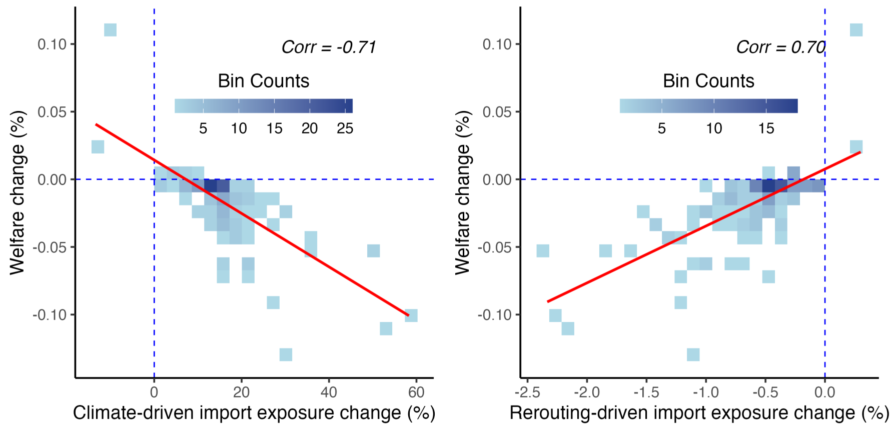

Figure 9: Regional welfare and import exposure to climate-affected ports

Notes: The figure relates the regional welfare change under the full-model RCP8.5 counterfactual to two components of the change in the region's port-climate import exposure. The climate component (left panel) holds baseline routing fixed and moves only the wind-speed field. The rerouting component (right panel) holds the counterfactual wind-speed field fixed and moves only the routing shares. Each panel is a 2D histogram with the fitted OLS line and correlation overlaid.

Equation (24) decomposes this change into two terms: the first holds routing fixed at its baseline values and moves only the wind-speed field; the second holds the wind-speed field fixed at its counterfactual values and moves only the routing shares. Both are normalised by $E_n^{(0)}$ to obtain percentage contributions. Figure 9 plots the regional welfare change against each component.

Welfare losses line up tightly with the climate component (correlation -0.71): regions for which a larger fraction of imports now passes through more cyclone-exposed ports suffer proportionally larger welfare losses, with climate-driven exposure changes that reach up to 60% of baseline import exposure for the hardest-hit regions. The rerouting component is nearly as strongly correlated with the welfare change (correlation $+0.70$), but operates on a much smaller scale: rerouting-driven exposure changes rarely exceed a few percent in absolute value. The positive sign reflects selection rather than a perverse effect of adaptation: the regions that reroute the most are precisely those whose baseline sourcing was most concentrated on the ports that the climate shock hits hardest, and they still absorb most of the welfare loss. Firms reroute just enough to shave a few percentage points off their exposure, leaving the bulk of the direct climate hit intact.

Spatially, the largest losses concentrate in sub-Saharan Africa and Southeast Asia, where baseline imports are routed through a small number of cyclone-exposed hubs;

parts of Northern Europe – where denser port networks provide alternative routes – are among the few regions that experience small welfare gains.

6.3 Congestion and Adaptation in General Equilibrium

The model comprises two endogenous channels mapping the exogenous wind-speed shift to trade costs that firms ultimately face. The first is behavioral: with trade elasticity ξ, firms reoptimize the port through which a given flow transits, reallocating trade towards less exposed ports as cyclone risk rises elsewhere. The second is an equilibrium price feedback: the port-level trade cost $\bar{t}_p$ responds to traffic through the elasticity λ_2, so that ports absorbing rerouted demand see their own costs rise while ports losing demand see theirs fall. Only the first channel is adaptation in the behavioral sense; the second is a congestion externality that firms do not internalize but that nonetheless reshapes trade costs in general equilibrium. Either channel can, in principle, amplify or dampen the direct effect of the shock. To isolate their contributions, I compare the full-model counterfactual to two nested restricted equilibria that successively suppress them.

In the *fixed-routing* counterfactual, the conditional probability $\Theta_{p|nn'}$ that a good travelling from n to n' transits through port p is held at its baseline value, so that bilateral trade flows continue to adjust to the shock through Equations (F.4)–(F.5), but the allocation of any given flow across ports is tied to the pre-shock transportation geography.[56] In the *fixed-congestion* counterfactual, the endogenous response of port-level trade costs to traffic is additionally suppressed: the resistance matrix is constructed once from the wind-speed shock alone, without any feedback from the induced reallocation of traffic.[57] The three equilibria form a nested decomposition: the fixed-congestion counterfactual isolates the direct trade-cost effect of the shock; the gap between the fixed-routing and fixed-congestion counterfactuals measures how much of that direct hit is absorbed by the endogenous response of port costs to traffic; and the gap between the full model and the fixed-routing counterfactual measures the addi-

[56]Formally, the conditional routing probabilities of Equation (17) are set to their baseline values, $\Theta_{p|nn'} = (\tau_{np}\tau_{pn'}/\tau_{nn'})^{-\xi}$ evaluated at $\{\tau_{nn'}\}$ rather than $\{\tau'_{nn'}\}$. This is implemented in the hatted system by replacing the counterfactual Leontief inverse $\mathbf{B}'$ with its baseline counterpart $\mathbf{B}$ in the traffic update of Equation (F.10), leaving all other equations of Appendix F.3 unchanged.

[57]Formally, the port-traffic ratio in Equation (F.7) is held at $\hat{\Xi}_p \equiv 1$ for every port, so that $\hat{\bar{t}}_p^{-\xi} = \left((1 + CycloneRisk'_p)/(1 + CycloneRisk_p)\right)^{\lambda_w}$. The counterfactual resistance matrix is then computed once from the wind-speed shock alone, and the outer fixed-point loop on traffic is bypassed.

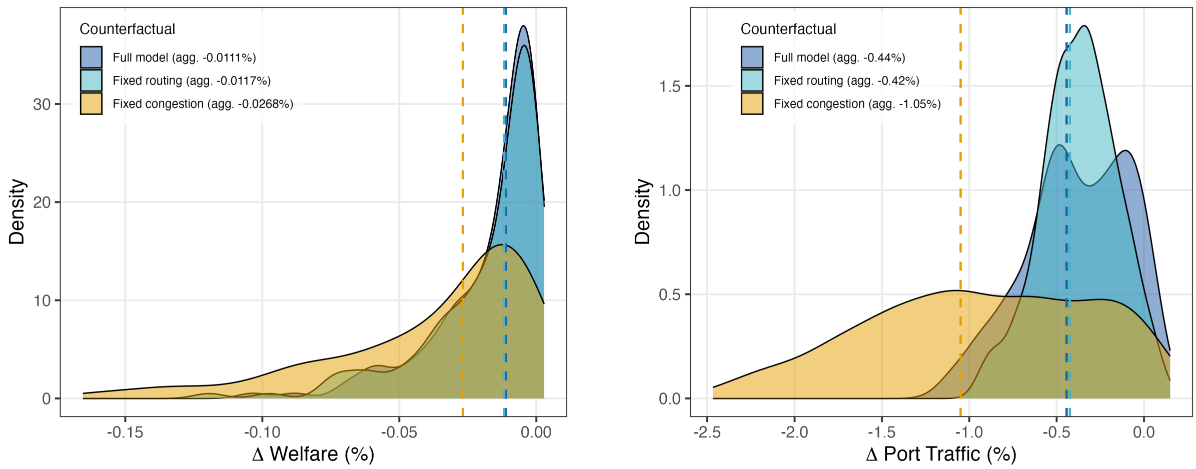

(a) Δ Welfare (%)

(b) Δ Port traffic (%)

Figure 10: Distribution of welfare and port traffic changes across the three counterfactuals

Notes: Overlaid kernel density estimates of regional welfare changes (panel a) and port traffic changes (panel b) under the full-model, fixed-routing, and fixed-congestion RCP8.5 counterfactuals. Vertical dashed lines mark the aggregate change for each scenario (GDP-weighted for welfare, total-traffic-weighted for port traffic), with the aggregate value reported in the legend. Tails are trimmed for readability. The corresponding maps and port-level scatters across the three scenarios are in Appendix F.5.

tional contribution of firm-level rerouting on top.

Figure 10 reports the three counterfactual distributions. The endogenous channels together dampen 74.3% of the direct welfare loss generated by the wind-speed shock.[58] The split between the two endogenous channels is, however, highly unbalanced: the congestion price feedback accounts for the bulk of the absorption, operating through the endogenous response of port costs to traffic even when routing shares are held at their baseline values, while firm-level rerouting contributes a residual that is economically negligible against the congestion channel. The ordering of the nested decomposition is itself a modelling choice – congestion is nested inside routing – and the two channels interact nonlinearly in the fixed point, so the reported split should be read as the contribution to absorption under this nesting, not as a clean orthogonal decomposition.

The congestion channel is a pecuniary externality that firms do not internalize. The wedge between private and social returns to port capacity is tied to the magnitude of

[58] In levels, the direct trade-cost effect alone yields an aggregate welfare loss of -0.06% (fixed-congestion counterfactual), against -0.01% in the full model. Of the 74.3% absorption, the congestion price feedback accounts for 73.3% of the direct loss (a contribution of $+0.04$ percentage points) and firm-level rerouting for 1.0% ($+0.0006$ pp).

the congestion feedback, which this section shows dominates the general-equilibrium response to climate change. The next section derives the welfare gain from marginal port-capacity investments and characterizes how the optimal allocation shifts under climate change.

7 Infrastructure policy

Evaluating infrastructure investment requires accounting for how private agents respond to the infrastructure itself. In transportation networks, firms reroute trade toward cheaper or less congested paths, and those routing responses generate congestion spillovers that reshape the welfare return to any single link or node (Allen and Arkolakis, 2022; Allen et al., 2025). When the infrastructure in question is long-lived and climate risk is spatially heterogeneous – as Section 6 documented for maritime ports – the problem acquires an additional dimension: a planner who ignores evolving climate exposure may direct investment to ports whose returns erode as the climate shifts (Balboni, 2025). This section asks two questions. First, what determines the welfare return to capacity expansion at a given port, and how do those returns vary across the global port network? Second, how much does the answer change once one accounts for the heterogeneous climate risk?

I develop an analytical framework, in the spirit of Allen et al. (2025), that delivers both objects – cross-port welfare returns and their climate sensitivity – in closed form. Rather than re-solving the general-equilibrium model introduced in Section 3 for port-by-port capacity improvements, I characterize the welfare elasticity to an increase in port capacity, $\partial \log V_n / \partial \log K_p$, expressed as the solution to a $(2N + P)$-dimensional linear system whose closed form makes the channel decomposition of the welfare gain transparent. The elasticity is computed under both the baseline and the RCP8.5 equilibria, and a closed-form channel decomposition identifies the general-equilibrium determinants of the welfare return to port capacity.

I then evaluate a concrete policy problem: The European Sea Ports Organisation reports that ports within the European Union (EU27) plan to commit approximately EUR 84 billion of capacity investment by 2034 (ESPO, 2024). How should this investment be distributed across EU27 ports, and how much does the answer change once one accounts for port-level climate risk? The framework is closed to data on EU27 port-investment pipelines and to an auxiliary first-stage estimation that translates dollars of investment into port capacity. The distributional content of both questions dominates the aggregate. A climate-blind allocation of EU27 port investment costs only 0.093 basis points of aggregate welfare relative to a climate-aware allocation, but at the country level the same myopia reshuffles welfare gains across the EU27.

7.1 A SOCIAL SAVINGS APPROACH TO PORT IMPROVEMENTS

This subsection develops the welfare-evaluation framework used throughout this section. Subsection 7.1.1 derives the sufficient-statistics characterization of the welfare elasticity to port-capacity expansions. Subsection 7.1.2 evaluates that elasticity at the calibration of Section 5 and decomposes the welfare return into its general-equilibrium determinants.

7.1.1 SUFFICIENT STATISTICS FOR PORT CAPACITY

I adopt a sufficient-statistics approach to recover the welfare elasticity of an arbitrary port-capacity expansion in closed form. The motivation is analytical: an explicit decomposition of the welfare gain into wage, factory-cost, and routing channels makes the underlying transmission mechanisms visible, in a way that a brute-force numerical sweep does not.[59] The label *social savings* echoes Fogel (1962), who priced the welfare contribution of U.S. railroads by computing the resource cost of next-best alternative routes in a partial-equilibrium accounting; the implementation here is closer to the modern general-equilibrium tradition of Allen et al. (2025), in which the welfare elasticity to a unit infrastructure improvement is recovered as a sufficient statistic over equilibrium primitives. The approach expresses the welfare elasticity to port capacity in terms of general equilibrium objects – trade shares, wage bills, and the routing kernel of Section 3 – and therefore recovers first-order welfare changes through a single linear solve, accounting for general-equilibrium adjustments and endogenous route choice.[60] The core result is characterized as follows.

[59] The standard alternative – adopted, for example, by Brancaccio et al. (2024) – is to numerically increase each port's capacity by 1% in turn and re-solve the general-equilibrium model. The analytical route adopted here is preferred because it exposes the structural determinants of port-improvement welfare gains.

[60] I depart from Allen et al. (2025) in three ways. First, I consider infrastructure improvements to nodes (ports) rather than to links (e.g., rail segments). Second, I abstract from mode-of-transport choice. Third, I explicitly allow for trade in intermediate inputs via production networks.

PROPOSITION 3. *The elasticity of region-level welfare V_n with respect to capacity K_p is*

$$\frac{\partial \log V_n}{\partial \log K_p} = \beta_w \, g^{(w)}_{n,p} + \beta_\tau \sum_{n'} \pi_{n'n} \left[-\xi \, g^{(c)}_{n',p} + \lambda_3 \, \Theta_{p|n'n} + \lambda_2 \sum_{p' \in \mathcal{P}} \Theta_{p'|n'n} \, g^{(\Xi)}_{p',p} \right], \qquad (25)$$

where $\beta_w = 1 + (\alpha - 1)(\sigma - 1)$, $\beta_\tau = \alpha(\sigma - 1)/\xi$. *The elasticities* $g^{(w)}_{n,p} \equiv \partial \log w_n / \partial \log K_p$, $g^{(\Xi)}_{p',p} \equiv \partial \log \Xi_{p'} / \partial \log K_p$, *and* $g^{(c)}_{n,p} \equiv \partial \log \bar{c}_n / \partial \log K_p$ *are the elements of the unique solution* $\boldsymbol{x} = \mathbf{A}^{-1}\boldsymbol{b}$ *to a* $(2N + P)$*-dimensional linear system derived in Appendix D.4.*

Proof. See Appendix D.4.

Proposition 3 characterizes *local* gains to port capacity improvements. Aggregation recovers a larger-scale object: the global (or multi-regional) welfare elasticity is the welfare-weighted average of region-specific elasticities,

$$\frac{\partial \log \bar{V}}{\partial \log K_p} = \sum_{n \in \mathcal{N}} \frac{V_n}{\bar{V}} \frac{\partial \log V_n}{\partial \log K_p}. \qquad (26)$$

Equation (25) decomposes the welfare elasticity into distinct channels. The *wage channel* ($\beta_w g^{(w)}_{n,p}$) captures the general-equilibrium response of wages to the capacity expansion; its sign is theoretically ambiguous, as lower trade costs at the expanded port can raise wages through improved market access but also depress them through intensified import competition. The *factory-cost channel* ($-\xi \beta_\tau \sum_{n'} \pi_{n'n} g^{(c)}_{n',p}$) reflects lower production costs at trading partners, which propagate downstream through the production network and reduce the consumer price index in region n. The *routing channel* ($\beta_\tau \sum_{n'} \pi_{n'n} [\lambda_3 \Theta_{p|n'n} + \lambda_2 \sum_{p'} \Theta_{p'|n'n} g^{(\Xi)}_{p',p}]$) combines the direct route-shortening effect of capacity expansion (λ_3) – the "shortcut" offered by the expanded port – with the congestion-relief spillover (λ_2) from the general-equilibrium reallocation of traffic across the rest of the port network. These channels are not independent: each elasticity is a general-equilibrium object, jointly determined by the linear system exposed in Appendix D.4.

7.1.2 WELFARE ELASTICITIES AND CHANNEL DECOMPOSITION

This subsection takes the elasticity of Proposition 3 to the calibration of Section 5 and reports the cross-port object that the rest of this section uses: the distribution of welfare elasticities across ports.

I evaluate Proposition 3 at the baseline and the RCP8.5 equilibria of Section 6, using the solution method detailed in Appendix D.4. Each port's global welfare elasticity is the GDP-weighted average across the 150 regions, following Equation (26).

Cross-port distribution. Figure 11a reports the port-level global welfare elasticities under RCP8.5. The distribution is highly right-skewed: the mean elasticity is 1.4 basis points per one-percent capacity expansion, the median only 0.38 basis points, and the 95^{th} percentile reaches 6.18 basis points – more than ten times the median. The lower tail is shaped by a non-trivial mass of inland-facing, low-traffic ports that carry negligible general-equilibrium weight and sit near zero. A back-of-the-envelope calculation reveals that a uniform 1% expansion of all 502 ports raises global welfare by roughly 502×1.4 basis points.[61] For comparison, Brancaccio et al. (2024) find that expanding a single U.S. dry-bulker port by one ship slot (approximately 1% of total U.S. capacity) raises aggregate welfare by 0.5% on average, with returns exceeding 1% at the best-located ports and near zero at others. Yet the skewness of the distribution implies that the bulk of this aggregate gain is concentrated in a small number of high-elasticity ports: a targeted investment rule would achieve a comparable welfare gain at a fraction of the cost.

Figure 11b maps the change in the port-level welfare elasticity between the baseline and the RCP8.5 equilibria. The cross-port mean elasticity falls by only -0.4%, but the distribution of port-level changes is asymmetric: the 5^{th} percentile of the percent change in port-level elasticity is -1.1%, while the 95^{th} percentile is $+0.2\%$. Ports that gain climate exposure under RCP8.5 see their welfare elasticity decline: the higher expected disruption cost reduces the marginal return to capacity expansion at those locations. Conversely, ports that remain unexposed see their elasticity rise, as the climate shock redirects trade toward them and raises the marginal value of their capacity. The resulting pattern tracks the geography of the RCP8.5 wind-speed shift: elasticities fall in the Caribbean, the Gulf of Mexico, and East and Southeast Asia – where tropical cyclone risk intensifies – and rise along less-exposed coastlines.

Channel decomposition. To understand the determinants of port-improvement welfare gains, I decompose the average welfare elasticity into the channels of Proposition 3. Figure 12 reports the cross-port mean contribution of each channel, in basis

[61] This calculation sums the per-port elasticities, thereby treating the welfare effects of capacity expansions at different ports as independent. Cross-port congestion spillovers would modify this figure in general equilibrium.

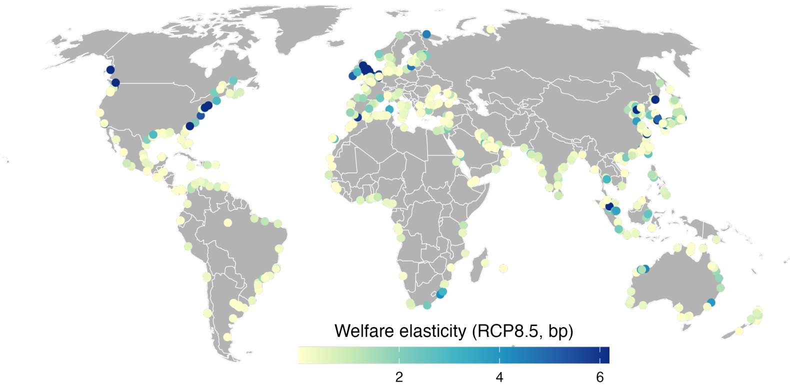

(a) Global welfare elasticity, RCP8.5

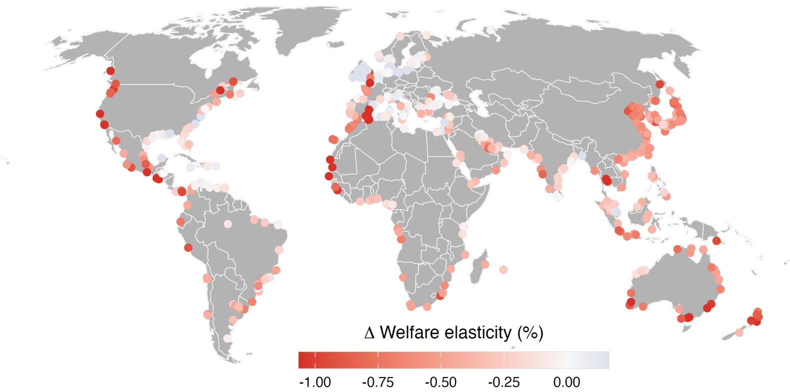

(b) Δ Welfare elasticity, RCP8.5 vs. baseline

Figure 11: Welfare elasticity to port capacity

Notes: Panel (a) plots the port-level GDP-weighted global welfare elasticity to port capacity under the RCP8.5 scenario. Panel (b) plots the change in the port-level welfare elasticity between the baseline and the RCP8.5 equilibria. Welfare elasticities are computed from the general-equilibrium outputs of Section 6 using the solution method of Appendix D.4. The color scales are truncated at the 5$^{\text{th}}$ and 95$^{\text{th}}$ percentiles.

points. Three facts stand out. First, the factory-cost and wage channels are large, nearly offsetting forces. The factory-cost channel accounts for 138% of the mean elasticity under RCP8.5, while the wage channel contributes -58%.[62] The factory-cost channel captures how lower transportation costs at expanded ports reduce input prices for trading partners, compounding along the production network; the wage channel reflects the general-equilibrium response of wages across trading partners to the same cost reduction – cheaper access through the expanded port intensifies import compe-

[62]Because the decomposition is additive and individual channels can partially offset, percentage shares need not lie between zero and one hundred. Across ports, the factory-cost and wage channels are nearly perfectly anti-correlated ($\rho = -0.99$): the same trade-cost reduction that lowers input prices (factory-cost channel) also intensifies import competition (wage channel), so the two forces largely cancel at every port.

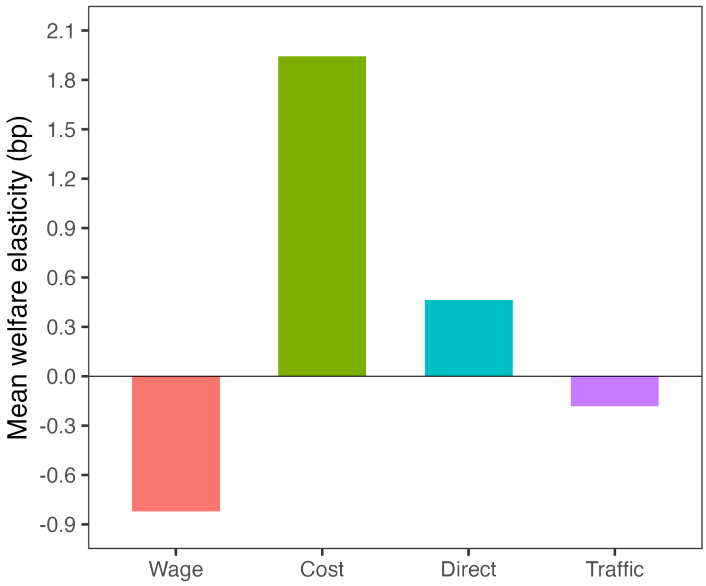

Figure 12: Channel decomposition of the average welfare elasticity

Notes: This figure decomposes the cross-port average welfare elasticity to port capacity into the channels of Proposition 3. The routing channel is further split into a direct "shortcut" component (λ_3) and a traffic-spillover component (λ_2). Bars report the cross-port mean contribution of each channel, in basis points per one-percent capacity expansion, under the baseline equilibrium. The channel shares are nearly invariant across baseline and RCP8.5. Appendix Figure G.3 reports the full cross-port distribution of each channel.

tition, depressing wages and partially offsetting the input-cost savings. On net, the production-network channels jointly contribute approximately 80% of the mean elasticity, with the remaining 20% from the routing channel. Second, the routing channel decomposes into a positive direct shortcut (33%) and a negative traffic-spillover leg (-13%). The direct shortcut captures the welfare gain from cheaper access through the expanded port, holding congestion fixed. The traffic-spillover leg reflects an "iron law of congestion" mechanism: expanding one port's capacity attracts additional traffic, which raises its congestion price and partially offsets the direct capacity gain; the congestion relief at alternative ports that lose traffic is insufficient to compensate, so the net traffic-spillover effect is negative. Third, only the direct routing channel is unambiguously positive in theory; the signs of the wage, factory-cost, and traffic-spillover channels are determined by general-equilibrium feedbacks and can vary across ports.

Ranking ports for investment. The cross-port heterogeneity in Figure 11a has a direct policy read: ranking ports by welfare elasticity defines a *heuristic* allocation rule in which the share of investment received by port p is proportional to its welfare elasticity,

$$g_p^\star = \frac{\partial \log \bar{V} / \partial \log K_p}{\sum_{p'} \partial \log \bar{V} / \partial \log K_{p'}}. \tag{27}$$

For a small aggregate investment ε distributed across ports according to shares $\{g_p\}$, the first-order welfare gain is $\varepsilon \sum_p g_p \left(\partial \log \bar{V} / \partial \log K_p\right)$, which – subject to $\sum_p g_p = 1$ – is maximized precisely when $g_p \propto \partial \log \bar{V} / \partial \log K_p$. The heuristic rule is therefore first-order welfare-maximizing in the $\varepsilon \to 0$ limit.[63]

Evaluating alternative allocation rules. How far do simpler, data-driven allocation rules deviate from the welfare-maximizing heuristic? I measure the distance between $g_p^\star$ and an alternative rule $g_p^{(i)}$ as

$$D(g^\star, g^{(i)}) = \frac{1}{2} \sum_p \left| g_p^\star - g_p^{(i)} \right|, \tag{28}$$

the share of any investment budget that would have to be redirected across ports to convert rule $g^{(i)}$ into the heuristic rule. Three alternative rules are instructive. A *capacity-share* rule that allocates investment in proportion to current port capacity implies $D = 46.1\%$; a *traffic-share* rule, $D = 46.0\%$; and an *equal-share* rule, $D = 58.6\%$. In other words, a planner who ranks ports by current capacity or traffic – rather than by the welfare elasticities of Figure 11a – would direct nearly half of every dollar to a different port. Traffic and capacity are poor sufficient statistics for the welfare return to port investment – an insight that mirrors the results of Allen et al. (2025) for highway links. Figure 13 compares the heuristic shares with the capacity- and traffic-share alternatives port by port: ports for which the welfare elasticity is large relative to current size sit far above the 45-degree line, and the bulk of the reallocation is concentrated on a handful of nodes. At the global ranking level, the climate state shifts the heuristic only at the margin: the distance between the baseline and RCP8.5 heuristics is only $D = 0.2\%$, because the structural determinants of the welfare elasticity – network position, traffic, and capacity – dominate the climate signal in the cross-port ranking.

[63] In the counterfactual exercise of Section 7.2.4, I ask how well that limit approximates welfare gains of the finite EUR 84 billion pipeline in port investment planned in the EU.

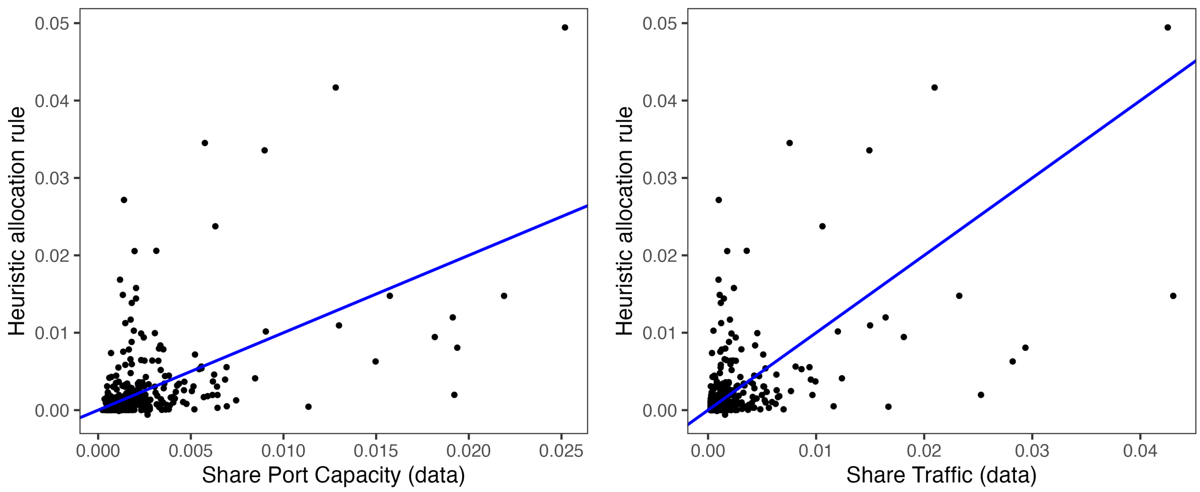

(a) Heuristic vs. capacity-share rule

(b) Heuristic vs. traffic-share rule

Figure 13: Heuristic allocation rule against capacity- and traffic-share alternatives

Notes: Each panel plots the port-level investment share under the heuristic rule of Equation (27) (vertical axis) against the share implied by an alternative rule (horizontal axis). Panel (a) uses the capacity-share rule; panel (b) uses the traffic-share rule. Welfare elasticities are evaluated at the RCP8.5 equilibrium. Points above the 45-degree line are ports that the heuristic rule prioritizes relative to the alternative; points below are de-prioritized. The reallocation share D of Equation (28) aggregates the absolute distance from the 45-degree line.

7.2 Evaluating port investments in the EU

This subsection evaluates the allocation of the EUR 84 billion EU27 port-investment budget reported by ESPO (2024). Subsection 7.2.1 fixes notation and data sources. Subsection 7.2.2 estimates a first-stage regression that maps dollars of port investment into TEU-day capacity, using the World Bank's PPI database. Subsection 7.2.3 reports a port-level benefit-cost ratio that combines the Section 7.1.2 elasticities with that first stage. Subsection 7.2.4 then runs the central policy exercise of this section: it distributes the EU27 investment across ports according to the heuristic rule of Equation (27) computed under both baseline and RCP8.5 climates, re-solves the general-equilibrium model, and compares the two allocations.

7.2.1 Setting and data

I apply the welfare elasticities of Section 7.1 to the allocation of EU27 port investment over the next decade. The choice of the EU27 is motivated both by data – the European Sea Ports Organisation publishes a comprehensive investment pipeline – and by the policy salience of the question. ESPO (2024) reports, on the basis of a port-level survey, that EU27 ports plan to commit approximately EUR 84 billion (USD 93 billion) of investment by 2034.[64] The aggregate budget is taken as exogenous throughout; the question is where it should go.

Two objects are needed to map this budget into a welfare evaluation. The first is the vector of welfare elasticities $\{\partial \log V^{\text{EU}} / \partial \log K_p\}_{p \in \mathcal{P}}$, where the welfare aggregate V^{EU} sums GDP-weighted regional welfare across EU27 countries only. These are computed exactly as in Section 7.1.2 but restricting the aggregation in Equation (26) to EU27 regions. The second is an investment-to-capacity elasticity that translates dollars into TEU-days of port capacity. That elasticity is estimated next.

7.2.2 Investment and port capacity: a first-stage estimate

This subsection estimates the investment-to-capacity elasticity that the framework of Section 7.2.1 requires to convert dollars of port investment into TEU-day units of port capacity. The counterfactual of Section 7.2.4 takes port-level capacity changes $\hat{K}_p$ as inputs to the exact-hat-algebra algorithm; the investment-to-capacity elasticity maps a fixed dollar budget into those capacity changes. I estimate this elasticity from the World Bank's Private Participation in Infrastructure (PPI) port-project database, which provides variation in port investment across middle-income countries, paired with IMF PortWatch port-day activity data as the source of the outcome. The subsection reports the full empirical specification, the headline estimate, and an external-validity discussion of the LMIC-to-EU27 extrapolation; a robustness check against the global port sample is collected in Appendix G.1.

Data. I combine World Bank PPI project-level data with IMF PortWatch port-year aggregates. The final estimation sample contains 38 treated ports and 238 within-country control ports, drawn from the 23 middle-income countries in which at least one port received a PPI investment between 2019 and 2023. I use all *Ports* projects from the PPI database for 2019–2023 (World Bank, 2025). The data contain the port identifier, the investment year, and the total committed investment for every port-infrastructure project in which the World Bank participated. For ports with multiple projects in the same year, I sum investment amounts to obtain a port-by-year aggregate. Recipient ports are matched to PortWatch identifiers by port name. I merge the investment data

[64] The ESPO survey covers 84 port managing bodies across EU core and comprehensive ports. I restrict the sample to the 79 ports retained in the calibration of Section 5, which requires IMF PortWatch traffic data and the bilateral resistance matrix to simultaneously cover the full 2019–2024 sample. The dropped ports are inland or small coastal nodes that account for a negligible share of the EUR 84 billion budget, so the policy implications below are not sensitive to the gap.

with PortWatch global traffic data aggregated at the yearly level (2019–2024), and define the outcome of interest – yearly port capacity – as the 99$^{\text{th}}$ percentile of daily TEU throughput over the calendar year. This quantile picks up the busiest days of the year and proxies the technological ceiling of a port's throughput. Ports are grouped into quartiles of annual total TEU traffic, $q_{p,t} \in \{1, \ldots, 4\}$, which are used to flexibly control for heterogeneous year-level shocks.

Empirical strategy. I estimate a staggered difference-in-differences model with continuous treatment intensity (the investment amount, in billion USD) to track how port capacity evolves around the investment year and let the dynamic effect scale with the investment amount. Let $\tau_{p,t} \equiv t - t_p^{\text{treat}}$ denote event time, with untreated ports assigned $\tau_{p,t} = 0$ and $I_p = 0$. The specification is

$$K_{p,t} = \sum_{\substack{k \in \mathcal{K} \\ k \neq -1}} \beta_k \mathbf{1}\{\tau_{p,t} = k\}\ I_p + \alpha_p + \gamma_{t \times q_{p,t}} + \varepsilon_{p,t}, \tag{29}$$

where $K_{p,t}$ is the 99$^{\text{th}}$ percentile of daily TEU traffic for port p in year t; $\mathbf{1}\{\tau_{p,t} = k\}$ are event-time dummies; I_p is the port's total investment amount (in USD billion); α_p are port fixed effects; and $\gamma_{t \times q_{p,t}}$ are year-by-traffic-quartile fixed effects that absorb flexible global shocks with heterogeneous impacts across the traffic distribution. The coefficient β_k measures the change in port capacity k years after the investment per USD 1 billion committed, relative to the pre-investment year (the omitted category is $\tau_{p,t} = -1$). Standard errors are clustered at the country (ISO3) level.

Estimate. Figure 14 reports the event-study coefficients scaled by a USD 1 billion investment. The pre-period coefficients are statistically indistinguishable from zero at conventional levels, consistent with the parallel-trends identifying assumption. Post-investment, port capacity rises by 3649 TEU-days per USD 1 billion of investment on average over the four years following project completion. Relative to the mean baseline capacity of 13668 TEU-days in the treated-country sample, the point estimate corresponds to a 27% average capacity gain per USD 1 billion. I use this elasticity to map the EU27 investment budget into port-level capacity changes in the counterfactual of Section 7.2.4.

External validity. The estimation sample is drawn from middle-income countries, for which the PPI database has non-trivial coverage. Applying an estimate obtained

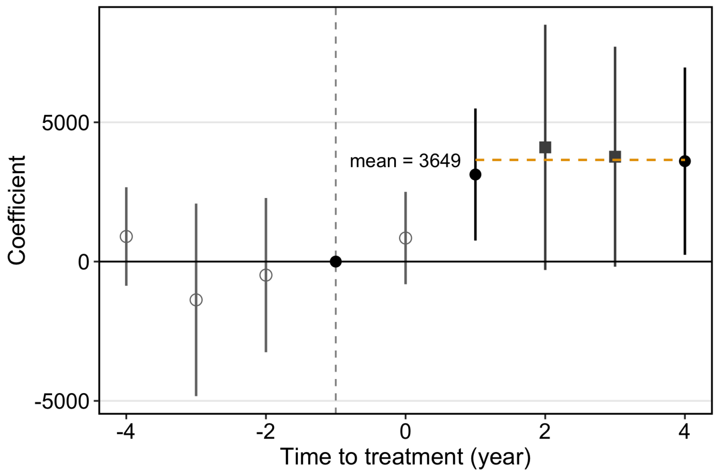

Figure 14: Port capacity response to a USD 1 billion PPI investment

Notes: Point estimates of the event-study coefficients β_k from Equation (29), scaled by a USD 1 billion investment. The outcome is the 99$^{\text{th}}$ percentile of daily TEU at the port-year level. The sample comprises the 38 treated ports and the 238 control ports located in the 23 treated countries. Bars show 95% confidence intervals, clustered at the country level. Black dots indicate point estimates significant at the 5% level, gray squares at the 10% level, and empty dots denote estimates not significant at the 10% level. The orange dashed line reports the mean post-treatment coefficient, which is used as the investment-to-capacity elasticity in the EU counterfactual of Section 7.2.4. Robustness against the global port sample is reported in Appendix G.1.

from middle-income ports to EU27 infrastructure raises a natural concern: if PPI-treated ports were systematically smaller or operated under different technological constraints than European ports, the estimated capacity response could be a poor guide for the counterfactual. Two considerations speak to this concern. First, in the PortWatch panel, the mean port capacity in the PPI estimation subsample (13668 TEU-days across the 23 treated countries) exceeds the EU27 mean (8222 TEU-days), and virtually all EU27 ports fall within the capacity range of the PPI subsample. PPI-treated ports span all 4 EU27 capacity quartiles, so the estimation draws on variation across the full port-size distribution. Appendix Figure G.2 overlays the two capacity distributions and confirms the extensive common support. Second, the year-by-traffic-quartile fixed effects $\gamma_{t\times q}$ in Equation (29) absorb any year-specific shock that hits ports differentially by size class: the identifying variation in the investment coefficient comes from within-quartile, within-country comparisons, so residual size differences between the PPI and EU27 samples do not contaminate the estimate.

7.2.3 Cost-benefit analysis of port investment

I explore the usefulness of the heuristic rule to perform cost-benefit analysis. For each of the 79 EU27 ports, I compute a port-level benefit-cost ratio (BCR) on a stand-alone basis. For each port p, the BCR is the ratio of the EU27 welfare gain of a 1% capacity expansion – computed from $\partial \log V^{\text{EU}}/\partial \log K_p$ evaluated at current-GDP EU27 levels – to the investment cost of that expansion, obtained by dividing $0.01 \times K_p$ (i.e., one percent of current capacity) by the investment-to-capacity elasticity of Section 7.2.2.[65] Benefits are measured in the metric of the underlying welfare function, and therefore include all channels of Proposition 3. Costs are the nominal investment required to achieve a one-percent capacity increase.

The EU-planner BCR averages 0.66 under RCP8.5, with a median of 0.25 and a maximum of 8.3 at the port of *Cork*. A mean BCR close to one is what one would expect from a network of ports operating near a decentralized investment equilibrium at the margin: the heterogeneity around the mean – not its level – is where the policy action lies. 20% of EU27 ports have a BCR above one: these are the ports at which the welfare gain to the EU27 exceeds the nominal cost of a 1% capacity expansion. The distribution is highly right-skewed, consistent with the elasticity heterogeneity of Figure 11. Figure 15 maps the spatial pattern of EU-planner BCRs under RCP8.5.[66] Climate change does not flip the sign of any port's BCR between the baseline and RCP8.5 climates, though it shifts the magnitudes slightly, consistent with the broader finding that climate operates on the distribution of welfare gains rather than on their level. The full port-level BCR table and country-level aggregates are collected in Appendix G.3.

7.2.4 The EU27 counterfactual

This subsection runs the headline exercise of this section. It compares two heuristic allocations of the EU27 investment – one computed under the baseline climate (the *myopic* rule) and one computed under RCP8.5 (the *climate-aware* rule) – by re-solving the general-equilibrium model of Section 3 under each.

[65]Formally, $\text{BCR}_p \equiv \frac{0.01 \cdot Y^{\text{EU}} \cdot (\partial \log V^{\text{EU}}/\partial \log K_p)}{(0.01 \cdot K_p)/\beta^{\text{PPI}}}$, where Y^{EU} is EU27 GDP (USD 15.1 trillion) and $\beta^{\text{PPI}} = 3649$ TEU-days per USD billion is the estimated investment-to-capacity elasticity.

[66]An analogous *national-planner* BCR replaces V^{EU} by the port country's own welfare – i.e., each port is evaluated against its home country's GDP rather than EU27 GDP. The EU-planner and national-planner rankings are highly correlated (Spearman rank correlation 0.90 under RCP8.5), diverging only at a handful of ports whose welfare-elasticity mass loads on trading partners outside the port's own country. See Appendix Figures G.6 and G.7a.

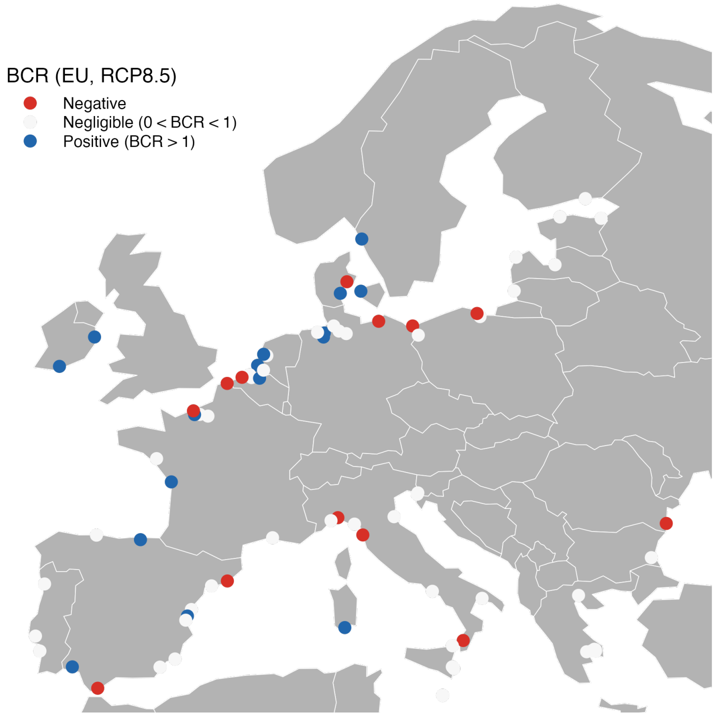

Figure 15: EU-planner benefit-cost ratio under RCP8.5

Notes: This figure maps the port-level benefit-cost ratio under the EU-planner perspective at the RCP8.5 climate. Benefits are the first-order welfare gain to the EU27 from a 1% capacity increase, priced at current EU27 GDP. Costs are the nominal investment required to expand port capacity by 1%, using the first-stage elasticity of Section 7.2.2. The port-level BCR distribution is reported in Appendix Figure G.5.

The mechanics are as follows. Each variant of the rule distributes the EUR 84 billion budget across the 79 EU27 ports in proportion to the corresponding EU27 welfare elasticity vector (Equation 27), and converts the implied investment shares into port-level capacity changes $\hat{K}_p$ via the first-stage elasticity of Section 7.2.2. Both counterfactuals are then solved by the exact-hat-algebra algorithm of Appendix F.4, with the underlying climate state set to RCP8.5 in both cases. What differs across the two is only the allocation of investment across ports, not the climate at which the equilibrium is evaluated.[67]

Aggregate results. Increasing port capacity is meaningful in aggregate: the heuristic allocation delivers a welfare gain on the order of 133.71 basis points. Climate change, however, affects this result only minimally – the climate-aware rule outperforms the myopic one by just 0.093 basis points. This is the expected finding: because the aggregate welfare hit of RCP8.5 in Section 6 is itself small (-0.01%), the cost of ignoring

[67] Appendix G.3 reports the EU27 welfare elasticity distribution and the climate-induced change at the port level.

that hit when allocating a fixed budget is mechanically bounded by the climate hit it fails to price in. Aggregate EU27 port traffic rises by 45.24% under the climate-aware allocation and by 45.21% under the myopic allocation, where both figures are percent gains relative to pre-investment EU27 traffic evaluated at the same RCP8.5 climate. The content of the exercise is not in the aggregate but in the distributional reshuffle documented below.

A unit walk-through. The 133.71 bp aggregate figure is worth reconciling against the primitives of Sections 7.1.2–7.2.2, since small welfare numbers invite the worry of a scaling error. The mean EU27 welfare elasticity to a 1% port-capacity expansion is 0.0308%, or about 3.1 basis points per port.[68] The PPI first-stage implies that USD 1 billion of investment buys, on average, a 27% capacity expansion at a treated port; with the EU budget of USD 93 billion spread uniformly across the 79 EU27 ports in the sample, each port would receive approximately USD 1.2 billion and expand by roughly 32%, or a log-change of about 0.28. Multiplying mean elasticity by this log-change and summing across ports delivers a uniform-rule back-of-the-envelope welfare gain of $79 \times 0.28 \times 3.1 \approx 68$ basis points. The heuristic rule concentrates investment on the right tail of the elasticity distribution and therefore delivers more welfare per dollar than the uniform benchmark – a concentration premium of roughly 2.0×[69] – which brings the back-of-the-envelope calculation to $\approx$ 134 basis points, in line with the observed 133.71 basis points. No free parameters intervene between the cross-port elasticity distribution, the PPI first-stage, and the aggregate welfare number.

Distributional results. The cost of myopia is concentrated. At the country level, the median welfare difference between the two rules is 0.097 basis points, but the tails are wide: the 5$^{\text{th}}$ percentile loses -0.17 basis points, while the 95$^{\text{th}}$ percentile gains 0.64 basis points. The key takeaway is that climate myopia is a distributional concern: the aggregate welfare payoff is virtually the same under either rule, but the cross-country incidence shifts materially. Figure 16 maps the spatial pattern. Appendix Figures G.8 and G.9 report the country-level cost of myopia and the level welfare gains under the climate-aware allocation, respectively.

[68] The EU27-level welfare elasticities are reported in Appendix G.3.

[69] The concentration premium arises because the heuristic rule allocates disproportionately to high-elasticity ports. Given the right-skewed elasticity distribution (Figure 11a), concentrating investment on the right tail delivers more welfare per dollar than spreading it uniformly.

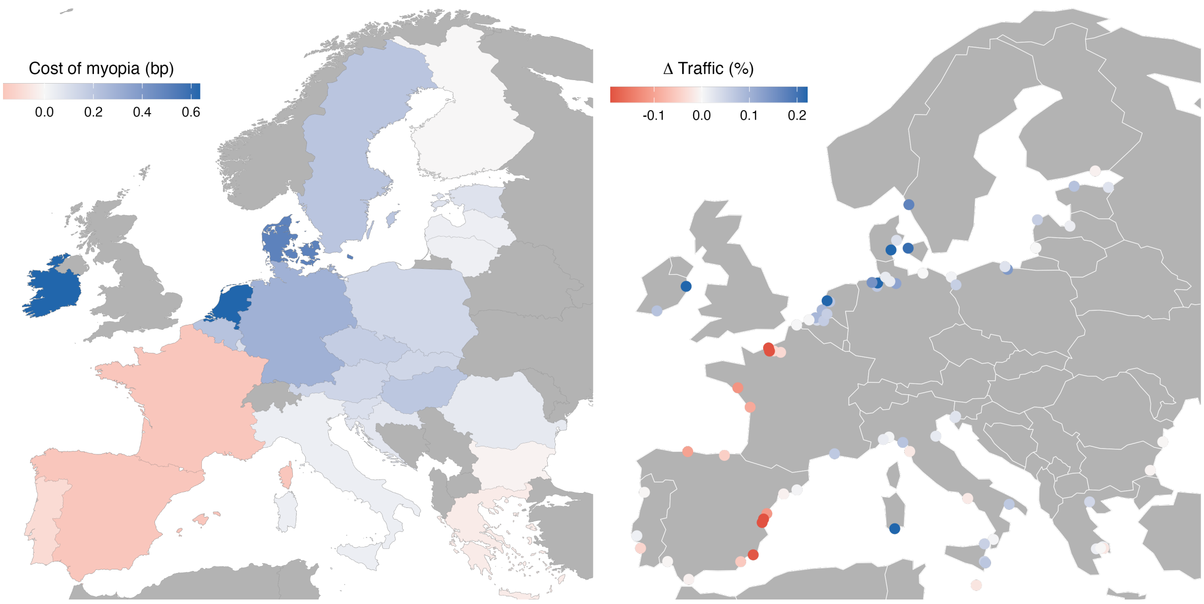

(a) Δ Welfare, myopic vs. climate-aware (bp) (b) Δ Port traffic, myopic vs. climate-aware (%)

Figure 16: Cost of myopia under the EU27 heuristic allocation

Notes: Both panels compare a general-equilibrium counterfactual in which the EUR 84 billion EU27 investment is distributed across ports according to the heuristic rule of Equation (27), computed under baseline climate conditions (myopic), against one in which the same budget is distributed according to the same rule computed under RCP8.5 (climate-aware). Climate conditions at ports are set to RCP8.5 in both counterfactuals. Panel (a) maps the region-level welfare difference (myopic − aware) in basis points. Panel (b) reports the port-level traffic difference (myopic − aware) in percent. Both counterfactuals are solved via the exact-hat-algebra algorithm of Appendix F.4. Color scales are truncated at the 1$^{\text{st}}$ and 99$^{\text{th}}$ percentiles.

8 Conclusion

This paper investigates the impacts of climate-induced disruptions on global supply chains, focusing on the role of disruptions to maritime transportation infrastructure. Leveraging high-frequency data on firm-to-firm shipments and detailed cyclone activity, I provide empirical evidence on how extreme weather events affect port operations and reshape trade. My findings show that rerouting along transportation networks is an adaptation mechanism with limited effectiveness: firms absorb a first port disruption by substituting toward alternative routes, but this margin is insufficient under subsequent shocks or when liner-schedule constraints limit route substitution. Despite rerouting, post-shock firm-to-firm relationship activity declines persistently, with the disruption concentrated among repeatedly exposed and containerized trade relationships.

I further develop a quantitative model of spatial production networks incorporating endogenous transportation costs and congestion spillovers, offering a framework to evaluate the broader economic implications of climate-induced transportation disruptions. The model reveals that the aggregate welfare consequences of a shift to an RCP8.5 port-level wind-speed distribution are small, yet conceal wide regional variation: the largest losses fall on regions most reliant on climate-exposed ports. A scenario decomposition highlights that the endogenous adjustment of port costs to traffic absorbs the bulk of the climate shock in general equilibrium, whereas firm-level rerouting mitigates comparatively little – consistent with the empirical evidence. This identifies the congestion externality as the channel through which infrastructure policy can operate.

I then explore infrastructure policy in a context of climate change. Using an analytical sufficient-statistics approach, I derive welfare elasticities that rank ports by the return to capacity expansion and decompose those returns into wage, factory-cost, and routing channels. The decomposition highlights that production-network propagation – through factory costs and wages, which are large, nearly offsetting forces – accounts for most of the welfare return, but that traffic spillovers across ports systematically dampen these gains. Applying the framework to EU27 port investment, I find that the cost of ignoring climate risk is small in aggregate but reshuffles which countries benefit from port investment.

These findings have clear policy relevance. Investments in port capacity can not only reduce the direct costs of disruptions but also alleviate the congestion externalities that this paper identifies as the dominant general-equilibrium channel. The distributional content of climate myopia – which countries gain and which lose when the planner ignores evolving weather risk – matters for the political economy of infrastructure allocation in settings where investment decisions are partly made at the national level and partly funded supranationally. More broadly, the paper highlights that assessments of where to expand transportation infrastructure must internalize both firms' routing responses and the congestion spillovers those responses generate. While I focus on maritime trade and tropical cyclone risk, the framework extends naturally to other modes of transport and other climate hazards affecting transportation networks, offering a broader lens on the vulnerability of global supply chains to climate risks at critical infrastructure nodes.

References

T. Allen and C. Arkolakis. The Welfare Effects of Transportation Infrastructure Improvements. *The Review of Economic Studies*, 89(6):2911–2957, 2022. ISSN 0034-6527, 1467-937X. doi: 10.1093/restud/rdac001. URL https://academic.oup.com/restud/article/89/6/2911/6519332.

T. Allen, S. Fuchs, and W. F. Wong. Evaluating Transportation Improvements Quantitatively: A Primer. *Working Paper*, 2025.

G. Amatulli, S. Domisch, M.-N. Tuanmu, B. Parmentier, A. Ranipeta, J. Malczyk, and W. Jetz. A suite of global, cross-scale topographic variables for environmental and biodiversity modeling. *Scientific Data*, 5(1):180040, Mar. 2018. ISSN 2052-4463. doi: 10.1038/sdata.2018.40. URL https://www.nature.com/articles/sdata201840. Publisher: Nature Publishing Group.

J. E. Anderson and E. van Wincoop. Gravity with Gravitas: A Solution to the Border Puzzle. *American Economic Review*, 93(1):170–192, 2003. doi: 10.1257/000282803321455214.

M. S. Arslanalp, M. R. Koepke, and J. Verschuur. Tracking Trade from Space: An Application to Pacific Island Countries. *IMF Working Papers*, Aug. 2021. URL https://ideas.repec.org//p/imf/imfwpa/2021-225.html. Number: 2021/225 Publisher: International Monetary Fund.

C. Balboni. In Harm's Way? Infrastructure Investments and the Persistence of Coastal Cities. *American Economic Review*, 115(1):77–116, Jan. 2025. ISSN 0002-8282. doi: 10.1257/aer.20191943. URL https://www.aeaweb.org/articles?id=10.1257/aer.20191943.

C. Balboni, J. Boehm, and M. Waseem. Firm Adaptation in Production Networks: Evidence from Extreme Weather Events in Pakistan. 2024.

J.-N. Barrot and J. Sauvagnat. Input Specificity and the Propagation of Idiosyncratic Shocks in Production Networks*. *The Quarterly Journal of Economics*, 131(3):1543–1592, Aug. 2016. ISSN 0033-5533, 1531-4650. doi: 10.1093/qje/qjw018. URL https://academic.oup.com/qje/article/131/3/1543/2461213.

A. Bilal and E. Rossi-Hansberg. Anticipating Climate Change Across the United States, June 2023. URL https://www.nber.org/papers/w31323.

J. Blaum, F. Esposito, and S. Heise. Input Sourcing under Supply Chain Risk:. *Working paper*, 2024.

N. Bloemendaal, H. de Moel, S. Muis, I. D. Haigh, and J. C. J. H. Aerts. Estimation of global tropical cyclone wind speed probabilities using the STORM dataset. *Scientific Data*, 7(1):377, Nov. 2020a. ISSN 2052-4463. doi: 10.1038/s41597-020-00720-x. URL https://www.nature.com/articles/s41597-020-00720-x. Publisher: Nature Publishing Group.

N. Bloemendaal, I. D. Haigh, H. de Moel, S. Muis, R. J. Haarsma, and J. C. J. H. Aerts. Generation of a global synthetic tropical cyclone hazard dataset using STORM. *Scientific Data*, 7(1):40, Feb. 2020b. ISSN 2052-4463. doi: 10.1038/s41597-020-0381-2. URL https://www.nature.com/articles/s41597-020-0381-2. Publisher: Nature Publishing Group.

C. E. Boehm, A. Flaaen, and N. Pandalai-Nayar. Input Linkages and the Transmission of Shocks: Firm-Level Evidence from the 2011 Tōhoku Earthquake. *The Review of Economics and Statistics*, 101(1):60–75, Mar. 2019. ISSN 0034-6535. doi: 10.1162/rest_a_00750. URL https://doi.org/10.1162/rest_a_00750.

I. Borchert, M. Larch, S. Shikher, and Y. V. Yotov. The international trade and production database for estimation (ITPD-E). *International Economics*, 166:140–166, 2022.

K. Borusyak, X. Jaravel, and J. Spiess. Revisiting Event-Study Designs: Robust and Efficient Estimation. *Review of Economic Studies*, 91(6):3253–3285, Nov. 2024. ISSN 0034-6527, 1467-937X. doi: 10.1093/restud/rdae007. URL https://academic.oup.com/restud/article/91/6/3253/7601390.

G. Brancaccio, M. Kalouptsidi, and T. Papageorgiou. Geography, Transportation, and Endogenous Trade Costs. *Econometrica*, 88(2):657–691, 2020. ISSN 1468-0262. doi: 10.3982/ECTA15455. URL https://onlinelibrary.wiley.com/doi/abs/10.3982/ECTA15455. _eprint: https://onlinelibrary.wiley.com/doi/pdf/10.3982/ECTA15455.

G. Brancaccio, M. Kalouptsidi, and T. Papageorgiou. Investment in Infrastructure and Trade: The Case of Ports, May 2024. URL https://papers.ssrn.com/abstract=4843062.

L. Caliendo and F. Parro. Estimates of the Trade and Welfare Effects of NAFTA. *The Review of Economic Studies*, 82(1):1–44, 2015. doi: 10.1093/restud/rdu035.

V. M. Carvalho, M. Nirei, Y. U. Saito, and A. Tahbaz-Salehi. Supply Chain Disruptions: Evidence from the Great East Japan Earthquake*. *The Quarterly Journal of Economics*, 136(2):1255–1321, May 2021. ISSN 0033-5533. doi: 10.1093/qje/qjaa044. URL https://doi.org/10.1093/qje/qjaa044.

J. Castro-Vincenzi. Climate Hazards and Resilience in the Global Car Industry. 2024.

J. Castro-Vincenzi, G. Khanna, N. Morales, and N. Pandalai-Nayar. Weathering the Storm: Supply Chains and Climate Risk, Mar. 2024. URL https://www.nber.org/papers/w32218.

D. Cengiz, A. Dube, A. Lindner, and B. Zipperer. The Effect of Minimum Wages on Low-Wage Jobs*. *The Quarterly Journal of Economics*, 134(3):1405–1454, Aug. 2019. ISSN 0033-5533. doi: 10.1093/qje/qjz014. URL https://doi.org/10.1093/qje/qjz014.

K. Chen. A Computation Method for Typhoon Wind Field. *Tropic Oceanology*, 13(2):41–48, 1994.

W. Chen, J. Fan, and W. Luo. Trade and Technology Compatibility in General Equilibrium. *SSRN Electronic Journal*, 2023. ISSN 1556-5068. doi: 10.2139/ssrn.4647210. URL https://www.ssrn.com/abstract=4647210.

D. P. Clark, V. Kozlova, and G. Schaur. Supply Chain Uncertainty in Ocean Transit as a Trade Barrier. 2024.

J.-L. Cruz and E. Rossi-Hansberg. The Economic Geography of Global Warming. *Review of Economic Studies*, 91(2):899–939, Mar. 2024. ISSN 0034-6527, 1467-937X. doi: 10.1093/restud/rdad042. URL https://academic.oup.com/restud/article/91/2/899/7107009.

R. Dekle, J. Eaton, and S. Kortum. Unbalanced Trade. *American Economic Review: Papers and Proceedings*, 97(2):351–355, 2007. doi: 10.1257/aer.97.2.351.

R. Dekle, J. Eaton, and S. Kortum. Global Rebalancing with Gravity: Measuring the Burden of Adjustment. *IMF Staff Papers*, 55(3):511–540, 2008. doi: 10.1057/imfsp.2008.17.

M. Deshpande and Y. Li. Who Is Screened Out? Application Costs and the Targeting of Disability Programs. *American Economic Journal: Economic Policy*, 11(4):213–248, Nov. 2019. ISSN 1945-7731, 1945-774X. doi: 10.1257/pol.20180076. URL https://pubs.aeaweb.org/doi/10.1257/pol.20180076.

K. Desmet and E. Rossi-Hansberg. On the spatial economic impact of global warming. *Journal of Urban Economics*, 88:16–37, July 2015. ISSN 00941190. doi: 10.1016/j.jue.2015.04.004. URL https://linkinghub.elsevier.com/retrieve/pii/S0094119015000339.

K. Desmet, R. E. Kopp, S. A. Kulp, D. K. Nagy, M. Oppenheimer, E. Rossi-Hansberg, and B. H. Strauss. Evaluating the Economic Cost of Coastal Flooding. *American Economic Journal: Macroeconomics*, 13(2):444–486, Apr. 2021. ISSN 1945-7707, 1945-7715. doi: 10.1257/mac.20180366. URL https://pubs.aeaweb.org/doi/10.1257/mac.20180366.

A. Dube, D. Girardi, Ò. Jordà, and A. M. Taylor. A Local Projections Approach to Difference-in-Differences, 2023. URL https://www.nber.org/papers/w31184.

C. Ducruet, R. Juhász, D. K. Nagy, and C. Steinwender. All aboard: The effects of port development. *Journal of International Economics*, 151:103963, Sept. 2024. ISSN 0022-1996. doi: 10.1016/j.jinteco.2024.103963. URL https://www.sciencedirect.com/science/article/pii/S0022199624000904.

ESPO. Port Investment Study 2024: The Investment Pipeline and Challenges of European Ports. Technical report, 2024. URL https://www.espo.be/media/ESPOPortInvestmentsStudy2024.pdf.

P. D. Fajgelbaum and E. Schaal. Optimal Transport Networks in Spatial Equilibrium. *Econometrica*, 88(4):1411–1452, 2020. ISSN 1468-0262. doi: 10.3982/ECTA15213. URL https://onlinelibrary.wiley.com/doi/abs/10.3982/ECTA15213. _eprint: https://onlinelibrary.wiley.com/doi/pdf/10.3982/ECTA15213.

D. J. Flynn. Mariner's Tropical Cyclone Guide. *National Weather Service*, 2023.

R. W. Fogel. A Quantitative Approach to the Study of Railroads in American Economic Growth: A Report of Some Preliminary Findings. *The Journal of Economic History*, 22(2):163–197, June 1962. ISSN 1471-6372, 0022-0507. doi: 10.1017/S0022050700062719. URL https://www.cambridge.org/core/journals/journal-of-economic-history/article/abs/quantitative-approach-to-the-study-of-railroads-in-american-economic-gr 72344209B9B3F06D69C9AA2BD3B0E1F7.

S. Fuchs and W. F. Wong. Multimodal Transport Networks. *SSRN Electronic Journal*, 2024. ISSN 1556-5068. doi: 10.2139/ssrn.4991910. URL https://www.ssrn.com/abstract=4991910.

S. Ganapati, W. F. Wong, and O. Ziv. Entrepôt: Hubs, Scale, and Trade Costs. *American Economic Journal: Macroeconomics*, 16(4):239–278, 2024. ISSN 1945-7707. doi: 10.1257/mac.20220250. URL https://www.aeaweb.org/articles?id=10.1257/mac.20220250.

Global Fishing Watch. AIS-based vessel voyages and named anchorages. https://globalfishingwatch.org/data-download/, 2024. Monthly vessel voyages and named anchorages v2, downloaded 2024.

S. M. Hsiang and A. S. Jina. The Causal Effect of Environmental Catastrophe on Long-Run Economic Growth: Evidence From 6,700 Cyclones, July 2014. URL https://www.nber.org/papers/w20352.

K. Klein Goldewijk. History Database of the Global Environment 3.3, Mar. 2024. URL https://public.yoda.uu.nl/geo/UU01/94FNH0.html. Publisher: Utrecht University.

K. R. Knapp, M. C. Kruk, D. H. Levinson, H. J. Diamond, and C. J. Neumann. The International Best Track Archive for Climate Stewardship (IBTrACS). Mar. 2010. doi: 10.1175/2009BAMS2755.1. URL https://journals.ametsoc.org/view/journals/bams/91/3/2009bams2755_1.xml. Section: Bulletin of the American Meteorological Society.

D. A. Kroodsma, J. Mayorga, T. Hochberg, N. A. Miller, K. Boerder, F. Ferretti, A. Wilson, B. Bergman, T. D. White, B. A. Block, P. Woods, B. Sullivan, C. Costello, and B. Worm. Tracking the global footprint of fisheries. *Science*, 359(6378):904–908, 2018. doi: 10.1126/science.aao5646.

J. Ksciuk, S. Kuhlemann, K. Tierney, and A. Koberstein. Uncertainty in maritime ship routing and scheduling: A Literature review. *European Journal of Operational Research*, 308(2):499–524, July 2023. ISSN 0377-2217. doi: 10.1016/j.ejor.2022.08.006. URL https://www.sciencedirect.com/science/article/pii/S037722172200649X.

A. Martinez. Trade Relationships During and After a Crisis: Evidence from Road Disruptions in Colombian Flower Exports. *Working Paper*, 2024.

E. Oberfield. A Theory of Input–Output Architecture. *Econometrica*, 86 (2):559–589, 2018. ISSN 1468-0262. doi: 10.3982/ECTA10731. URL https://onlinelibrary.wiley.com/doi/abs/10.3982/ECTA10731. _eprint: https://onlinelibrary.wiley.com/doi/pdf/10.3982/ECTA10731.

N. M. C. Pankratz and C. Schiller. Climate Change and Adaptation in Global Supply-Chain Networks, June 2021. URL https://papers.ssrn.com/abstract=3475416.

A. Rabano and J. N. Rosas. The Transmission of Climate Shocks: The Case of Floods in India. *Working Paper*, 2024.

S. J. Redding and M. A. Turner. Chapter 20 - Transportation Costs and the Spatial Organization of Economic Activity. In G. Duranton, J. V. Henderson, and W. C. Strange, editors, *Handbook of Regional and Urban Economics*, volume 5 of *Handbook of Regional and Urban Economics*, pages 1339–1398. Elsevier, Jan. 2015.

doi: 10.1016/B978-0-444-59531-7.00020-X. URL https://www.sciencedirect.com/science/article/pii/B978044459531700020X.

E. Rossi-Hansberg and J. Zhang. Local GDP Estimates Around the World, Feb. 2025. URL https://www.nber.org/papers/w33458.

I. Rudik, G. Lyn, W. Tan, and A. Ortiz-Bobea. The Economic Effects of Climate Change in Dynamic Spatial Equilibrium, June 2021. URL https://osf.io/usghb_v1.

J. Verschuur, E. E. Koks, and J. W. Hall. Port disruptions due to natural disasters: Insights into port and logistics resilience. *Transportation Research Part D: Transport and Environment*, 85:102393, Aug. 2020. ISSN 1361-9209. doi: 10.1016/j.trd.2020.102393. URL https://www.sciencedirect.com/science/article/pii/S1361920920305800.

J. Verschuur, E. E. Koks, and J. W. Hall. Systemic risks from climate-related disruptions at ports. *Nature Climate Change*, 13(8):804–806, Aug. 2023a. ISSN 1758-6798. doi: 10.1038/s41558-023-01754-w. URL https://www.nature.com/articles/s41558-023-01754-w. Publisher: Nature Publishing Group.

J. Verschuur, E. E. Koks, S. Li, and J. W. Hall. Multi-hazard risk to global port infrastructure and resulting trade and logistics losses. *Communications Earth & Environment*, 4(1):1–12, Jan. 2023b. ISSN 2662-4435. doi: 10.1038/s43247-022-00656-7. URL https://www.nature.com/articles/s43247-022-00656-7. Publisher: Nature Publishing Group.

H. E. Willoughby, R. W. R. Darling, and M. E. Rahn. Parametric Representation of the Primary Hurricane Vortex. Part II: A New Family of Sectionally Continuous Profiles. Apr. 2006. doi: 10.1175/MWR3106.1. URL https://journals.ametsoc.org/view/journals/mwre/134/4/mwr3106.1.xml. Section: Monthly Weather Review.

C. Wing, S. M. Freedman, and A. Hollingsworth. Stacked Difference-in-Differences, Jan. 2024. URL https://www.nber.org/papers/w32054.

W. F. Wong and S. Fuchs. Multimodal Transport Networks, Oct. 2022. URL https://papers.ssrn.com/abstract=4277194.

World Bank. Data on Private Participation in Infrastructure (PPI) - World Bank Group, 2025. URL https://ppi.worldbank.org/en/ppidata.

Appendix

Climate Trade Costs: Extreme Weather, Transportation, and Supply Chains

Hubert Massoni

University of Bologna

Contents

A Anecdotal evidence

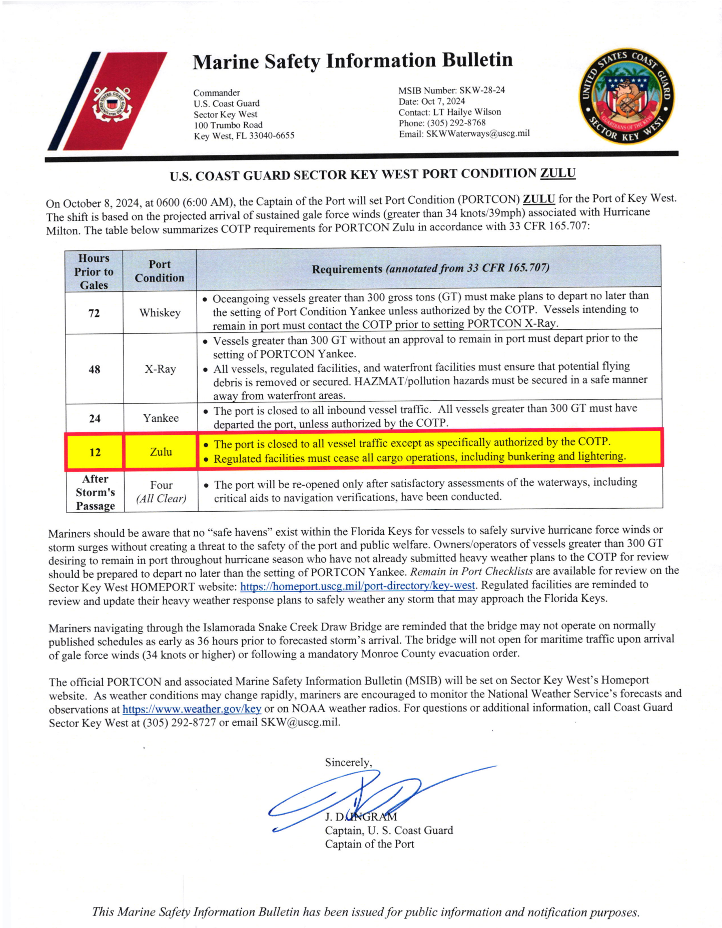

Marine Safety Information Bulletin

Commander
U.S. Coast Guard
Sector Key West
100 Trumbo Road
Key West, FL 33040-6655

MSIB Number: SKW-28-24
Date: Oct 7, 2024
Contact: LT Hailye Wilson
Phone: (305) 292-8768
Email: SKWWaterways@uscg.mil

U.S. COAST GUARD SECTOR KEY WEST PORT CONDITION ZULU

On October 8, 2024, at 0600 (6:00 AM), the Captain of the Port will set Port Condition (PORTCON) **ZULU** for the Port of Key West. The shift is based on the projected arrival of sustained gale force winds (greater than 34 knots/39mph) associated with Hurricane Milton. The table below summarizes COTP requirements for PORTCON Zulu in accordance with 33 CFR 165.707:

Hours Prior to Gales	**Port Condition**	**Requirements** *(annotated from 33 CFR 165.707)*
72	Whiskey	• Oceangoing vessels greater than 300 gross tons (GT) must make plans to depart no later than the setting of Port Condition Yankee unless authorized by the COTP. Vessels intending to remain in port must contact the COTP prior to setting PORTCON X-Ray.
48	X-Ray	• Vessels greater than 300 GT without an approval to remain in port must depart prior to the setting of PORTCON Yankee. • All vessels, regulated facilities, and waterfront facilities must ensure that potential flying debris is removed or secured. HAZMAT/pollution hazards must be secured in a safe manner away from waterfront areas.
24	Yankee	• The port is closed to all inbound vessel traffic. All vessels greater than 300 GT must have departed the port, unless authorized by the COTP.
12	Zulu	• The port is closed to all vessel traffic except as specifically authorized by the COTP. • Regulated facilities must cease all cargo operations, including bunkering and lightering.
After Storm's Passage	Four *(All Clear)*	• The port will be re-opened only after satisfactory assessments of the waterways, including critical aids to navigation verifications, have been conducted.

Mariners should be aware that no "safe havens" exist within the Florida Keys for vessels to safely survive hurricane force winds or storm surges without creating a threat to the safety of the port and public welfare. Owners/operators of vessels greater than 300 GT desiring to remain in port throughout hurricane season who have not already submitted heavy weather plans to the COTP for review should be prepared to depart no later than the setting of PORTCON Yankee. *Remain in Port Checklists* are available for review on the Sector Key West HOMEPORT website: https://homeport.uscg.mil/port-directory/key-west. Regulated facilities are reminded to review and update their heavy weather response plans to safely weather any storm that may approach the Florida Keys.

Mariners navigating through the Islamorada Snake Creek Draw Bridge are reminded that the bridge may not operate on normally published schedules as early as 36 hours prior to forecasted storm's arrival. The bridge will not open for maritime traffic upon arrival of gale force winds (34 knots or higher) or following a mandatory Monroe County evacuation order.

The official PORTCON and associated Marine Safety Information Bulletin (MSIB) will be set on Sector Key West's Homeport website. As weather conditions may change rapidly, mariners are encouraged to monitor the National Weather Service's forecasts and observations at https://www.weather.gov/key or on NOAA weather radios. For questions or additional information, call Coast Guard Sector Key West at (305) 292-8727 or email SKW@uscg.mil.

Sincerely,

J. D. INGRAM
Captain, U. S. Coast Guard
Captain of the Port

This Marine Safety Information Bulletin has been issued for public information and notification purposes.

Figure A.1: Example of port condition ZULU (US)

Notes: This document is the Marine Safety Information Bulletin issued on October 8, 2024, by the US Coast Guards of Port Key West (Florida), before the landfall of Hurricane Milton.

B Data sources

This appendix describes all data sources used in the paper. Table B.1 provides a summary. Exercise-specific data construction is documented separately: the reduced-form estimation sample and instruments in Appendix E, and the calibration data assembly in Appendix F.1.

Table B.1: Data sources and time coverage

Data type/variable	Time coverage	Source
Bills of lading (Brazil)	2014–2023	S&P Panjiva
Global port-level traffic	2019–2023	IMF PortWatch
Port capacity	2019–2023	IMF PortWatch
Tropical cyclone tracks	2014–2023	IBTrACS (Knapp et al., 2010)
GAUL1 subnational polygons	-	GAUL1 (geocoding overlay)
Tropical cyclone climate	1980–2015 / 2015–2050	STORM (Bloemendaal et al., 2020a,b)
Bilateral trade flows	2019	ITPD-E (Borchert et al., 2022)
Country polygons	-	Natural Earth (admin 0)
Distances (land)	-	Great-circle between country centroids
Distances (sea)	-	Eurostat `SeaRoute`
Vessel voyages (AIS)	2017	Global Fishing Watch (Global Fishing Watch, 2024)
Population (1° grid)	2012–2020	Rossi-Hansberg and Zhang (2025)
GDP per capita (1° grid, 2017 PPP)	2012–2020	Rossi-Hansberg and Zhang (2025)
Historical population (1950)	1950	HYDE 3.3 (Klein Goldewijk, 2024)
Terrain Ruggedness Index	-	Amatulli et al. (2018)

Notes: This table reports all data sources used in the paper. Appendices B.1–B.5 describe each source in detail.

B.1 Bill of Lading Data – Brazil (2014–2023)

Source and coverage. I use firm-to-firm bills of lading assembled by S&P Panjiva for all maritime import transactions recorded as entering a Brazilian port between June 2014 and December 2023. The raw data contains shipment identifiers (`panjivaRecordId`), the date the shipment entered the first domestic port (`shpmtDate`), company names for the consignee/importer and shipper/exporter (`conName`, `shpName`), party address fields (street, city, state/region, postal code, country), party type (`shpType`, `conType`: *Real Cargo Owner* vs. *NVO/Forwarder*), maritime ports of lading/origin and unlading/destination (names and UNLOCODEs), transport mode, indicators for containerization, and physical/value measures (TEU volume, gross weight in kg, USD value).[70] The empirical analysis focuses on maritime shipments only; if non-maritime records are present in the extract, they are dropped.

[70]The data also contains Panjiva-assigned establishment identifiers for the consignee and shipper (`conPanjivaId`, `shpPanjivaId`), but these are prone to errors. E.g., small variations in street names can lead to wrongly-assigned separate establishment identifiers. I address this issue by constructing new establishment identifiers, based on (cleaned) company names and addresses.

Defining geocoded establishments (firms). Empty strings in Panjiva address fields are treated as missing. For both sides of the transaction I build full-address tokens by concatenating the available street, city, state/region, postal code, and country fields. These tokens are used for geocoding and as intermediate keys to define establishments. Company names are standardized prior to consolidation: I transliterate non-Latin scripts to Latin and then to ASCII, harmonize special characters, and remove legal-form affixes using a comprehensive cross-walk of entity-type abbreviations. The resulting sanitized parent names are then passed through a generic string-cleaning routine.

I geocode the full addresses via the ArcGIS service (through `tidygeocoder`). Minimum information for geolocalization is a city or postal code; street addresses are not required. I define a *firm* as the set of co-located establishments belonging to the same (cleaned) parent name. Concretely, within each parent, I cluster all geocoded points using single-linkage hierarchical clustering with a 10km cutoff and assign a unique establishment identifier to each cluster (constructed from the parent name and the cluster centroid). I then overlay cluster centroids onto GAUL1 polygons to assign a unique GAUL1 location identifier to each buyer and supplier. Observations without a city/postal code or without a successful GAUL1 assignment are excluded.

Defining geocoded ports. I parse Panjiva's port names and countries, normalize them via the same transliteration/ASCII pipeline used for firm names, and remove unknown UNLOCODEs. For a limited set of ports with commonly used variants, I apply targeted name corrections (e.g., major Ukrainian, Chinese, and North African ports). To link Panjiva ports with the IMF PortWatch global port universe, I proceed in two steps. First, I match Panjiva ports to PortWatch ports by UNLOCODE (exact match). Second, for remaining unmatched ports, I match cleaned port names within country using fuzzy matching (Jaro–Winkler), retaining only exact post-cleaning matches. Port coordinates are obtained from the PortWatch database. The resulting matched sample retains ports with a unique mapping between Panjiva UNLOCODEs and PortWatch identifiers.

Useful identifiers. I construct a set of unit identifiers used throughout the analysis. Let b denote a Brazilian buyer establishment and s a foreign supplier establishment. The buyer–supplier establishment pair is $\{b, s\}$. Each shipment lists a port of lading p_o and a port of unlading p_d, which define a sea route. The identifiers are:

- `BS.establishment.id`: buyer-supplier establishment pair;

- `route.id`: route (p_o, p_d);
- `BS.route.id`: buyer-supplier establishment pair $\times$ route (p_o, p_d).

Calendar time is built from shipment dates by constructing a complete daily grid between the first and last observed shipment dates and then indexing months by their first day (`time.ym`). These normalized indices are merged back to shipments.

Aggregation and sample restrictions. I exclude records with missing Panjiva party identifiers (`conPanjivaId` or `shpPanjivaId`), with establishments not geocoded at the city or postal code level, or transiting through ports not matched to the PortWatch universe. I keep only shipments where (i) both parties are labeled as *Real Cargo Owner* (i.e., I exclude *NVO/Forwarder* on either side), and (ii) the buyer geocodes to Brazil and the supplier does not geocode to Brazil.

I build two main aggregated datasets, at the `BS.establishment.id` (relationship) level, and at the `BS.route.id` (relationship-route) level. For each relationship (relationship-route) identifier, I aggregate shipment quantities and values at the monthly level. I compute the sum of USD value, gross weight (kg), and TEU volume, the number of distinct shipments, and the number of containerized shipments. I finally drop infrequent relationships (relationship-routes), by keeping only `BS.establishment.id` (`BS.route.id`) identifiers that trade at least two months within the sample.

Table B.2 reports the effect of the data cleaning procedure on firm- and relationship-related variables. Table B.3 focuses on ports and routes. Table B.4 presents summary statistics on firm-to-firm trade when infrequent relationships are removed, while Table B.5 presents summary statistics on firm-to-firm trade when infrequent relationships or relationships-routes are removed.

Table B.2: Data Cleaning - Firms and Relationships

	Desc.	Num. Shipments	Num. Importers	Num. Exporters	Num. Rel.
Full Sample					
(1)	Raw Panjiva	9017154	44556	37973	185708
(2)	Drop missing parent company ID	8950897	44509	37868	185355
(3)	Drop poorly geolocalized firms	2205290	27136	31537	126811
(4)	Drop NVO/forwarders	1044786	17886	23622	74290
(5)	Keep Brazilian imp., foreign exp.	1039652	17695	23301	73600
(6)	Drop unmatched ports (PortWatch)	915587	16149	21387	62728
Estimation Sample					
(7)	Drop infrequent rel.	876802	9605	12641	32592
(8)	Drop infrequent rel.-routes	835211	8696	11497	28434

Note: This table reports the effect of the data cleaning procedure on firm-related variables. Firms refer to geolocalized establishments. "Num. Shipments" refers to the number of distinct shipments, as identified by the bill of lading ID. "Num. Importers" refers to the number of establishments importing goods. "Num. Exporters" refers to the number of establishments exporting goods. "Num. Rel." refers to the number of trading establishment pairs.

Table B.3: Data Cleaning - Maritime Ports and Routes

	Desc.	Num. Exit Ports	Num. Entry Ports	Num. Routes	Num. Rel.-Routes
Full Sample					
(1)	Raw Panjiva	597	30	3567	565699
(2)	Drop missing parent company ID	583	30	3383	562213
(3)	Drop poorly geolocalized firms	319	26	1427	240272
(4)	Drop NVO/forwarders	306	25	1338	127425
(5)	Keep Brazilian imp., foreign exp.	302	25	1325	126449
(6)	Drop unmatched ports (PortWatch)	286	24	1147	102796
Estimation Sample					
(7)	Drop infrequent rel.	239	22	941	72082
(8)	Drop infrequent rel.-routes	183	22	676	42131

Note: This table reports the effect of the data cleaning procedure on route-related variables. Routes refer to port of exit-port of entry pairs. "Num. Exit Ports" refers to the number of ports of lading, as identified by the PortWatch port ID. "Num. Entry Ports" refers to the number of ports of unlading, as identified by the PortWatch port ID. "Num. Routes" refers to the number of observed port pairs. "Num. Rel.Routes" refers to the number of importer-exporter-route triplets.

Table B.4: Summary Statistics - Relationship Sample

Desc.	Mean	25%	50%	75%	90%	95%
Per Buyer - Month						
Num. transactions	6.35	1.00	2.00	4.00	10.00	19.00
Num. suppliers	1.68	1.00	1.00	2.00	3.00	4.00
Num. exit ports	1.69	1.00	1.00	2.00	3.00	4.00
Num. entry ports	1.07	1.00	1.00	1.00	1.00	2.00
Num. routes	1.72	1.00	1.00	2.00	3.00	5.00
Log weight (kg)	10.93	9.90	10.74	11.90	13.11	13.93
Log volume (TEU)	1.55	0.69	1.39	2.40	3.47	4.16
Log value (USD)	12.08	10.99	11.89	13.01	14.18	14.98
Per Supplier - Month						
Num. transactions	5.81	1.00	2.00	4.00	9.00	17.00
Num. buyers	1.54	1.00	1.00	1.00	2.00	4.00
Num. exit ports	1.31	1.00	1.00	1.00	2.00	3.00
Num. entry ports	1.19	1.00	1.00	1.00	2.00	2.00
Num. routes	1.46	1.00	1.00	1.00	2.00	3.00
Log weight (kg)	10.64	9.69	10.51	11.63	12.81	13.59
Log volume (TEU)	1.45	0.69	1.39	2.30	3.33	3.99
Log value (USD)	12.10	11.02	11.94	13.06	14.20	15.01
Per Relationship - Month						
Num. transactions	3.78	1.00	1.00	3.00	6.00	10.00
Num. exit ports	1.15	1.00	1.00	1.00	2.00	2.00
Num. entry ports	1.02	1.00	1.00	1.00	1.00	1.00
Num. routes	1.17	1.00	1.00	1.00	2.00	2.00
Log weight (kg)	10.50	9.71	10.24	11.38	12.46	13.21
Log volume (TEU)	1.21	0.41	0.69	1.95	2.89	3.58
Log value (USD)	11.76	10.81	11.60	12.59	13.67	14.43

Note: The table reports summary statistics of the relationship sample. "Num. Shipments" refers to the number of distinct shipments, as identified by the bill of lading ID. "Num. exit ports" refers to the number of ports of exit, as identified by the PortWatch port ID. "Num. entry ports" refers to the number of ports of entry, as identified by the PortWatch port ID. "Num. routes" refers to the number of pairs or ports of exit and entry. "Log weight (kg)" refers to the total weight of shipments, in kilograms. "Log volume (TEU)" refers to the total volume of shipments, in Twenty-foot Equivalent Units. "Log value (USD)" refers to the total value of shipments, in current USD.

Table B.5: Summary Statistics - Relationship-Route Sample

Desc.	Mean	25%	50%	75%	90%	95%
Per Buyer - Month						
Num. shipments	6.63	1.00	2.00	4.00	10.00	20.00
Num. suppliers	1.67	1.00	1.00	2.00	3.00	4.00
Num. exit ports	1.65	1.00	1.00	2.00	3.00	4.00
Num. entry ports	1.06	1.00	1.00	1.00	1.00	2.00
Num. routes	1.67	1.00	1.00	2.00	3.00	4.00
Log weight (kg)	10.94	9.91	10.76	11.91	13.12	13.92
Log volume (TEU)	1.57	0.69	1.39	2.48	3.50	4.20
Log value (USD)	12.09	10.99	11.90	13.02	14.21	15.02
Per Supplier - Month						
Num. shipments	6.02	1.00	2.00	4.00	10.00	18.00
Num. buyers	1.52	1.00	1.00	1.00	2.00	3.00
Num. exit ports	1.27	1.00	1.00	1.00	2.00	3.00
Num. entry ports	1.18	1.00	1.00	1.00	2.00	2.00
Num. routes	1.41	1.00	1.00	1.00	2.00	3.00
Log weight (kg)	10.65	9.70	10.53	11.65	12.82	13.59
Log volume (TEU)	1.47	0.69	1.39	2.30	3.33	4.02
Log value (USD)	12.11	11.03	11.96	13.08	14.23	15.03
Per Relationship - Month						
Num. shipments	3.97	1.00	1.00	3.00	6.00	11.00
Num. exit ports	1.13	1.00	1.00	1.00	1.00	2.00
Num. entry ports	1.02	1.00	1.00	1.00	1.00	1.00
Num. routes	1.15	1.00	1.00	1.00	2.00	2.00
Log weight (kg)	10.50	9.71	10.26	11.41	12.47	13.21
Log volume (TEU)	1.24	0.69	1.10	2.06	3.00	3.58
Log value (USD)	11.78	10.81	11.61	12.62	13.71	14.48

Note:
The table reports summary statistics of the relationship-route sample. It contains only treated relationships. "Num. Shipments" refers to the number of distinct shipments, as identified by the bill of lading ID. "Num. exit ports" refers to the number of ports of exit, as identified by the PortWatch port ID. "Num. entry ports" refers to the number of ports of entry, as identified by the PortWatch port ID. "Num. routes" refers to the number of pairs or ports of exit and entry. "Log weight (kg)" refers to the total weight of shipments, in kilograms. "Log volume (TEU)" refers to the total volume of shipments, in Twenty-foot Equivalent Units. "Log value (USD)" refers to the total value of shipments, in current USD.

B.2 Global Port-Level Traffic (2019–2023)

Source and coverage. I use the IMF PortWatch daily data on port activity and estimated trade flows for 1,666 global ports from 2019 to 2023. The data reports, at a daily $\times$ port level, counts of port calls and estimated import/export trade flows (in metric tons) disaggregated by ship type (container, dry bulk, general cargo, tanker, and ro–ro).[71] These indicators are derived from raw AIS traces processed by the PortWatch team following the methodology in Arslanalp et al. (2021).[72] I link PortWatch ports to the Panjiva port universe using the UNLOCODE and fuzzy name matching described in Appendix B.1, which yields a stable mapping between PortWatch port IDs and UNLOCODEs. To avoid ambiguous joins, I retain only PortWatch IDs that map to a single UNLOCODE. The resulting linked sample contains 621 ports that can be used jointly with the Brazilian bill-of-lading data.

Construction of daily traffic measures. For each port–day (p, t), I compute (i) total vessel calls, (ii) container vessel calls, (iii) total traffic in TEU, and (iv) container traffic in TEU. To construct daily total vessel calls, I sum the PortWatch port-call counts across all ship types. To construct TEU traffic estimates, I sum import/export series across all ship types within port–day and rescale it by a factor of $1/10$ so that the stored variables represent average TEU units.[73] Container vessel calls and TEU traffic estimates are constructed using the same logic, although they only account for container ships, and containerized import/export weights.

Unless noted, I use *total* daily TEU as the proxy for port traffic; container-specific TEU and vessel-call measures are used for robustness and by-ship-type checks. When higher-frequency noise is undesirable, I aggregate these series to the relevant time unit (e.g., week) by summation, as indicated in the empirical design.

Port capacity. I measure port capacity from PortWatch daily TEU flows. For each port, I compute the 99$^{\text{th}}$ percentile of daily total TEU (imports + exports) over 2019–2023, and I use this as the capacity proxy K_p. Unless noted, I use a normalized capacity measure (capacity divided by the global maximum).

[71] Container ships carry standardized containers, mostly containing manufactured goods. Dry bulk carriers transport unpackaged commodities such as coal, iron ore, and grain in large holds. General cargo vessels move breakbulk items – often on pallets or in crates – using multipurpose ships with their own gear. Tankers carry liquid bulk – crude oil, refined products, chemicals, or liquefied gases – in segregated tanks. Ro-ro ships carry wheeled cargo such as cars and trucks that roll on and off via ramps.

[72] Downloaded from IMF PortWatch. Estimates are based on AIS data via the United Nations Global Platform; see Arslanalp et al. (2021) for details.

[73] Twenty-foot equivalent units carry on average 10 tons of goods.

B.3 Tropical Cyclone Tracks (2014–2023)

Source and coverage. I use the International Best Track Archive for Climate Stewardship (IBTrACS) global archive (Knapp et al., 2010). IBTrACS provides a harmonized record of tropical cyclones with 3-hourly observations and $\approx 0.1^\circ$ track coordinates. For each country hosting at least one port in the Panjiva sample, I use the `StormR` package to select all storms observed within 300 km of the country polygon between 2014 and 2023, using country polygons as the location of interest. The analysis centers on cyclones that affect ports. Operationally, I compute wind fields for each selected storm and evaluate wind exposure at geocoded ports that export to Brazil (Appendix B.1). For descriptive figures (e.g., Figure 2a), I display the full tracks of selected cyclones to illustrate coastal exposure.

Wind fields and exposure surfaces. For each selected storm, I compute gridded surfaces of (i) maximum sustained wind (MSW) and (ii) an exposure index conditional on winds exceeding 18m/s (hours of exposure) using the `spatialBehaviour` function in `StormR` at 10-arc-minute spatial resolution. The 18m/s threshold ($\approx$ 35 knots) aligns closely with the 34-knot operational threshold commonly used for port closure conditions (e.g., condition ZULU in the US).

Port-level extraction and variables. For each port–storm pair, I extract cell means at the port's coordinates from the MSW and exposure rasters, yielding (i) the port's expected sustained wind in m/s and (ii) the storm-specific exposure index above 18m/s. I also record the first observed timestamp of the storm, which serves as the shock time for this event to avoid anticipation from port authorities/firms. Ports with missing raster values are set to zero exposure for that storm.

Port-level shocks. The resulting dataset at the port $\times$ storm level is later merged to the PortWatch port data (Appendix B.2) at the daily level, and to the bill of lading data (Appendix B.1) at the monthly level. These joins yield the port-level treatment indicators used in the empirical analysis.

Table B.6: Summary Statistics - Tropical Cyclones at Ports

Desc.	Mean	10%	25%	50%	75%	90%
(a) Panjiva sample						
Per Tropical Cyclone Event						
Num. ports of lading	7.17	1.00	1.00	4.00	10.00	17.00
Windspeed (m/s)	25.61	19.48	20.95	24.32	28.76	33.59
Exposure - 18m/s (hours)	10.94	4.60	6.55	9.32	13.56	19.63
Per Port - Year						
Num. cyclones	1.62	1.00	1.00	1.00	2.00	3.00
Windspeed (m/s)	26.77	19.51	21.76	25.26	30.04	36.05
Exposure - 18m/s (hours)	11.75	3.88	6.42	9.89	15.33	21.78
(b) Portwatch sample						
Per Tropical Cyclone Event						
Num. ports of lading	4.88	1.00	1.00	3.00	7.00	10.00
Windspeed (m/s)	26.37	19.55	20.74	25.23	29.75	34.60
Exposure - 18m/s (hours)	11.63	4.71	6.83	9.67	14.56	20.71
Per Port - Year						
Num. cyclones	1.61	1.00	1.00	1.00	2.00	3.00
Windspeed (m/s)	26.91	19.55	21.72	25.51	30.03	36.34
Exposure - 18m/s (hours)	11.87	4.00	7.08	9.90	15.33	21.57

Note: The table reports summary statistics for the exposure of ports to tropical cyclones. Panel (a) reports statistics for ports recorded in the Brazilian bill of lading data. Panel (b) reports statistics for ports recorded in IMF Portwatch data. "Per Tropical Cyclone Event: Num. ports of lading" refers to the number of ports exposed to at least 18m/s of wind speed, per cyclone event. "Per Tropical Cyclone Event: Windspeed (m/s)" refers to the mean maximum sustained wind speed experienced by ports, per cyclone event. "Per Tropical Cyclone Event: Exposure - 18m/s (hours)" refers to the mean exposure of ports, measured in hours of exposition to at least 18m/s of wind speeds, per cyclone event. "Per Port - Year: Num. cyclones" refers to the number of cyclones in which the port experiences at least 18m/s of maximum sustained wind speed, per port-year. "Per Port - Year: Windspeed (m/s)" refers to the mean maximum sustained wind speed from tropical cyclones experienced by ports, per port - year. "Per Port - Year: Exposure - 18m/s (hours)" refers to the mean exposure of ports during tropical cyclones, measured in hours of exposition to at least 18m/s of wind speeds, per port-year.

B.4 Tropical Cyclones Climate – STORM

Source and coverage. I use the STORM tropical cyclone hazard dataset (Bloemendaal et al., 2020a,b), which simulates 10,000 years of synthetic storm tracks to estimate wind hazards at $\approx$ 10 km resolution. In practice, I use the global-scale `.tiff` files derived by Russel (2022).[74] The data consists of gridded *fixed return period* rasters for (i) a present-day climate (1980–2015; hereafter *baseline*) and (ii) a future climate scenarios consistent with RCP8.5/SSP5 (2015–2050). The RCP8.5 scenarios correspond to the climate simulations of several climate models: CMCC-CM2-VHR4, CNRM-CM6-1-HR, EC-Earth3P-HR, and HadGEM3-GC31-HM. For each scenario, STORM provides the maximum sustained wind speed (m/s) associated with a set of return periods $R = \{10, 20, \ldots, 10{,}000\}$ years.

Defining expected wind speed. For each grid cell g and scenario s, I compute a simple expected (annual) windspeed proxy by weighting the return-period rasters by their annual probability:

$$windspeed_g^{(s)} = \sum_{r \in R} \frac{1}{r} V_{g,r}^{(s)},$$

where $V_{g,r}^{(s)}$ is the STORM raster of maximum sustained wind (m/s) for return period r. I implement this by dividing each raster by its return period and summing across $r \in R$; missing cells are treated as zeros. For display and merging, I spatially aggregate the resulting surface to $\approx 2^\circ$ resolution.

The baseline expected wind speed field $windspeed^{(0)}$ is built from the STORM "constant" (present-day) raster. The RCP8.5 expected wind speed field $windspeed^{(\mathrm{RCP8.5})}$ is the mean of the climate models. Figures B.1a and B.1b report the respective baseline and RCP8.5 expected wind speed fields.

Port-level exposure (climate). To link climate hazards to ports, I buffer each port by 50km and extract the mean expected wind speed from the baseline and RCP8.5 rasters. Missing values in the baseline raster are set to zero before extraction; extraction uses area means over the buffer. The resulting port-level measure is denoted $CycloneRisk_p^{(s)}$ for scenario s:

$$CycloneRisk_p^{(s)} = \frac{1}{|B_{50}(p)|} \sum_{g \in B_{50}(p)} windspeed_g^{(s)},$$

where $B_{50}(p)$ is the set of grid cells within 50km of port p. I implement this both for the Panjiva-linked ports and for the IMF PortWatch global port set. The baseline and RCP8.5

[74] The data is available here.

values $CycloneRisk_p^{(0)}$ and $CycloneRisk_p^{(1)}$ are treated as port fundamentals both in the reduced-form estimation of Section 4.2 and in the structural calibration and counterfactuals of Sections 5–6.

Figure B.1: Present and future (RCP8.5) tropical cyclone climates

(a) Present-day (1980-2015)

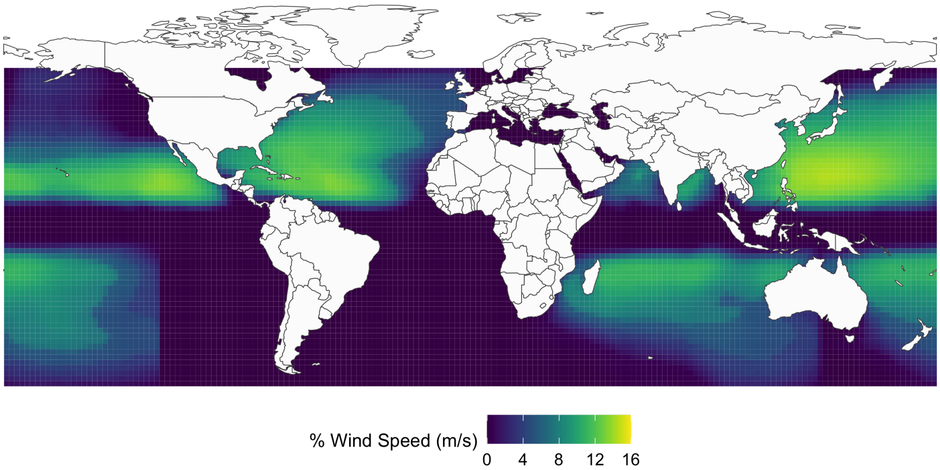

(b) RCP8.5 (2015-2050)

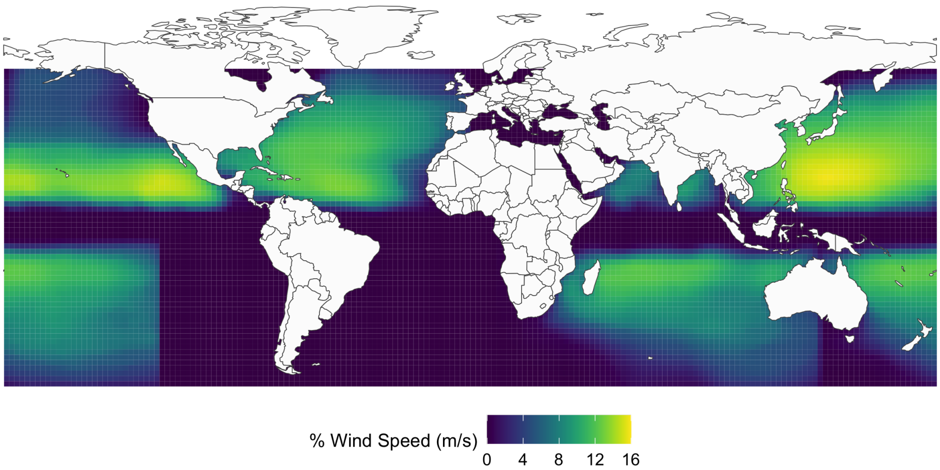

Notes: This map reports expected wind speeds (m/s) induced by tropical cyclones, in the present-day (Panel a) and the future RCP8.5 scenario (Panel b) of the STORM model.

B.5 Other data sources

Bilateral trade flows – ITPD-E. I use the International Trade and Production Database for Estimation (ITPD-E), release 1.1 (Borchert et al., 2022). The dataset reports bilateral trade values in millions of current US dollars for all sectors and country pairs. I use the 2019 cross-section. The aggregation of ITPD-E trade flows to the model's country-level bilateral matrix is documented in Appendix F.1.

Land and sea distances. Land route distances are approximated by great-circle distances between Natural Earth admin-0 country centroids. In the reduced-form regression of Section 4.2, land distances enter as the sum of two great-circle legs: from the supplier country centroid to the port of lading, and from the port of unlading to the buyer country centroid. Shortest maritime distances between ports are computed with the Eurostat `SeaRoute` program, yielding a directed port-to-port matrix with entries equal to the shortest-path length in kilometres. I also attach port-to-country distances by recording, for each port, the great-circle distance from the port's coordinates to every country centroid. The assembly of the economy-wide distance matrix for the calibration – including contiguity masking, voyage-based sparsification, and block-matrix stacking – is documented in Appendix F.1.

Vessel voyages – Global Fishing Watch. I use the Global Fishing Watch (GFW) vessel-voyage dataset (Kroodsma et al., 2018; Global Fishing Watch, 2024), covering the universe of AIS-tracked commercial vessel trips over the twelve monthly files of 2017. A voyage is a pair of (start, end) anchorage visits for a given vessel. Each voyage is tagged with an anchorage identifier drawn from the GFW named-anchorages database (v2), which records the location, the country ISO3 code, and a human-readable label/sublabel for every anchorage. I build a crosswalk from GFW anchorages to PortWatch ports by (i) restricting to dock-side anchorages and anchorages lying within 20 km of the shore, (ii) keeping, for each anchorage, the PortWatch port in the same ISO3 country within a 50 km buffer, and (iii) selecting the best candidate by Jaro–Winkler similarity between the normalized anchorage label/sublabel and the PortWatch port name or full name, with a similarity threshold of 0.80. For each origin port, I compute the empirical transit probability to each destination port as $\text{prob}_{pp'} = n_{pp'} / \sum_{\tilde{p}'} n_{p\tilde{p}'}$, where $n_{pp'}$ is the number of voyages from p to p'. The resulting sparse matrix of empirical transit probabilities drives the sparsification of the port-to-port sea-distance block in Appendix F.1.

Population and GDP per capita. For fundamentals at the country level, I use the global 1°

grid of population and GDP per capita from Rossi-Hansberg and Zhang (2025), averaged over 2012–2020. GDP per capita is expressed in constant 2017 PPP dollars. I aggregate the gridded population field to each Natural Earth admin-0 polygon by summing grid cells, yielding country population L_n. Country GDP per capita is obtained as the area-weighted mean of the grid-cell GDP per capita over the polygon. Both series are used as calibration inputs in Section 5: population L_n enters the model directly, and GDP per capita is the starting point for the balanced-trade wage fixed point of Section 5.3.

Historical population – HYDE 3.3. To proxy historical coastal population at port, I use the HYDE 3.3 global gridded population for year 1950 at 5-arc-minute resolution (Klein Goldewijk, 2024). For each port p, I build a 100km radius buffer, and extract the sum of 1950 inhabitants within the buffer. I construct a share of 1950 coastal population by normalizing this count by the total population around the estimation-sample ports. This share enters the port-traffic instrument $z^1_{p_o,t}$ of Appendix E.1, interacted with the contemporaneous country-out global PortWatch TEU traffic.

Terrain Ruggedness Index. To capture hinterland topography, I use the global Terrain Ruggedness Index based on GMTED at 30-arc-second resolution (Amatulli et al., 2018). For each port, I form a 20km radius buffer and extract the mean TRI over raster cells that fall within the buffer. The resulting port-level TRI serves as the capacity instrument $z^2_{p_o}$ in the route-level regression of Appendix E.1.

Private Participation in Infrastructure (PPI). The World Bank PPI database records individual infrastructure projects with private-sector involvement across developing and emerging economies. I extract all port-sector projects with positive total investment and a financial-close year between 2000 and 2020, retaining the project's country, financial-close year, and total investment in current USD. I then aggregate investments to the country $\times$ year level and merge them with the PortWatch port-capacity panel, yielding a country-year panel of port investments and port-level capacity measures used in the first-stage estimation of Section 7.2.2.

C Robustness and alternative specifications

C.0.1 Port-level disruptions

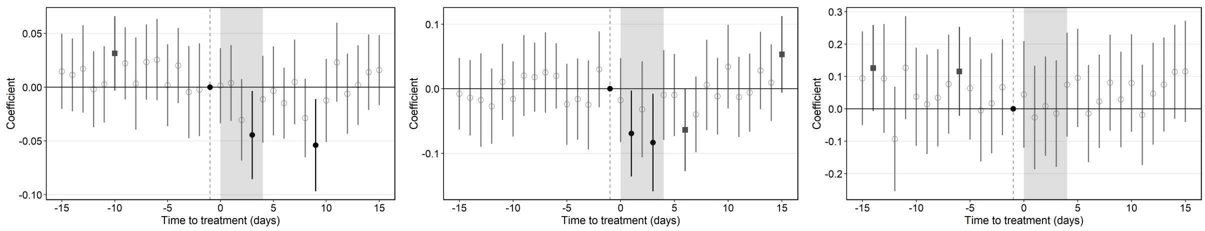

(a) Port activity (b) Log vessel count (c) Log volume (TEU)

Figure C.1: Port exposure to weak cyclones

Notes: These panels plot the effect of exposure to tropical cyclones on daily port-level outcomes, as specified by Equation (1). The sample is constructed analogously to the one in Section 2.3.1, but treatment is defined as exposure to wind speed between 9 and 18 m/s (weak cyclones), removing any port treated by wind speed above 18 m/s. The outcome in Panel C.1a is a binary variable taking the value 1 if at least one vessel entered the port on day t (port activity), and 0 otherwise. The outcome in Panel C.1b is the log number of vessels that use the port on day t, conditional on the port being active. The outcome in Panel C.1c is the log volume (TEU) transiting through the port on day t, conditional on the port being active. Standard errors are clustered at the port level. The bars correspond to 95% confidence intervals. Black dots are point estimates significant at the 5% level, gray squares are point estimates significant at the 10% level, and empty dots are point estimates non-significant at the 10% level.

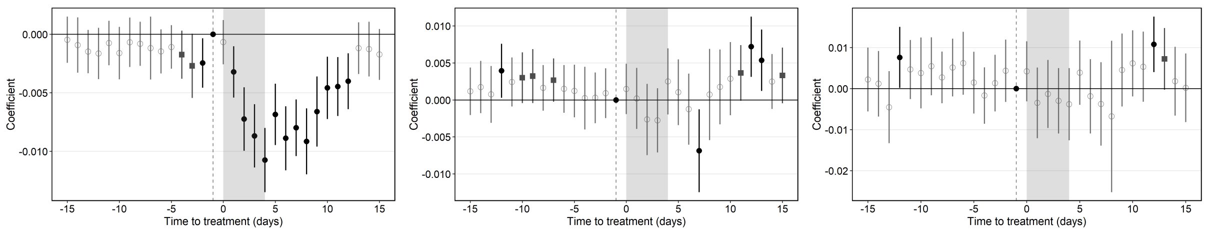

(a) Port activity (b) Log vessel count (c) Log TEU

Figure C.2: Port exposure to cyclones, continuous treatment (hours of exposure)

Notes: These panels plot the effect of exposure to tropical cyclones on daily port-level outcomes, as specified by Equation (1). The outcome in Panel C.2a is a binary variable taking the value 1 if at least one vessel entered the port on day t (port activity), and 0 otherwise. The outcome in Panel C.2b is the log number of vessels that use the port on day t, conditional on the port being active. The outcome in Panel C.2c is the log volume (TEU) transiting through the port on day t, conditional on the port being active. Standard errors are clustered at the port level. The bars correspond to 95% confidence intervals. Black dots are point estimates significant at the 5% level, gray squares at the 10% level, and empty dots are non-significant at the 10% level.

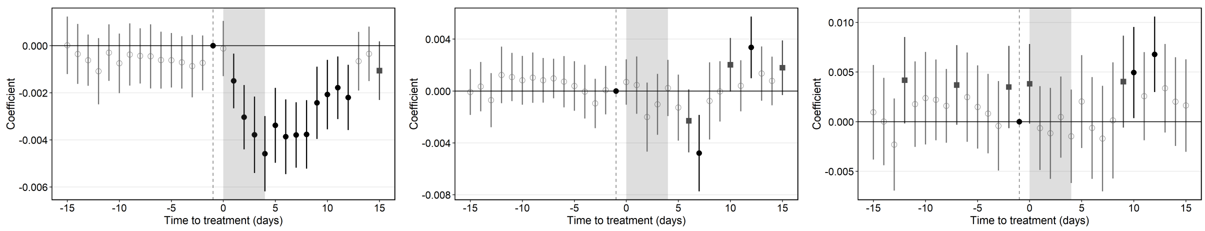

(a) Port activity (b) Log vessel count (c) Log TEU

Figure C.3: Port exposure to cyclones, continuous treatment (wind speed m/s)

Notes: These panels plot the effect of exposure to tropical cyclones on daily port-level outcomes, as specified by Equation (1). The outcome in Panel C.3a is a binary variable taking the value 1 if at least one vessel entered the port on day t (port activity), and 0 otherwise. The outcome in Panel C.3b is the log number of vessels that use the port on day t, conditional on the port being active. The outcome in Panel C.3c is the log volume (TEU) transiting through the port on day t, conditional on the port being active. Standard errors are clustered at the port level. The bars correspond to 95% confidence intervals. Black dots are point estimates significant at the 5% level, gray squares at the 10% level, and empty dots are non-significant at the 10% level.

C.0.2 Route choice

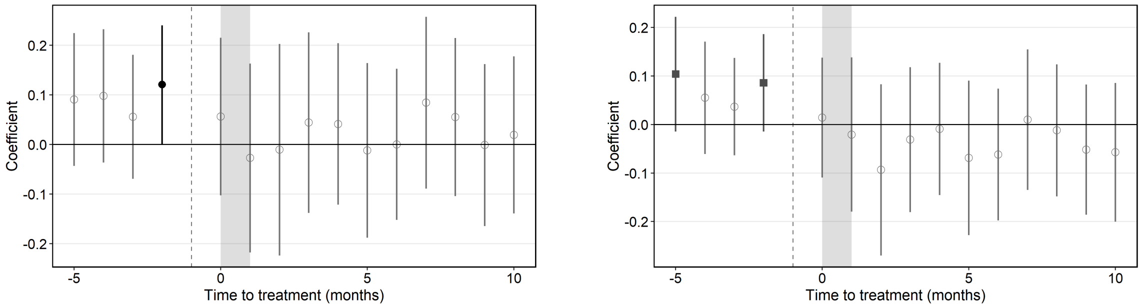

(a) Log weight (kg)

(b) Log # shipments

Figure C.4: Exposure to cyclones & route choice (additional intensive margins)

Notes: These panels plot the effect of port exposure to tropical cyclones on monthly firm-to-firm–route-level outcomes, as specified by Equation (2). The outcome in Panel C.4a is the log of total weight (kg) shipped through route r in month t, conditional on the relationship–route being active. The outcome in Panel C.4b is the log number of shipments through route r in month t, conditional on the relationship–route being active. Regressions include relationship–month fixed effects, and control for time dummies interacted with relationship-routes' pre-treatment characteristics. Standard errors are clustered at the relationship level. The bars show 95% confidence intervals. Black dots indicate point estimates significant at the 5% level, gray squares at the 10% level, and empty dots denote estimates that are not significant at the 10% level.

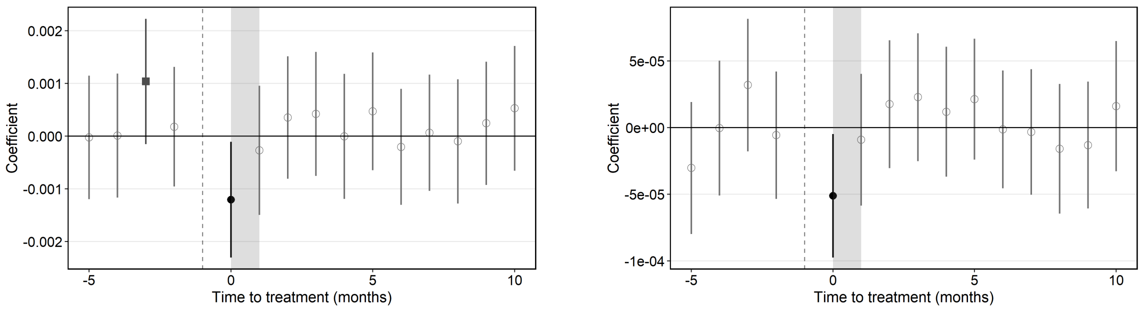

(a) Route activity, windspeed (m/s)

(b) Route activity, exposure (hours)

Figure C.5: Exposure to cyclones & route choice, continuous treatments

Notes: These panels plot the effect of port exposure to tropical cyclones on monthly firm-to-firm–route-level outcomes, as specified by Equation (2). In Panel C.5a, the treatment variable is interacted with the windspeed (in m/s) experienced by the exposed port. In Panel C.5b, the treatment variable is interacted with the number of hours of exposure to at least 18 m/s experienced by the exposed port.The outcome in both panels is a binary variable equal to 1 if at least one shipment is observed for the trading pair through route r in month t (active route), and 0 otherwise. Regressions include relationship–month fixed effects, and control for time dummies interacted with relationship-routes' pre-treatment characteristics. Standard errors are clustered at the relationship level. The bars show 95% confidence intervals. Black dots indicate point estimates significant at the 5% level, gray squares at the 10% level, and empty dots denote estimates that are not significant at the 10% level.

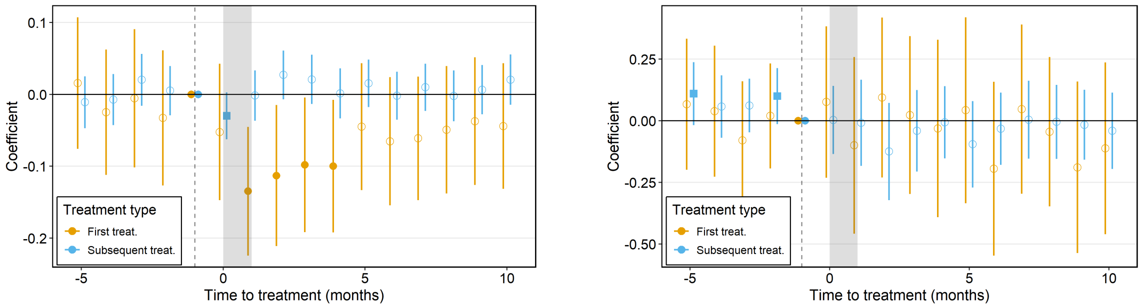

(a) Route activity

(b) Log # shipments

Figure C.6: Exposure to cyclones & route choice (first vs. subsequent treatments)

Notes: These panels plot the effect of port exposure to tropical cyclones on monthly firm-to-firm-route-level outcomes, as specified by Equation (2). The treatment variable is interacted with two indicator variables, taking value 1 if the treatment is respectively (i) the first treatment experienced by the relationship (b, s), or (ii) a subsequent treatment. The outcome in Panel C.6a is a binary variable equal to 1 if at least one shipment is observed for the trading pair through route r in month t (active route), and 0 otherwise. The outcome in Panel C.6b is the log number of shipments of the relationship using route r in month t, conditional on the relationship-route being active. Regressions include relationship–month fixed effects, and control for time dummies interacted with relationship-routes' pre-treatment characteristics. Standard errors are clustered at the relationship level. The bars correspond to 95% confidence intervals. Black dots are point estimates significant at the 5% level, gray squares are point estimates significant at the 10% level, and empty dots are point estimates non-significant at the 10% level.

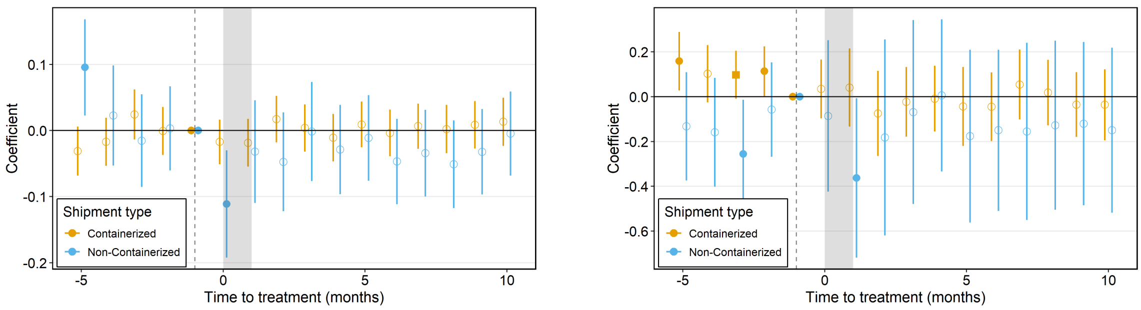

(a) Route activity

(b) Log # shipments

Figure C.7: Exposure to cyclones & route choice (by good type)

Notes: These panels plot the effect of port exposure to tropical cyclones on monthly firm-to-firm-route-level outcomes, as specified by Equation (2). The treatment variable is interacted with two indicator variables, taking value 1 if the relationship-route traded respectively (i) only containerized goods, or (ii) at least one non-containerized good, in the 5-month period preceding the shock. The outcome in Panel C.7a is a binary variable equal to 1 if at least one shipment is observed for the trading pair through route r in month t (active route), and 0 otherwise. The outcome in Panel C.7b is the log number of shipments of the relationship using route r in month t, conditional on the relationship-route being active. Regressions include relationship–month fixed effects, and control for time dummies interacted with relationship-routes' pre-treatment characteristics. Standard errors are clustered at the relationship level. The bars correspond to 95% confidence intervals. Black dots are point estimates significant at the 5% level, gray squares are point estimates significant at the 10% level, and empty dots are point estimates non-significant at the 10% level.

C.0.3 Firm-to-firm disruptions

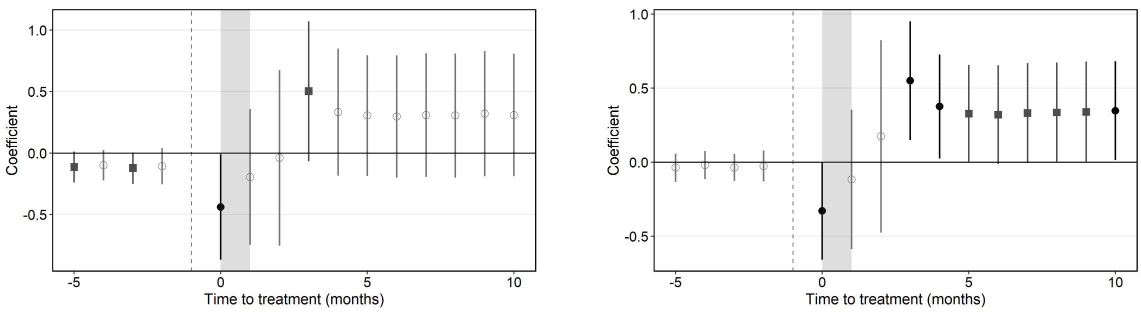

(a) Log weight (kg)

(b) Log volume (TEU)

Figure C.8: Exposure to cyclones & firm-to-firm relationship (additional intensive margins)

Notes: These panels plot the effect of port exposure to tropical cyclones on monthly firm-to-firm-level outcomes, as specified by Equation (3). The outcome in Panel C.8a is the log total weight shipped by the relationship, conditional on the relationship being active. The outcome in Panel C.8b is the log total volume shipped by the relationship, conditional on the relationship being active. Regressions include buyer–time and supplier–time fixed effects, and control for time dummies interacted with relationships' pre-treatment characteristics. Standard errors are clustered at the buyer level. The bars denote 95% confidence intervals. Black dots indicate point estimates significant at the 5% level, gray squares at the 10% level, and empty dots denote non-significant estimates at the 10% level.

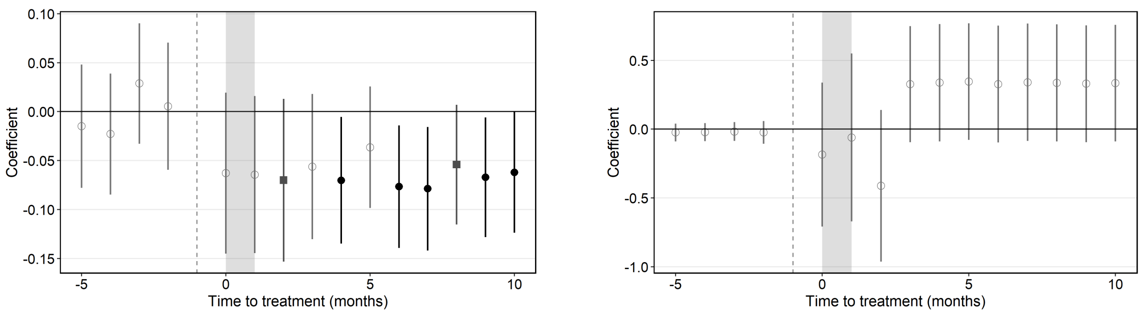

(a) Relationship activity

(b) Log # shipments

Figure C.9: Exposure to cyclones & firm-to-firm relationship (continuous treatment)

Notes: These panels plot the effect of port exposure to tropical cyclones on monthly firm-to-firm-level outcomes, as specified by Equation (3). The treatment variable is interacted with share of buyers' trade transiting through affected routes during the pre-treatment period (measured by the number of shipments). The outcome in Panel C.9a is a binary variable, taking the value 1 if at least one shipment is observed for the trading pair at month t (active relationship), and 0 otherwise. Relationship activity is conditioned on the entry of both the buyer and the supplier. The outcome in Panel C.9b is the log number of shipments by the relationship, conditioning on activity. Regressions include buyer–time and supplier–time fixed effects, and control for time dummies interacted with relationships' pre-treatment characteristics. Standard errors are clustered at the buyer level. The bars correspond to 95% confidence intervals. Black dots are point estimates significant at the 5% level, gray squares are point estimates significant at the 10% level, and empty dots are point estimates non-significant at the 10% level.

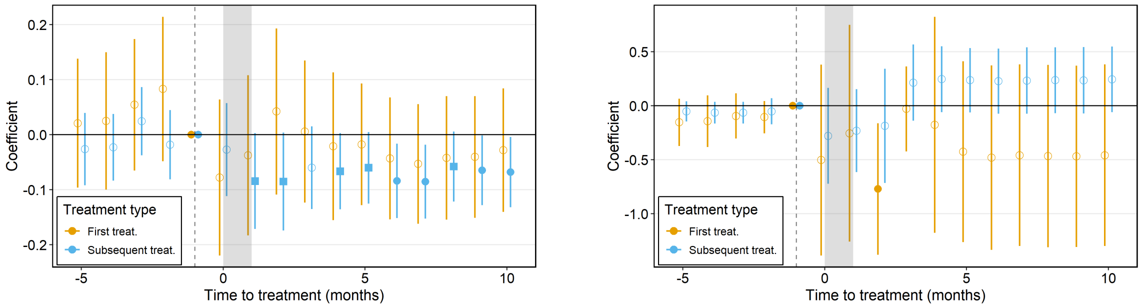

(a) Relationship activity

(b) Log # shipments

Figure C.10: Exposure to cyclones & firm-to-firm relationship (first vs. subsequent treatments)

Notes: These panels plot the effect of port exposure to tropical cyclones on monthly firm-to-firm-level outcomes, as specified by Equation (3). The treatment variable is interacted with two indicator variables, taking value 1 if the treatment is respectively (i) the first treatment experienced by the relationship (b, s), or (ii) a subsequent treatment. The outcome in Panel C.10a is a binary variable equal to 1 if at least one shipment is observed for the trading pair in month t (active relationship), and 0 otherwise. Relationship activity is conditioned on the entry of both the buyer and the supplier. The outcome in Panel C.10b is the log number of shipments by the relationship, conditional on activity. Regressions include buyer–time and supplier–time fixed effects, and control for time dummies interacted with relationships' pre-treatment characteristics. Standard errors are clustered at the buyer level. The bars correspond to 95% confidence intervals. Black dots are point estimates significant at the 5% level, gray squares are point estimates significant at the 10% level, and empty dots are point estimates non-significant at the 10% level.

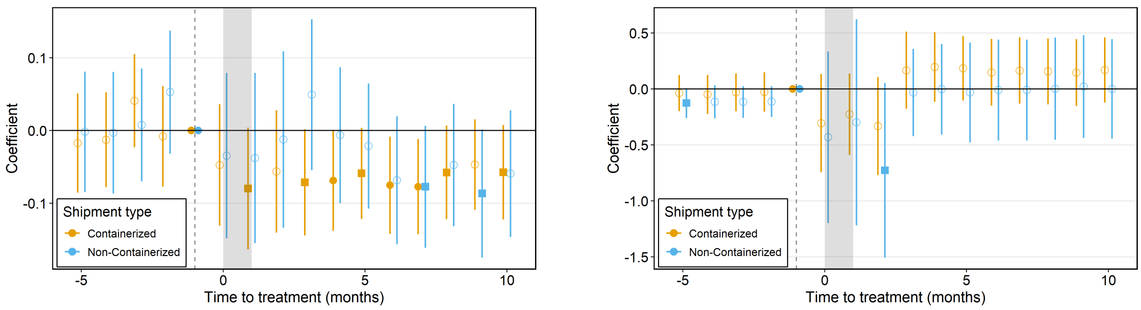

(a) Relationship activity

(b) Log # shipments

Figure C.11: Port exposure to cyclones & firm-to-firm relationship (by good type)

Notes: These panels plot the effect of port exposure to tropical cyclones on monthly firm-to-firm-level outcomes, as specified by Equation (3). The treatment variable is interacted with two indicator variables, taking value 1 if the relationship shipped respectively (i) only containerized goods, or (ii) at least one non-containerized good, in the 5-month period preceding the shock. The outcome in Panel C.11a is a binary variable equal to 1 if at least one shipment is observed for the trading pair in month t (active relationship), and 0 otherwise. Relationship activity is conditioned on the entry of both the buyer and the supplier. The outcome in Panel C.11b is the log number of shipments by the relationship, conditional on activity. Regressions include buyer–time and supplier–time fixed effects, and control for time dummies interacted with relationships' pre-treatment characteristics. Standard errors are clustered at the buyer level. The bars correspond to 95% confidence intervals. Black dots are point estimates significant at the 5% level, gray squares are point estimates significant at the 10% level, and empty dots are point estimates non-significant at the 10% level.

D Theory

D.1 Proofs

Proof: Proposition 1. Denote by $\lambda_j(\phi, r) = \frac{c_j}{z(\phi)} \prod_{k=1}^{|\mathcal{B}_r|} d_{r_{k-1},r_k} \prod_{m=1}^{|\mathcal{P}_r|} t_{p(r)_m}$ the *effective* costs of using input from supplier j in technique ϕ, along route r. Consider the probability that the effective cost of supplier $j \in M_{n'}$ available to $i \in M_n$ through route r is strictly lower than a threshold λ,

$$P(\lambda_j(\phi, r) \leq \lambda) = P\left(\frac{c_j}{z(\phi)} \prod_{k=1}^{|\mathcal{B}_r|} d_{r_{k-1},r_k} \prod_{m=1}^{|\mathcal{P}_r|} t_{p(r)_m} \leq \lambda\right) = F_r(\lambda).$$

Integrating F_r over realizations of z and $t_{p(r)_1}, \cdots, t_{p(r)_M}$, we obtain that the number of potential suppliers that deliver effective cost weakly less than λ through route r follows a Poisson distribution with mean

$$\begin{aligned}
\Lambda_{jr} &= \int_0^\infty \left[\int_1^\infty \cdots \int_1^\infty F_r(\lambda) dF_{p(r)_1}(\theta) \cdots dF_{p(r)_M}(\theta)\right] dF_r(z) \\
&= \int_0^\infty \left[\int_1^\infty \cdots \int_1^\infty \left[\int_0^\infty \mathbb{1}\left(\frac{c_j}{z(\phi)} \prod_{k=1}^{|\mathcal{B}_r|} d_{r_{k-1},r_k} \prod_{m=1}^{|\mathcal{P}_r|} t_{p(r)_m} \leq \lambda\right) dF_{n'}(c_j)\right] dF_{p(r)_1}(\theta) \cdots dF_{p(r)_M}(\theta)\right] \xi a_{n'} z^{-\xi-1} dz \\
&= a_{n'} \lambda^\xi \prod_{k=1}^{|\mathcal{B}_r|} d_{r_{k-1},r_k}^{-\xi} \int_0^\infty \left[\int_1^\infty \cdots \int_1^\infty \left[\int_0^\infty \mathbb{1}\left(c_j \leq u\right) dF_{n'}(c_j)\right] \prod_{m=1}^{|\mathcal{P}_r|} t_{p(r)_m}^{-\xi} dF_{p(r)_1}(\theta) \cdots dF_{p(r)_M}(\theta)\right] \xi u^{-\xi-1} du \\
&= a_{n'} \lambda^\xi \prod_{k=1}^{|\mathcal{B}_r|} d_{r_{k-1},r_k}^{-\xi} \left[\int_1^\infty \int_1^\infty \cdots \int_1^\infty \left[\int_0^\infty c_j^{-\xi} dF_{n'}(c_j)\right] \prod_{m=1}^{|\mathcal{P}_r|} t_{p(r)_m}^{-\xi} dF_{p(r)_1}(\theta) \cdots dF_{p(r)_M}(\theta)\right] \xi s^{-\xi-1} ds \\
&= a_{n'} \lambda^\xi \bar{c}_j^{-\xi} \prod_{k=1}^{|\mathcal{B}_r|} d_{r_{k-1},r_k}^{-\xi} \prod_{m=1}^{|\mathcal{P}_r|} \bar{t}_{p(r)_m}^{-\xi},
\end{aligned} \tag{D.1}$$

where

$$\bar{c}_j^{-\xi} = \int_0^\infty c_j^{-\xi} dF_{n'}(c_j) \quad \text{and} \quad \bar{t}_{p(r)_m}^{-\xi} = \int_1^\infty t_{p(r)_m}^{-\xi} dF_{p(r)_m}(\theta) \tag{D.2}$$

The second equality follows when applying the transformation

$$z\lambda / \left(\prod_{k=1}^{|\mathcal{B}_r|} d_{r_{k-1},r_k} \prod_{m=1}^{|\mathcal{P}_r|} t_{p(r)_m}\right) = u,$$

while the third equality follows when applying the transformation $u/c_j = s$. Therefore, number of potential suppliers along route r that deliver effective cost strictly greater than λ is such that:

$$P(\lambda_j(\phi, r) > \lambda) = e^{-\Lambda_{jr}} = e^{-a_{n'} \lambda^\xi \bar{c}_j^{-\xi} \prod_{k=1}^{|\mathcal{B}_r|} d_{r_{k-1},r_k}^{-\xi} \prod_{m=1}^{|\mathcal{P}_r|} \bar{t}_{p(r)_m}^{-\xi}}. \tag{D.3}$$

Consider now the cost distribution of firm $i \in M_n$ with a supplier $j \in M_{n'}$ along route r. Using the marginal cost of firm i, one obtains

$$\begin{aligned}
P\left(c_i(\phi, r) > c\right) &= P\left(\frac{w_n^{1-\alpha}}{a_n}\left(\tau_{n(i)n(j)}(r)\frac{c_j}{z(\phi)}\right)^{\alpha} > c\right) \\
&= P\left(\lambda_j(\phi, r) > \left(a_n w_n^{\alpha-1} c\right)^{\frac{1}{\alpha}}\right) \\
&= exp\left[-\left(a_{n'} c^{\frac{\xi}{\alpha}}\left(a_n w_n^{\alpha-1}\right)^{\frac{\xi}{\alpha}} \prod_{k=1}^{|\mathcal{B}_r|} d_{r_{k-1},r_k}^{-\xi} \prod_{m=1}^{|\mathcal{P}_r|} \bar{t}_{p(r)_m}^{-\xi} \bar{c}_j^{-\xi}\right)\right].
\end{aligned} \tag{D.4}$$

Then the probability that firm i's minimal cost from sourcing from n' through route r is higher than a threshold, $P\left(c_i(\phi, r)_{\min,r} > c\right)$ is as follows:

$$\begin{aligned}
P\left(c_i(\phi, r)_{\min,r} > c\right) &= P\left(\lambda_j(\phi, r)_{\min,r} > \left(a_n w_n^{\alpha-1} c\right)^{\frac{1}{\alpha}}\right) \\
&= exp\left[-a_{n'} c^{\frac{\xi}{\alpha}}\left(a_n w_n^{\alpha-1}\right)^{\frac{\xi}{\alpha}} \prod_{k=1}^{|\mathcal{B}_r|} d_{r_{k-1},r_k}^{-\xi} \prod_{m=1}^{|\mathcal{P}_r|} \bar{t}_{p(r)_m}^{-\xi} \bar{c}_{n'}^{-\xi}\right].
\end{aligned} \tag{D.5}$$

Consider finally the minimum cost at which firm i can produce (sourcing from any supplier through any route $r \in \mathcal{R}$), given realizations of a_n:

$$\begin{aligned}
P(c_i(\phi, r)_{\min,r\in\mathcal{R}} > c) &= \prod_{r\in\mathcal{R}} P\left(c_i(\phi, r)_{\min,r} > c\right) \\
&= \prod_{r\in\mathcal{R}} exp\left[-a_{n'} c^{\frac{\xi}{\alpha}}\left(a_n w_n^{\alpha-1}\right)^{\frac{\xi}{\alpha}} \prod_{k=1}^{|\mathcal{B}_r|} d_{r_{k-1},r_k}^{-\xi} \prod_{m=1}^{|\mathcal{P}_r|} \bar{t}_{p(r)_m}^{-\xi} \bar{c}_{n'}^{-\xi}\right] \\
&= exp\left[-\left(a_n w_n^{\alpha-1}\right)^{\frac{\xi}{\alpha}}\left(\sum_{n'} a_{n'} \bar{c}_{n'}^{-\xi} \sum_{r\in\mathcal{R}_{n'n}} \prod_{k=1}^{|\mathcal{B}_r|} d_{r_{k-1},r_k}^{-\xi} \prod_{m=1}^{|\mathcal{P}_r|} \bar{t}_{p(r)_m}^{-\xi}\right) c^{\frac{\xi}{\alpha}}\right].
\end{aligned} \tag{D.6}$$

which is Weibull distributed. It remains to characterize $\bar{c}_n$ and $\bar{\theta}_r$, both moments of the respective marginal cost and trade cost distributions. Consider first

$$\begin{aligned}
\bar{c}_n^{-\xi} &= \int_0^{\infty} c^{-\xi} d\left\{1 - exp\left[-\left(a_n w_n^{\alpha-1}\right)^{\frac{\xi}{\alpha}}\left(\sum_{n'} a_{n'} \bar{c}_{n'}^{-\xi} \sum_{r\in\mathcal{R}_{n'n}} \prod_{k=1}^{|\mathcal{B}_r|} d_{r_{k-1},r_k}^{-\xi} \prod_{m=1}^{|\mathcal{P}_r|} \bar{t}_{p(r)_m}^{-\xi}\right) c^{\frac{\xi}{\alpha}}\right]\right\} \\
&= a_n^{\xi} w_n^{(\alpha-1)\xi}\left(\sum_{n'} a_{n'} \bar{c}_{n'}^{-\xi} \sum_{r\in\mathcal{R}_{n'n}} \prod_{k=1}^{|\mathcal{B}_r|} d_{r_{k-1},r_k}^{-\xi} \prod_{m=1}^{|\mathcal{P}_r|} \bar{t}_{p(r)_m}^{-\xi}\right)^{\alpha} \int_0^{\infty} u^{-\xi} d\left\{1 - exp\left[-u^{\frac{\xi}{\alpha}}\right]\right\} \\
&= a_n^{\xi} w_n^{(\alpha-1)\xi}\left(\sum_{n'} a_{n'} \bar{c}_{n'}^{-\xi} \sum_{r\in\mathcal{R}_{nn'}} \prod_{k=1}^{|\mathcal{B}_r|} d_{r_{k-1},r_k}^{-\xi} \prod_{m=1}^{|\mathcal{P}_r|} \bar{t}_{p(r)_m}^{-\xi}\right)^{\alpha} \int_0^{\infty} v^{-\alpha} d\left\{1 - e^{-v}\right\} \\
&= a_n^{\xi} w_n^{(\alpha-1)\xi}\left(\sum_{n'} a_{n'} \bar{c}_{n'}^{-\xi} \sum_{r\in\mathcal{R}_{n'n}} \prod_{k=1}^{|\mathcal{B}_r|} d_{r_{k-1},r_k}^{-\xi} \prod_{m=1}^{|\mathcal{P}_r|} \bar{t}_{p(r)_m}^{-\xi}\right)^{\alpha} \int_0^{\infty} v^{-\alpha} e^{-v} dv \\
&= a_n^{\xi} w_n^{(\alpha-1)\xi}\left(\sum_{n'} a_{n'} \bar{c}_{n'}^{-\xi} \sum_{r\in\mathcal{R}_{n'n}} \prod_{k=1}^{|\mathcal{B}_r|} d_{r_{k-1},r_k}^{-\xi} \prod_{m=1}^{|\mathcal{P}_r|} \bar{t}_{p(r)_m}^{-\xi}\right)^{\alpha} \Gamma\left(1-\alpha\right).
\end{aligned} \tag{D.7}$$

The second equality follows from applying the transformation

$$a_n w_n^{\alpha-1}\left(\sum_{n'} a_{n'}\bar{c}_{n'}^{-\xi} \sum_{r\in\mathcal{R}_{n'n}} \prod_{k=1}^{|\mathcal{B}_r|} d_{r_{k-1},r_k}^{-\xi} \prod_{m=1}^{|\mathcal{P}_r|} \bar{t}_{p(r)_m}^{-\xi}\right)^{\frac{\alpha}{\xi}} c = u.$$

The third equality follows from applying the transformation $v = u^{\frac{\xi}{\alpha}}$.

Moreover, $\bar{t}_{p(r)_m}^{-\xi}$ follows immediately from its definition and the Pareto assumptions on its distribution:

$$\begin{aligned}
\bar{t}_{p(r)_m}^{-\xi} &= \int_1^\infty t_{p(r)_m}^{-\xi} dF_{p(r)_m}(\theta) \\
&= \int_1^\infty t_{p(r)_m}^{-\xi} d\{1-\theta^{-\psi_{p(r)m}}\} \\
&= t(\Xi, K_p)^{-\xi}\frac{\psi_{p(r)_m}}{\psi_{p(r)_m}+\xi}.
\end{aligned} \tag{D.8}$$

Proof: Corollary 1. From the cost distribution of firm $i \in M_{n'}$ sourcing from route r, the number of suppliers located in n and using route r available to firm i in region n', such that i achieves a cost below c is distributed Poisson with parameter

$$\rho_{i,r} = a_n c^{\frac{\xi}{\alpha}}\left(a_{n'}w_{n'}^{\alpha-1}\right)^{\frac{\xi}{\alpha}} \prod_{k=1}^{|\mathcal{B}_r|} d_{r_{k-1},r_k}^{-\xi} \prod_{m=1}^{|\mathcal{P}_r|} \bar{t}_{p(r)_m}^{-\xi}\bar{c}_n^{-\xi}. \tag{D.9}$$

Moreover, from the cost distribution of firm $i \in M_{n'}$ sourcing from any route, the number of suppliers available to firm i from any route, such that i achieves a cost below c is distributed Poisson with parameter

$$\rho_i = \left(a_{n'}w_{n'}^{\alpha-1}\right)^{\frac{\xi}{\alpha}}\left(\sum_{\tilde{n}} a_{\tilde{n}}\bar{c}_{\tilde{n}}^{-\xi} \sum_{r\in\mathcal{R}_{\tilde{n}n'}} \prod_{k=1}^{|\mathcal{B}_r|} d_{r_{k-1},r_k}^{-\xi} \prod_{m=1}^{|\mathcal{P}_r|} \bar{t}_{p(r)_m}^{-\xi}\right) c^{\frac{\xi}{\alpha}}. \tag{D.10}$$

The probability that a firm i in location n (able to deliver costs below c) supplies from location n' through route r is the ratio of $\rho_{i,r}$ and ρ_i:

$$\begin{aligned}
\pi_{i,r} &= \frac{a_n c^{\frac{\xi}{\alpha}}\left(a_{n'}w_{n'}^{\alpha-1}\right)^{\frac{\xi}{\alpha}} \prod_{k=1}^{|\mathcal{B}_r|} d_{r_{k-1},r_k}^{-\xi} \prod_{m=1}^{|\mathcal{P}_r|} \bar{t}_{p(r)_m}^{-\xi}\bar{c}_n^{-\xi}}{\left(a_{n'}w_{n'}^{\alpha-1}\right)^{\frac{\xi}{\alpha}}\left(\sum_{\tilde{n}} a_{\tilde{n}}\bar{c}_{\tilde{n}}^{-\xi}\sum_{r\in\mathcal{R}_{\tilde{n}n}} \prod_{k=1}^{|\mathcal{B}_r|} d_{r_{k-1},r_k}^{-\xi} \prod_{m=1}^{|\mathcal{P}_r|} \bar{t}_{p(r)_m}^{-\xi}\right) c^{\frac{\xi}{\alpha}}} \\
&= \frac{a_n\bar{c}_n^{-\xi} \prod_{k=1}^{|\mathcal{B}_r|} d_{r_{k-1},r_k}^{-\xi} \prod_{m=1}^{|\mathcal{P}_r|} \bar{t}_{p(r)_m}^{-\xi}}{\sum_{\tilde{n}} a_{\tilde{n}}\bar{c}_{\tilde{n}}^{-\xi}\sum_{r\in\mathcal{R}_{\tilde{n}n}} \prod_{k=1}^{|\mathcal{B}_r|} d_{r_{k-1},r_k}^{-\xi} \prod_{m=1}^{|\mathcal{P}_r|} \bar{t}_{p(r)_m}^{-\xi}}
\end{aligned} \tag{D.11}$$

Note that the probability of sourcing from r is the same for any firm in n'. Since there are a continuum of firms in n', $\pi_{i,r}$ is also the *bilateral trade share* of route r in the total absorption of goods of destination n', denoted $\pi_{n',r}$.

Proof: Corollary 2

$$\begin{aligned}\pi_{nn'} &= \sum_{r\in\mathcal{R}_{nn'}} \pi_{n',r} \\ &= \frac{a_n \bar{c}_n^{-\xi} \tau_{nn'}^{-\xi}}{\sum_{\tilde{n}} a_{\tilde{n}} \bar{c}_{\tilde{n}}^{-\xi} \tau_{n\tilde{n}}^{-\xi}}\end{aligned} \tag{D.12}$$

where

$$\tau_{nn'} = \left(\sum_{r\in\mathcal{R}_{nn'}} \left(\prod_{k=1}^{|\mathcal{B}_r|} d_{r_{k-1},r_k}^{-\xi}\right)\left(\prod_{m=1}^{|\mathcal{P}_r|} \bar{t}_{p(r)_m}^{-\xi}\right)\right)^{-\frac{1}{\xi}} \tag{D.13}$$

Proof. Proposition 2. Define welfare in location d as:

$$\begin{aligned}V_n &= \frac{L_n(w_n + \Pi_n)}{\left(\int_{i\in M_n} p_i^{1-\sigma} di\right)^{\frac{1}{1-\sigma}}} \\ &= \frac{L_n w_n \tilde{\sigma}}{\left(\int_{i\in M_n} (\tilde{\sigma} c_i)^{1-\sigma} di\right)^{\frac{1}{1-\sigma}}} \\ &= \frac{L_n w_n}{\left(M_n \int c^{1-\sigma} dF_i(c)\right)^{\frac{1}{1-\sigma}}}\end{aligned} \tag{D.14}$$

It remains to characterize $\int c^{1-\sigma} dF_i(c)$:

$$\begin{aligned}\int c^{1-\sigma} dF_i(c) &= \int_0^\infty c^{1-\sigma} d\left\{1 - exp\left[-\left(a_n w_n^{\alpha-1}\right)^{\frac{\xi}{\alpha}} \left(\sum_{n'} a_{n'} \bar{c}_{n'}^{-\xi} \sum_{r\in\mathcal{R}_{n'n}} \prod_{k=1}^{|\mathcal{B}_r|} d_{r_{k-1},r_k}^{-\xi} \prod_{m=1}^{|\mathcal{P}_r|} \bar{t}_{p(r)_m}^{-\xi}\right) c^{\frac{\xi}{\alpha}}\right]\right\} \\ &= \int_0^\infty c^{1-\sigma} d\left\{1 - exp\left[-\left(a_n w_n^{\alpha-1}\right)^{\frac{\xi}{\alpha}} \left(\sum_{n'} a_{n'} \bar{c}_{n'}^{-\xi} \tau_{n'n}^{-\xi}\right) c^{\frac{\xi}{\alpha}}\right]\right\} \\ &= \left[a_n w_n^{\alpha-1} \left(\sum_{n'} a_{n'} \bar{c}_{n'}^{-\xi} \tau_{n'n}^{-\xi}\right)^{\frac{\alpha}{\xi}}\right]^{\sigma-1} \int_0^\infty u^{1-\sigma} d\left\{1 - exp\left[-u^{\frac{\xi}{\alpha}}\right]\right\} \\ &= \left[a_n w_n^{\alpha-1} \left(\sum_{n'} a_{n'} \bar{c}_{n'}^{-\xi} \tau_{n'n}^{-\xi}\right)^{\frac{\alpha}{\xi}}\right]^{\sigma-1} \int_0^\infty v^{-\frac{\alpha(\sigma-1)}{\xi}} d\left\{1 - e^{-v}\right\} \\ &= \left[a_n w_n^{\alpha-1} \left(\sum_{n'} a_{n'} \bar{c}_{n'}^{-\xi} \tau_{n'n}^{-\xi}\right)^{\frac{\alpha}{\xi}}\right]^{\sigma-1} \int_0^\infty v^{-\frac{\alpha(\sigma-1)}{\xi}} e^{-v} dv \\ &= \left[a_n w_n^{\alpha-1} \left(\sum_{n'} a_{n'} \bar{c}_{n'}^{-\xi} \tau_{n'n}^{-\xi}\right)^{\frac{\alpha}{\xi}}\right]^{\sigma-1} \Gamma\left(1 - \frac{\alpha(\sigma-1)}{\xi}\right),\end{aligned} \tag{D.15}$$

The third equality follows from applying the transformation $a_n w_n^{\alpha-1} \left(\sum_{n'} a_{n'} \bar{c}_{n'}^{-\xi} \tau_{n'n}^{-\xi}\right)^{\frac{\alpha}{\xi}} c = u$.

The fourth equality follows from applying the transformation $v = u^{\frac{\xi}{\alpha}}$. The sixth equality follows from the definition of the Gamma function $\Gamma(z) = \int_0^\infty t^{z-1}e^{-t}dt$. Therefore, assuming a unit measure of firms in each region, welfare writes:

$$V_n = L_n w_n \left[a_n w_n^{\alpha-1} \left(\sum_{n'} a_{n'} \bar{c}_{n'}^{-\xi} \tau_{n'n}^{-\xi} \right)^{\frac{\alpha}{\xi}} \right]^{\sigma-1} \Gamma\left(1 - \frac{\alpha(\sigma-1)}{\xi}\right) \tag{D.16}$$

D.2 Closing the model

Labor market clearing: Labor demand for a firm i in location n is given by $l_i = (1-\alpha)y_i c_i / w_n$. Plugging this condition into the labor market clearing gives:

$$L_n = \int_{i \in M_n} l_i di \Rightarrow \frac{w_n L_n}{1-\alpha} = \int_{i\in M_n} y_i c_i di. \tag{D.17}$$

Good market clearing:

$$y_i = L_n q_i + \sum_{n'} \int_{j \in M_{n'}} \tau_{n(j)n(j)} x_{ij} dj, \quad x_{ij} = x_j \times \mathbf{1}\{i = i^*\} \tag{D.18}$$

Multiplying both sides by marginal costs c_j and aggregating over firms in $M_{n'}$:

$$\underbrace{\int_{i\in M_n} c_i y_i di}_{\text{(1) Supply}} = \underbrace{L_n \int_{i\in M_n} c_i q_i di}_{\text{(2) Final good demand}} + \underbrace{\int_{i\in M_n} c_i \left[\sum_{n'} \int_{j\in M_{n'}} \tau_{n(i)n(j)} (x_j \times \mathbf{1}\{i = i^*\}) dj \right] di}_{\text{(3) Intermediate input demand}}. \tag{D.19}$$

Term (1) simplifies using the labor market clearing condition, $\int_{i\in M_n} c_i y_i di = w_n L_n/(1-\alpha)$. Term (2) simplifies as follows: With isoelastic preferences and monopolistic competition, households in region n demand $q_j = q_n p_n^\sigma p_j^{-\sigma}$, where $p_i = c_i \frac{\sigma}{\sigma-1}$. Realizing that $q_n = (w_n + \Pi_n)/p_n$, where w_n is the wage rate and Π_n is the per-capita profits of firms in n rebated to labor, implies:

$$\begin{aligned} L_n \int_{i\in M_n} c_i q_i di &= L_n (w_n + \Pi_n) p_n^{\sigma-1} \left(\frac{\sigma}{\sigma-1}\right)^{-\sigma} \int_{i\in M_n} c_i^{1-\sigma} di \\ &= L_n(w_n + \Pi_n) \left(\left(\int_{i\in M_n} p_i^{1-\sigma} di \right)^{\frac{1}{1-\sigma}} \right)^{\sigma-1} \left(\frac{\sigma}{\sigma-1}\right)^{-\sigma} \int_{i\in M_n} c_i^{1-\sigma} di \\ &= L_n(w_n+\Pi_n) \left(\frac{\sigma}{\sigma-1}\right)^{-1} \left(\int_{i\in M_n} c_i^{1-\sigma} di \right)^{-1} \int_{i\in M_n} c_i^{1-\sigma} di \\ &= L_n (w_n + \Pi_n) \tilde{\sigma}^{-1}. \end{aligned} \tag{D.20}$$

[Note: term (2) simplifies also easily when considering that $q_n p_n = \int_{i\in M_n} \tilde{\sigma} c_i q_i di$, where $\tilde{\sigma} = \sigma/(\sigma-1)$, and $q_n p_n = w_n + \Pi_n$.] It remains to characterize per-capita profit rebated to households in region n. Note that firms only gain profits from selling final goods to local households:

$$\text{Profit}_i = p_i q_i L_n - c_i q_i L_n. \tag{D.21}$$

Therefore, total profit per capita (aggregating over all firms in M_n) yields:

$$
\begin{aligned}
\Pi_n &= L_n^{-1} \int_{i \in M_n} L_n (p_i q_i - c_i q_i) di \\
&= \int_{i \in M_n} (\tilde{\sigma} c_i q_i - c_i q_i) di \\
&= (\tilde{\sigma} - 1) \int_{i \in M_n} c_i q_i di \\
&= (\tilde{\sigma} - 1) \tilde{\sigma}^{-1} q_n p_n \\
&= \frac{1}{\sigma} (w_n + \Pi_n).
\end{aligned}
\tag{D.22}
$$

Solving for per-capita profits yields $\Pi_n = \frac{w_n}{\sigma - 1}$. Therefore, term (2) simplifies to:

$$
\begin{aligned}
L_n \int_{i \in M_n} c_i q_i di &= L_n \left(w_n + \frac{w_n}{\sigma - 1} \right) \tilde{\sigma}^{-1} \\
&= L_n w_n.
\end{aligned}
\tag{D.23}
$$

Term (3) simplifies as follows: Firms demand $x_j = \frac{(1-\alpha) y_j c_j}{c_i \tau_{n(i)n(j)}}$ units of intermediate inputs. This implies:

$$
\begin{aligned}
\int_{i \in M_n} c_i \left(\sum_{n'} \int_{j \in M_{n'}} \tau_{nn'} (x_j \times \mathbf{1}\{i = i^*\}) dj \right) di &= \alpha \int_{i \in M_n} \left(\sum_{n'} \int_{j \in M_{n'}} \mathbf{1}\{i = i^*\} y_j c_j dj \right) di \\
&= \alpha \sum_{n'} \int_{j \in M_{n'}} \mathbf{1}\{i^* \in M_n\} y_j c_j dj \\
&= \alpha \sum_{n'} \pi_{nn'} \int_{j \in M_{n'}} y_j c_j dj \\
&= \alpha \sum_{n'} \pi_{nn'} \frac{w_{n'} L_{n'}}{1 - \alpha}
\end{aligned}
\tag{D.24}
$$

Putting terms (1), (2) and (3) together yields the following system for region-level wages:

$$
w_n L_n = \sum_{n'} \pi_{nn'} w_{n'} L_{n'}. \tag{D.25}
$$

Finally, to obtain traffic, we recover the value of bilateral flows (i.e. the level of expenditures from firms in n' to firms in n):

$$
\begin{aligned}
X_{nn'} &= \int_{i \in M_n} \int_{j \in M_{n'}} c_i \tau_{nn'} (x_j \times \mathbf{1}\{i = i^*\}) dj di \\
&= \alpha \int_{i \in M_n} \int_{j \in M_{n'}} \mathbf{1}\{i = i^*\} y_j c_j dj di \\
&= \alpha \int_{j \in M_{n'}} \mathbf{1}\{i^* \in M_n\} y_j c_j dj \\
&= \alpha \pi_{nn'} \int_{j \in M_{n'}} y_j c_j dj \\
&= \alpha \pi_{nn'} \frac{w_{n'} L_{n'}}{1 - \alpha}
\end{aligned}
\tag{D.26}
$$

D.3 General equilibrium: definition

Given a geography $\mathcal{G} = \{\mathcal{N}, \mathcal{P}, \mathcal{L}, \mathcal{M}, \mathcal{A}, \mathcal{D}, \mathcal{K}, \Psi\}$ and a set of model parameters $\{\sigma, \alpha, \xi, \lambda_1, \lambda_2, \lambda_3, \kappa_d, \kappa_p\}$, an equilibrium is defined as a distribution of wages and factory-gate prices $\{w_n, \bar{c}_n\}_{n \in \mathcal{N}}$, such that:

1. Given the equilibrium transportation network $\delta_{ll'} \in \{\delta_{ll'}\}_{l,l' \in \mathcal{N} \cup \mathcal{P} \times \mathcal{N} \cup \mathcal{P}}$, (i) consumers maximize utility; (ii) firms choose the techniques and the routes that minimize costs, and markups that maximize profits; and (iii) markets clear.[75]

2. Given the transportation network fundamentals $\{\mathcal{D}, \mathcal{K}\}$ and equilibrium prices, the equilibrium transportation network $\delta_{ll'} \in \{\delta_{ll'}\}_{l,l' \in \mathcal{N} \cup \mathcal{P} \times \mathcal{N} \cup \mathcal{P}}$ is determined by the equilibrium levels of traffic $\{\Xi_p\}$.

This leads the equilibrium to be characterized by the following set of equations:[76]

$$w_n L_n = \sum_{n'} \pi_{nn'} \, w_{n'} L_{n'} \qquad \text{(wage bill)} \tag{D.27}$$

$$\pi_{nn'} = \frac{a_n \bar{c}_n^{-\xi} \, \tau_{nn'}^{-\xi}}{\sum_{\tilde{n}} a_{\tilde{n}} \bar{c}_{\tilde{n}}^{-\xi} \, \tau_{\tilde{n}n'}^{-\xi}} \qquad \text{(bilateral trade shares)} \tag{D.28}$$

$$\bar{c}_n^{-\xi} = a_n^{\xi} \, w_n^{(\alpha-1)\xi} \left(\sum_{\tilde{n}} a_{\tilde{n}} \bar{c}_{\tilde{n}}^{-\xi} \, \tau_{\tilde{n}n}^{-\xi} \right)^{\alpha} \Gamma(1-\alpha) \qquad \text{(factory-gate cost indices)} \tag{D.29}$$

$$\tau_{nn'}^{-\xi} = \begin{cases} 1 & n = n' \\ \left[(\mathbf{I} - \mathbf{\Delta})^{-1} \right]_{nn'} & n \neq n' \end{cases} \qquad \text{(transportation costs)} \tag{D.30}$$

$$\mathbf{\Delta} = [\delta_{ll'}], \quad \delta_{ll'} = \begin{cases} 0 & l = l' \text{ or } l \not\sim l' \\ d_{ll'}^{-\xi} \, \bar{t}_{l'}^{-\xi} & l \sim l', \; l' \in \mathcal{P} \\ d_{ll'}^{-\xi} & l \sim l', \; l' \notin \mathcal{P} \end{cases} \qquad \text{(resistance matrix)} \tag{D.31}$$

$$d_{ll'}^{-\xi} = \kappa_d \, \epsilon_{ll'}^{\lambda_1}, \quad \bar{t}_p^{-\xi} = \kappa_p \, \Xi_p^{\lambda_2} \, K_p^{\lambda_3} \, \frac{\psi_p}{\psi_p + \xi} \qquad \text{(link- and port-level costs)} \tag{D.32}$$

$$\Xi_p = \sum_{n} \sum_{n' \neq n} \frac{\tau_{np}^{-\xi} \, \tau_{pn'}^{-\xi}}{\tau_{nn'}^{-\xi}} X_{nn'} \qquad \text{(port traffic)} \tag{D.33}$$

$$X_{nn'} = \frac{\alpha}{1-\alpha} \pi_{nn'} w_{n'} L_{n'} \qquad \text{(bilateral trade volumes)} \tag{D.34}$$

---

[75] Formally, the economy admits ports as locations. However, I assume that ports have a zero measure of households and firms, such that they do not consume or produce. It follows that equilibrium prices have dimension $|\mathcal{N}|$, while the transportation network has dimensions $(|\mathcal{N}| + |\mathcal{P}|)^2$.

[76] Up to a numeraire: $w_1 = 1$.

D.4 WELFARE ELASTICITY

Proof: Proposition 3. Recall that the general equilibrium of the model is characterised by set of equations described in Appendix D.3. Consider the region-level welfare function (Proposition 2):

$$V_n = L_n w_n \left[a_n w_n^{\alpha-1} \left(\sum_{n'} a_{n'} \bar{c}_{n'}^{-\xi} \tau_{n'n}^{-\xi} \right)^{\frac{\alpha}{\xi}} \right]^{\sigma-1} \Gamma\left(1 - \frac{\alpha(\sigma-1)}{\xi}\right). \tag{D.35}$$

Collecting constants, write

$$V_n = L_n\, w_n^{\beta_w}\, \mathcal{T}_n^{\beta_\tau}\, C_n, \tag{D.36}$$

where

$$C_n = a_n^{\sigma-1}\Gamma\left(1-\frac{\alpha(\sigma-1)}{\xi}\right), \qquad \beta_w = 1+(\alpha-1)(\sigma-1), \qquad \beta_\tau = \frac{\alpha(\sigma-1)}{\xi},$$

are constants, and $\mathcal{T}_n = \sum_{n'} a_{n'}\bar{c}_{n'}^{-\xi}\tau_{n'n}^{-\xi}$ is the market-access term. Recalling that $\pi_{n'n} = a_{n'}\bar{c}_{n'}^{-\xi}\tau_{n'n}^{-\xi}/\mathcal{T}_n$, log-differentiating Equation (D.36) gives

$$\frac{\partial \log V_n}{\partial \log K_p} = \beta_w \underbrace{\frac{\partial \log w_n}{\partial \log K_p}}_{(1)} + \beta_\tau \sum_{n'} \pi_{n'n} \left[-\xi \underbrace{\frac{\partial \log \bar{c}_{n'}}{\partial \log K_p}}_{(2)} - \xi \underbrace{\frac{\partial \log \tau_{n'n}}{\partial \log K_p}}_{(3)} \right]. \tag{D.37}$$

I derive each term in turn.

(1) Wage elasticity. Log-differentiating the wage bill Equation (D.27), using $X_{nn'} = \frac{\alpha}{1-\alpha}\pi_{nn'}w_{n'}L_{n'}$:

$$w_n L_n \frac{\partial \log w_n}{\partial \log K_p} = \frac{1-\alpha}{\alpha} \sum_{n'} X_{nn'} \left[\frac{\partial \log \pi_{nn'}}{\partial \log K_p} + \frac{\partial \log w_{n'}}{\partial \log K_p} \right]. \tag{D.38}$$

Log-differentiating the trade share $\pi_{nn'}$ in Equation (D.28):

$$\frac{\partial \log \pi_{nn'}}{\partial \log K_p} = -\xi \left[\frac{\partial \log \bar{c}_n}{\partial \log K_p} + \frac{\partial \log \tau_{nn'}}{\partial \log K_p} \right] + \xi \sum_{\tilde{n}} \pi_{\tilde{n}n'} \left[\frac{\partial \log \bar{c}_{\tilde{n}}}{\partial \log K_p} + \frac{\partial \log \tau_{\tilde{n}n'}}{\partial \log K_p} \right]. \tag{D.39}$$

Substituting Equation (D.39) into Equation (D.38) yields

$$\frac{\partial \log w_n}{\partial \log K_p} = \frac{1-\alpha}{\alpha w_n L_n} \sum_{n'} X_{nn'} \left[-\xi \left[\frac{\partial \log \bar{c}_n}{\partial \log K_p} + \frac{\partial \log \tau_{nn'}}{\partial \log K_p} \right] + \xi \sum_{\tilde{n}} \pi_{\tilde{n}n'} \left[\frac{\partial \log \bar{c}_{\tilde{n}}}{\partial \log K_p} + \frac{\partial \log \tau_{\tilde{n}n'}}{\partial \log K_p} \right] + \frac{\partial \log w_{n'}}{\partial \log K_p} \right]. \tag{D.40}$$

The normalization $w_1 = 1$ implies $g_{1,p}^{(w)} \equiv 0$; Equation (D.40) is therefore solved for $n = 2, \ldots, N$ only.

(2) Factory-gate cost elasticity. Log-differentiating Equation (D.29):

$$-\frac{\partial \log \bar{c}_n}{\partial \log K_p} = (\alpha - 1)\frac{\partial \log w_n}{\partial \log K_p} + \frac{\alpha}{\xi}\frac{\partial \log \mathcal{T}_n}{\partial \log K_p}$$

$$= (\alpha-1)\frac{\partial \log w_n}{\partial \log K_p} - \alpha \sum_{n'} \pi_{n'n}\left[\frac{\partial \log \bar{c}_{n'}}{\partial \log K_p} + \frac{\partial \log \tau_{n'n}}{\partial \log K_p}\right], \tag{D.41}$$

where the second line uses $\partial \log \mathcal{T}_n/\partial \log K_p = -\xi \sum_{n'} \pi_{n'n}[\partial \log \bar{c}_{n'}/\partial \log K_p + \partial \log \tau_{n'n}/\partial \log K_p]$.

(3) Transportation cost elasticity. Define $\mathbf{B} = (\mathbf{I}-\mathbf{\Delta})^{-1}$, so that $\tau_{ll'}^{-\xi} = B_{ll'}$ for $l \neq l'$. Differentiating the identity $(\mathbf{I}-\mathbf{\Delta})\mathbf{B} = \mathbf{I}$ gives the standard result

$$\frac{\partial \mathbf{B}}{\partial \log K_p} = \mathbf{B}\left(\frac{\partial \mathbf{\Delta}}{\partial \log K_p}\right)\mathbf{B}. \tag{D.42}$$

Element-wise,

$$\frac{\partial B_{ll'}}{\partial \log K_p} = \sum_i \sum_j B_{li}\left(\frac{\partial \delta_{ij}}{\partial \log K_p}\right) B_{jl'}. \tag{D.43}$$

Since $\partial \delta_{ij}/\partial \log K_p = 0$ for $j \notin \mathcal{P}$:

$$\frac{\partial \log B_{ll'}}{\partial \log K_p} = \frac{1}{B_{ll'}} \sum_i \sum_{j\in\mathcal{P}} B_{li}\left(\frac{\partial \delta_{ij}}{\partial \log K_p}\right) B_{jl'}. \tag{D.44}$$

With $\delta_{ll'} = d_{ll'}^{-\xi}\bar{t}_{l'}^{-\xi}$ for $l' \in \mathcal{P}$ and $\bar{t}_p^{-\xi} = \kappa_p\, \Xi_p^{\lambda_2} K_p^{\lambda_3} \psi_p/(\psi_p+\xi)$:

$$\frac{\partial \delta_{ij}}{\partial \log K_p} = \delta_{ij}\left(\lambda_3\, \mathbf{1}_{j=p} + \lambda_2 \frac{\partial \log \Xi_j}{\partial \log K_p}\right). \tag{D.45}$$

Substituting Equation (D.45) into Equation (D.44) yields

$$\frac{\partial \log B_{ll'}}{\partial \log K_p} = \sum_{j\in\mathcal{P}}\left(\lambda_3 \mathbf{1}_{j=p} + \lambda_2 \frac{\partial \log \Xi_j}{\partial \log K_p}\right)\frac{(\mathbf{B\Delta})_{lj}\, B_{jl'}}{B_{ll'}}. \tag{D.46}$$

Now, since $\mathbf{B\Delta} = \mathbf{B}-\mathbf{I}$, we have $(\mathbf{B\Delta})_{lj} = B_{lj} - \mathbf{1}_{l=j}$, which equals B_{lj} whenever $l \neq j$. Using the routing kernel

$$\Theta_{q|ll'} \equiv \begin{cases} 0 & l = l' \\ \dfrac{B_{lq}\, B_{ql'}}{B_{ll'}} & l \neq l' \end{cases}, \qquad \Theta \in \mathbb{R}^{N\times N\times P}, \quad \Theta_p \in \mathbb{R}^{N\times N}. \tag{D.47}$$

The restriction $\Theta_{q|ll} = 0$ reflects the domestic cost normalization $\tau_{ll} = 1$: domestic transactions use the direct route and do not transit through port infrastructure.

Equation Equation (D.46) becomes, for **general** locations l, l':

$$\frac{\partial \log \tau_{ll'}}{\partial \log K_p} = -\frac{1}{\xi}\sum_{q\in\mathcal{P}}\left(\lambda_3\, \mathbf{1}_{q=p} + \lambda_2 \frac{\partial \log \Xi_q}{\partial \log K_p}\right)\left[\Theta_{q|ll'} - \frac{\delta_{lq}\, B_{ql'}}{B_{ll'}}\right]. \tag{D.48}$$

When $l \notin \mathcal{P}$ (in particular when l is a region), $\delta_{lq} = 0$ for all $q \in \mathcal{P}$ and Equation (D.48) reduces to

$$\frac{\partial \log \tau_{ll'}}{\partial \log K_p} = -\frac{\lambda_3}{\xi}\Theta_{p|ll'} - \frac{\lambda_2}{\xi}\sum_{q\in\mathcal{P}} \Theta_{q|ll'} \frac{\partial \log \Xi_q}{\partial \log K_p} \qquad (l \notin \mathcal{P}). \tag{D.49}$$

This simplified form is the only one needed in the wage block Equation (D.40), the cost block Equation (D.41), and the welfare formula Equation (D.37), because all transport costs there run between *regions*. When $l \in \mathcal{P}$ – specifically $l = p'$, a port – the Kronecker term δ_{lq} is non-zero for $q = p'$, producing an extra **self-correction**:

$$-\xi \frac{\partial \log \tau_{p'l'}}{\partial \log K_p} = \lambda_3 \Theta_{p|p'l'} + \lambda_2 \sum_{q \in \mathcal{P}} \Theta_{q|p'l'} \frac{\partial \log \Xi_q}{\partial \log K_p} - \left(\lambda_3 \mathbf{1}_{p'=p} + \lambda_2 \frac{\partial \log \Xi_{p'}}{\partial \log K_p} \right). \tag{D.50}$$

This distinction matters in the traffic block, where $\partial \log \tau_{p'n'} / \partial \log K_p$ appears explicitly. $\Theta_{p|ll'}$ is the probability that the least-cost path from l to l' passes through port p.

(4) Traffic elasticity. Port traffic is

$$\Xi_{p'} = \sum_n \sum_{n' \neq n} \Theta_{p'|nn'} X_{nn'}, \qquad \Theta_{p'|nn'} = (\tau_{np'} \tau_{p'n'} \tau_{nn'}^{-1})^{-\xi}. \tag{D.51}$$

Define the bilateral traffic weights

$$\omega_{p',nn'} = \frac{\Theta_{p'|nn'} X_{nn'}}{\Xi_{p'}}, \qquad \sum_n \sum_{n'} \omega_{p',nn'} = 1. \tag{D.52}$$

Log-differentiating Equation (D.51):

$$\frac{\partial \log \Xi_{p'}}{\partial \log K_p} = \sum_n \sum_{n'} \omega_{p',nn'} \left[\frac{\partial \log \Theta_{p'|nn'}}{\partial \log K_p} + \frac{\partial \log X_{nn'}}{\partial \log K_p} \right]. \tag{D.53}$$

Routing kernel term. From $\Theta_{p'|nn'} = (\tau_{np'} \tau_{p'n'} / \tau_{nn'})^{-\xi}$ and equations Equation (D.49)–Equation (D.50). Note that $\tau_{np'}$ has origin $n \in \mathcal{N}$ so the simplified form Equation (D.49) applies, while $\tau_{p'n'}$ has origin $p' \in \mathcal{P}$ so the corrected form Equation (D.50) is required:

$$\begin{aligned} \frac{\partial \log \Theta_{p'|nn'}}{\partial \log K_p} &= -\xi \frac{\partial \log \tau_{np'}}{\partial \log K_p} - \xi \frac{\partial \log \tau_{p'n'}}{\partial \log K_p} + \xi \frac{\partial \log \tau_{nn'}}{\partial \log K_p} \\ &= \lambda_3 \left[\Theta_{p|np'} + \Theta_{p|p'n'} - \Theta_{p|nn'} \right] + \lambda_2 \sum_{\tilde{p} \in \mathcal{P}} \left[\Theta_{\tilde{p}|np'} + \Theta_{\tilde{p}|p'n'} - \Theta_{\tilde{p}|nn'} \right] \frac{\partial \log \Xi_{\tilde{p}}}{\partial \log K_p} \\ &\quad \underbrace{- \left(\lambda_3 \mathbf{1}_{p'=p} + \lambda_2 \frac{\partial \log \Xi_{p'}}{\partial \log K_p} \right)}_{\text{self-correction from Equation (D.50)}}. \end{aligned} \tag{D.54}$$

Trade volume term. From $X_{nn'} = \frac{\alpha}{1-\alpha} \pi_{nn'} w_{n'} L_{n'}$ and Equation (D.39):

$$\begin{aligned} \frac{\partial \log X_{nn'}}{\partial \log K_p} &= \frac{\partial \log \pi_{nn'}}{\partial \log K_p} + \frac{\partial \log w_{n'}}{\partial \log K_p} \\ &= -\xi \frac{\partial \log \bar{c}_n}{\partial \log K_p} + \lambda_3 \Theta_{p|nn'} + \lambda_2 \sum_{\tilde{p}} \Theta_{\tilde{p}|nn'} \frac{\partial \log \Xi_{\tilde{p}}}{\partial \log K_p} \end{aligned}$$

$$
+ \xi \sum_{\tilde{n}} \pi_{\tilde{n}n'} \frac{\partial \log \bar{c}_{\tilde{n}}}{\partial \log K_p} - \sum_{\tilde{n}} \pi_{\tilde{n}n'} \left[\lambda_3 \Theta_{p|\tilde{n}n'} + \lambda_2 \sum_{\tilde{p}} \Theta_{\tilde{p}|\tilde{n}n'} \frac{\partial \log \Xi_{\tilde{p}}}{\partial \log K_p} \right] + \frac{\partial \log w_{n'}}{\partial \log K_p}. \tag{D.55}
$$

Compact form. Define

$$
\Delta_{np'n',p} = \Theta_{p|np'} + \Theta_{p|p'n'} - \sum_{\tilde{n}} \pi_{\tilde{n}n'} \Theta_{p|\tilde{n}n'}. \tag{D.56}
$$

Substituting Equation (D.54) and Equation (D.55) into Equation (D.53) and collecting terms by their unknown elasticities. The self-correction in Equation (D.54) contributes $-(\lambda_3 \mathbf{1}_{p'=p} + \lambda_2 g^{(\Xi)}_{p',p})$ inside the ω-weighted sum; since $\sum_n \sum_{n'} \omega_{p',nn'} = 1$, this passes through as an additive constant:

$$
\begin{aligned}
\frac{\partial \log \Xi_{p'}}{\partial \log K_p} = \sum_n \sum_{n'} \omega_{p',nn'} \Bigg[& \lambda_3 \Delta_{np'n',p} + \lambda_2 \sum_{\tilde{p} \in \mathcal{P}} \Delta_{np'n',\tilde{p}} \frac{\partial \log \Xi_{\tilde{p}}}{\partial \log K_p} + \xi \left(\sum_{\tilde{n}} \pi_{\tilde{n}n'} \frac{\partial \log \bar{c}_{\tilde{n}}}{\partial \log K_p} - \frac{\partial \log \bar{c}_n}{\partial \log K_p} \right) + \frac{\partial \log w_{n'}}{\partial \log K_p} \Bigg] \\
& - \lambda_3 \mathbf{1}_{p'=p} - \lambda_2 \frac{\partial \log \Xi_{p'}}{\partial \log K_p}.
\end{aligned} \tag{D.57}
$$

Moving the last term to the left-hand side gives $(1 + \lambda_2)\, g^{(\Xi)}_{p',p}$ on the left, which shifts the diagonal of the traffic-block coefficient matrix by $-\lambda_2$ (see Equation (D.66)).

D.5 The linear system in matrix form.

Notation. I collect the three vectors of unknown elasticities:

$$
\begin{aligned}
\boldsymbol{g}_w &= \{ g^{(w)}_{n,p} \}_{n \in \mathcal{N}} \in \mathbb{R}^N, & g^{(w)}_{n,p} &\equiv \frac{\partial \log w_n}{\partial \log K_p}, \\
\boldsymbol{g}_\Xi &= \{ g^{(\Xi)}_{p',p} \}_{p' \in \mathcal{P}} \in \mathbb{R}^P, & g^{(\Xi)}_{p',p} &\equiv \frac{\partial \log \Xi_{p'}}{\partial \log K_p}, \\
\boldsymbol{g}_c &= \{ g^{(c)}_{n,p} \}_{n \in \mathcal{N}} \in \mathbb{R}^N, & g^{(c)}_{n,p} &\equiv \frac{\partial \log \bar{c}_n}{\partial \log K_p}.
\end{aligned}
$$

All three vectors depend on the single capacity shock $\mathrm{d} \log K_p$, so for a given port p each is a column vector; the full stacked solution is $\boldsymbol{x} = [\boldsymbol{g}_w^\top\ \boldsymbol{g}_\Xi^\top\ \boldsymbol{g}_c^\top]^\top \in \mathbb{R}^{2N+P}$.

Auxiliary matrices. I define auxiliary matrices built from equilibrium objects $\{\pi_{nn'}, X_{nn'}, \Theta_{p|nn'}, \omega_{p',nn'}, B_n$

$$
\mathbf{Z}^{(1)} \in \mathbb{R}^{N \times P}, \qquad Z^{(1)}_{n,p} = \left[(\boldsymbol{\Pi} \odot \boldsymbol{\Theta}_p)^\top \mathbf{1}_N \right]_n = \sum_{n'} \pi_{n'n} \Theta_{p|n'n} \tag{D.58}
$$

$$
\mathbf{Z}^{(2)} \in \mathbb{R}^{N \times P}, \qquad Z^{(2)}_{n,p} = \sum_{n'} \left[X_{nn'} \Theta_{p|nn'} - X_{nn'} \sum_{\tilde{n}} \pi_{\tilde{n}n'} \Theta_{p|\tilde{n}n'} \right] \tag{D.59}
$$

$$
\mathbf{Z}^{(3)} \in \mathbb{R}^{P \times N}, \qquad Z^{(3)}_{p',n'} = \sum_{n} \omega_{p',nn'} \tag{D.60}
$$

$$\mathbf{Z}^{(4)} \in \mathbb{R}^{P\times P}, \qquad Z^{(4)}_{p',p} = \sum_n \sum_{n'} \omega_{p',nn'}\, \Delta_{np'n',p} \tag{D.61}$$

$$\mathbf{Z}^{(5)} \in \mathbb{R}^{P\times N}, \qquad Z^{(5)}_{p',\tilde{n}} = \sum_n \sum_{n'} \omega_{p',nn'}\, \pi_{\tilde{n}n'} \tag{D.62}$$

$$\mathbf{Z}^{(6)} \in \mathbb{R}^{P\times N}, \qquad Z^{(6)}_{p',n} = \sum_{n'} \omega_{p',nn'} \tag{D.63}$$

where $\mathbf{\Pi} = [\pi_{nn'}] \in \mathbb{R}^{N\times N}$, $\mathbf{X} = [X_{nn'}] \in \mathbb{R}^{N\times N}$, and $\odot$ denotes the Hadamard (element-wise) product.

THREE SUB-SYSTEMS. *Cost block* (from Equation (D.41), rearranged):

$$\underbrace{(\alpha-1)\mathbb{I}_N}_{\mathbf{A}_{cw}} \boldsymbol{g}_w + \underbrace{\frac{\alpha\lambda_2}{\xi}\mathbf{Z}^{(1)}}_{\mathbf{A}_{c\Xi}} \boldsymbol{g}_\Xi + \underbrace{\left(\mathbb{I}_N - \alpha\mathbf{\Pi}^\top\right)}_{\mathbf{A}_{cc}} \boldsymbol{g}_c = \underbrace{-\frac{\alpha\lambda_3}{\xi}\mathbf{Z}^{(1)}_{\cdot p}}_{\boldsymbol{b}_c}, \tag{D.64}$$

where $\mathbf{Z}^{(1)}_{\cdot p} \in \mathbb{R}^N$ denotes the p-th column of $\mathbf{Z}^{(1)}$.

Wage block (from Equation (D.40), rearranged):

$$\underbrace{\left[\operatorname{diag}(\boldsymbol{w}\odot\boldsymbol{L}) - \tfrac{1-\alpha}{\alpha}\mathbf{X}\right]}_{\mathbf{A}_{ww}} \boldsymbol{g}_w + \underbrace{\lambda_2\tfrac{1-\alpha}{\alpha}\mathbf{Z}^{(2)}}_{\mathbf{A}_{w\Xi}} \boldsymbol{g}_\Xi + \underbrace{\left[-\xi\tfrac{1-\alpha}{\alpha}\left(\operatorname{diag}(\mathbf{X}\mathbf{1}_N) - \mathbf{X}\mathbf{\Pi}^\top\right)\right]}_{\mathbf{A}_{wc}} \boldsymbol{g}_c = \underbrace{\lambda_3\tfrac{1-\alpha}{\alpha}\mathbf{Z}^{(2)}_{\cdot p}}_{\boldsymbol{b}_w}. \tag{D.65}$$

where $\mathbf{Z}^{(2)}_{\cdot p} \in \mathbb{R}^N$ denotes the p-th column of $\mathbf{Z}^{(2)}$. The normalization $w_1 = 1$ is imposed by setting $g^{(w)}_{1,p} = 0$ and replacing row 1 of $\mathbf{A}_{ww}$ with $\boldsymbol{e}_1^\top = [1, 0, \ldots, 0]$ and zeroing the corresponding entries of $\mathbf{A}_{w\Xi}$, $\mathbf{A}_{wc}$, and $\boldsymbol{b}_w$.

Traffic block (from Equation (D.57), rearranged). After absorbing the self-correction $-\lambda_2\, g^{(\Xi)}_{p'}$ from Equation (D.57) into the left-hand side, the diagonal of the coefficient matrix shifts by $-\lambda_2$:

$$\underbrace{-\mathbf{Z}^{(3)}}_{\mathbf{A}_{\Xi w}} \boldsymbol{g}_w + \underbrace{\left((1-\lambda_2)\mathbb{I}_P - \lambda_2\mathbf{Z}^{(4)}\right)}_{\mathbf{A}_{\Xi\Xi}} \boldsymbol{g}_\Xi + \underbrace{(-\xi)\left(\mathbf{Z}^{(5)} - \mathbf{Z}^{(6)}\right)}_{\mathbf{A}_{\Xi c}} \boldsymbol{g}_c = \underbrace{\lambda_3\left(\mathbf{Z}^{(4)}_{\cdot p} - \boldsymbol{e}_p\right)}_{\boldsymbol{b}_\Xi}, \tag{D.66}$$

where $\mathbf{Z}^{(4)}_{\cdot p} \in \mathbb{R}^P$ is the p-th column of $\mathbf{Z}^{(4)}$ and $\boldsymbol{e}_p \in \mathbb{R}^P$ is the p-th standard basis vector.

STACKED SYSTEM. Stacking the three blocks gives the $(2N+P)\times(2N+P)$ linear system:

$$\underbrace{\begin{bmatrix} \mathbf{A}_{ww} & \mathbf{A}_{w\Xi} & \mathbf{A}_{wc} \\ \mathbf{A}_{\Xi w} & \mathbf{A}_{\Xi\Xi} & \mathbf{A}_{\Xi c} \\ \mathbf{A}_{cw} & \mathbf{A}_{c\Xi} & \mathbf{A}_{cc} \end{bmatrix}}_{\mathbf{A}\ \in\ \mathbb{R}^{(2N+P)\times(2N+P)}} \underbrace{\begin{bmatrix} \boldsymbol{g}_w \\ \boldsymbol{g}_\Xi \\ \boldsymbol{g}_c \end{bmatrix}}_{\boldsymbol{x}\ \in\ \mathbb{R}^{2N+P}} = \underbrace{\begin{bmatrix} \boldsymbol{b}_w \\ \boldsymbol{b}_\Xi \\ \boldsymbol{b}_c \end{bmatrix}}_{\boldsymbol{b}\ \in\ \mathbb{R}^{2N+P}}. \tag{D.67}$$

Table D.1 summarises the dimensions and definitions of all blocks.

Table D.1: Block decomposition of the linear system $\mathbf{A}\boldsymbol{x} = \boldsymbol{b}$.

Block	Size	Expression	Economic content
$\mathbf{A}_{ww}$	$N \times N$	$\mathrm{diag}(\boldsymbol{w} \odot \boldsymbol{L}) - \frac{1-\alpha}{\alpha}\mathbf{X}$	Own-wage effect on wage bill
$\mathbf{A}_{w\Xi}$	$N \times P$	$\lambda_2 \frac{1-\alpha}{\alpha}\mathbf{Z}^{(2)}$	Traffic congestion $\rightarrow$ wages
$\mathbf{A}_{wc}$	$N \times N$	$-\xi\frac{1-\alpha}{\alpha}[\mathrm{diag}(\mathbf{X}\mathbf{1}_N) - \mathbf{X}\mathbf{\Pi}^\top]$	Factory costs $\rightarrow$ wages
$\mathbf{A}_{\Xi w}$	$P \times N$	$-\mathbf{Z}^{(3)}$	Wages $\rightarrow$ traffic
$\mathbf{A}_{\Xi\Xi}$	$P \times P$	$(1-\lambda_2)\mathbb{I}_P - \lambda_2\mathbf{Z}^{(4)}$	Traffic $\rightarrow$ traffic (congestion)
$\mathbf{A}_{\Xi c}$	$P \times N$	$-\xi(\mathbf{Z}^{(5)} - \mathbf{Z}^{(6)})$	Factory costs $\rightarrow$ traffic
$\mathbf{A}_{cw}$	$N \times N$	$(\alpha - 1)\mathbb{I}_N$	Wages $\rightarrow$ factory costs
$\mathbf{A}_{c\Xi}$	$N \times P$	$\frac{\alpha\lambda_2}{\xi}\mathbf{Z}^{(1)}$	Traffic congestion $\rightarrow$ factory costs
$\mathbf{A}_{cc}$	$N \times N$	$\mathbb{I}_N - \alpha\mathbf{\Pi}^\top$	Factory cost propagation
$\boldsymbol{b}_w$	$N \times 1$	$\lambda_3\frac{1-\alpha}{\alpha}\mathbf{Z}^{(2)}_{\cdot p}$	Direct capacity effect on wages
$\boldsymbol{b}_\Xi$	$P \times 1$	$\lambda_3(\mathbf{Z}^{(4)}_{\cdot p} - \boldsymbol{e}_p)$	Direct capacity effect on traffic
$\boldsymbol{b}_c$	$N \times 1$	$-\frac{\alpha\lambda_3}{\xi}\mathbf{Z}^{(1)}_{\cdot p}$	Direct capacity effect on costs

E Reduced-form estimation

This appendix documents the sample, variables, and instruments used in the route-level reduced-form regression of Section 4.2. The underlying data sources – including the two port-level instruments (HYDE 1950 and TRI) – are documented in Appendix B.

E.1 Route-level reduced-form regression

Script and output. The estimation routine produces the main-text Table 1 (volume as outcome) and the alternative-outcome Table E.1 reported below.

Sample. The estimation sample is the balanced route $\times$ month panel of Brazilian maritime imports between 2019 and 2023. A *route* is the quadruplet (n_o, n_d, p_o, p_d) formed by the supplier country, the buyer country (always Brazil), the port of lading, and the port of unlading.

I first extract the universe of routes observed at least once in 2019–2023 from the Panjiva data and cross it with the monthly timeline, yielding a fully balanced route-month panel in which months without observed shipments are filled with zeros for value, weight, volume, and shipment counts.

Dependent variables. For each route r and month t, I compute four alternative route-level shares of Brazilian inward imports – in value, weight, volume (TEU), and number of shipments – defined as

$$\pi^k_{n_d,r,t} = \frac{k_{r,t}}{\sum_{r'} k_{r',t}}, \qquad k \in \{\text{value}, \text{weight}, \text{volume}, \text{shipments}\},$$

where the denominator sums over all routes entering Brazil in month t. I use $\log \pi^k_{n_d,r,t}$ as the dependent variable; the four alternatives are reported side by side in Table E.1.[77]

Regressors. I construct four right-hand-side variables at the port of lading p_o:

- *Port traffic.* $\Xi_{p_o,t}$ is the monthly sum of daily PortWatch TEU $(\text{imports} + \text{exports})/10$ at p_o. It enters the regression as $\log \Xi_{p_o,t}$.
- *Port capacity.* K_{p_o} is the 99th percentile of daily PortWatch TEU at p_o over 2019–2023 (time-invariant). It enters as $\log K_{p_o}$.
- *Cyclone risk.* CycloneRisk_{p_o} is the baseline expected wind speed at p_o built from the STORM return-period rasters within a 50km buffer (Appendix B.4). It enters as $\log(1 + \text{CycloneRisk}_{p_o})$.
- *Distance.* Route distance is decomposed into a sea component (Eurostat `SeaRoute` port-to-port) and a land component (great-circle distance from supplier country centroid to p_o plus from p_d to Brazil), both entering as $\log(1 + x)$ in kilometers.

Fixed effects and clustering. All specifications include supplier-country $\times$ month and port-of-unlading $\times$ month fixed effects, which absorb any destination-time and origin-time shocks common to the error term of Equation 22. Standard errors are clustered at the four-way supplier-country $\times$ port-of-lading $\times$ port-of-unlading $\times$ month level.

Instruments. The 2SLS specifications instrument port traffic and port capacity with two exogenous shifters constructed from dedicated datasets (Appendices B.5 and B.5):

[77] Because the panel is zero-filled, months in which a route reports no shipments generate $\log 0 = -\infty$ and are dropped by the estimator. The OLS and 2SLS estimates are therefore identified off the subsample of active route-months.

Table E.1: Estimation of transportation costs: alternative outcomes

	$\pi^{value}_{n_d,r,t}$ (1)	$\pi^{weight}_{n_d,r,t}$ (2)	$\pi^{volume}_{n_d,r,t}$ (3)	$\pi^{shipments}_{n_d,r,t}$ (4)	$\pi^{value}_{n_d,r,t}$ (5)	$\pi^{weight}_{n_d,r,t}$ (6)	$\pi^{volume}_{n_d,r,t}$ (7)	$\pi^{shipments}_{n_d,r,t}$ (8)
Log Port Origin Traffic	0.25	-0.23	0.55	0.60	-2.09	-4.50	-1.79	-0.41
	(0.03)	(0.03)	(0.02)	(0.02)	(0.18)	(0.17)	(0.14)	(0.10)
Log Port Origin Capacity	-0.13	0.37	-0.47	-0.54	2.62	5.39	2.24	0.63
	(0.04)	(0.04)	(0.03)	(0.02)	(0.22)	(0.21)	(0.17)	(0.13)
Log Distance (sea)	-0.39	-0.16	-0.39	-0.34	-0.15	0.25	-0.09	-0.21
	(0.02)	(0.02)	(0.01)	(0.01)	(0.03)	(0.03)	(0.02)	(0.02)
Log Distance (land)	-0.97	-1.12	-0.93	-0.85	-0.94	-0.99	-0.89	-0.82
	(0.01)	(0.01)	(0.01)	(0.01)	(0.01)	(0.01)	(0.01)	(0.01)
Log Cyclone Risk	-0.05	-0.01	0.05	0.00	-0.12	-0.13	-0.02	-0.03
	(0.01)	(0.01)	(0.01)	(0.00)	(0.01)	(0.01)	(0.01)	(0.01)
Observations	71,853	105,119	98,039	105,119	71,853	105,119	98,039	105,119
Adjusted R^2	0.27	0.34	0.30	0.32	0.21	0.13	0.21	0.30
Wald-F, Log Port Origin Traffic					9,924.61	12,846.34	14,116.91	12,846.34
Wald-F, Log Port Origin Capacity					9,938.83	12,903.09	14,260.68	12,903.09
n_o-month fixed effects	✓	✓	✓	✓	✓	✓	✓	✓
p_d-month fixed effects	✓	✓	✓	✓	✓	✓	✓	✓

Notes: This table reports the reduced-form estimation of transportation costs, as specified by Equation 22, using four alternative definitions of the route-level bilateral trade share: value, weight, volume (TEU), and number of shipments. Panel (1) reports the OLS estimates; Panel (2) reports the 2SLS estimates. The specification, sample, fixed effects, and instruments are identical to those of the main-text Table 1. Robust standard errors are clustered at the $\{n_o, p_o, p_d\}$-month level.

- *Port traffic instrument.* $z^1_{p_o,t} = \widetilde{\Xi}^{world}_{-c(p_o),t} \times s^{1950}_{p_o}$, where $\widetilde{\Xi}^{world}_{-c(p_o),t}$ is the monthly global PortWatch TEU traffic net of the country hosting p_o, and $s^{1950}_{p_o}$ is the share of total 1950 population within a 100km buffer of p_o (HYDE 3.3).
- *Port capacity instrument.* $z^2_{p_o}$ is the mean Terrain Ruggedness Index within a 20km buffer of p_o (GMTED).

Both instruments enter the first-stage and reduced-form regressions as $\log(1+z)$ to accommodate port-months with zero values.

Alternative outcome definitions. Table E.1 re-estimates Equation 22 using the four alternative definitions of the route-level bilateral trade share: value, weight, volume (TEU), and number of shipments. The specification, sample, fixed effects, and instruments are identical to those of the main-text Table 1. The estimated elasticities are quantitatively stable across outcome definitions; volume is retained in the main text because it offers the highest coverage of the raw Panjiva data (see footnote in Section 4.2).

F QUANTITATIVE IMPLEMENTATION

F.1 DATA ASSEMBLY FOR THE CALIBRATION

This subsection documents the assembly of inputs to the country-level structural calibration of Section 5. The underlying data sources are documented in Appendix B: port traffic and capacity (Appendix B.2), tropical-cyclone climate (Appendix B.4), and bilateral trade flows, distances, vessel voyages, and population (Appendix B.5).

F.1.1 COUNTRIES, PORTS, AND CALIBRATION INPUTS

Inputs assembled. The geography and macro pipeline writes the input files consumed by the calibration routine of Appendix F.2: country and port identifiers, the full economy-wide distance matrix D, bilateral trade shares π, balanced wages w, country population L, port capacity K, the target moment Ξ^{data}, and port-level baseline and RCP8.5 cyclone climate.

Countries. The geography backbone is the Natural Earth admin-0 polygons (10-scale, `ADM0_A3` identifier). Geometries are validated and the date line is wrapped before computing country centroids. After dropping countries with missing population or GDP per capita, dropping countries absent from the ITPD-E trade matrix, and keeping the largest connected component of the transportation graph, the final geography contains $N = 150$ countries.

Ports. Starting from the 1,666 PortWatch ports, I drop ports with zero 99$^{\text{th}}$-percentile daily TEU and keep those whose cumulative share of total 2019–2023 TEU reaches 95%. I further drop ports that are isolated in the voyage-based adjacency and keep only ports inside the largest connected component of the transportation graph. This yields $P = 502$ ports. Ports are assigned to countries via the `ISO3` field in the PortWatch metadata. Figure F.1 shows the cumulative distribution of global port traffic as a function of the number of ports retained in the sample.

Global bilateral trade flows. Country-by-country bilateral trade flows $X_{nn'}$ are aggregated from the ITPD-E data (Appendix B.5). I aggregate across all sectors within each ordered country pair to obtain a single bilateral trade matrix $X_{nn'} = \sum_s X^s_{nn'}$. Trade shares are recovered by column normalization $\pi_{nn'} = X_{nn'} / \sum_{\tilde{n}} X_{\tilde{n}n'}$. Country coverage in ITPD-E is aligned with the Natural Earth admin-0 ISO3 list by country-code matching; countries outside the intersection are dropped before the connectivity filter.

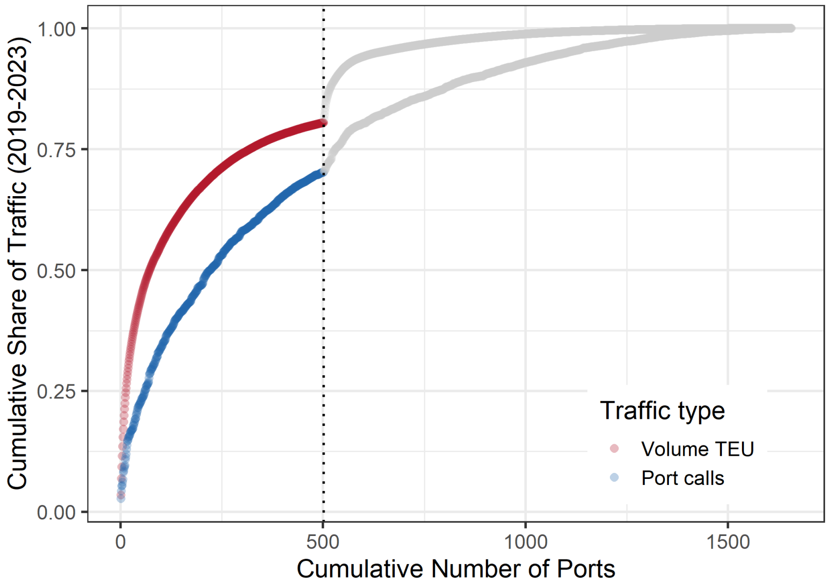

Figure F.1: Cumulative Share of Global Port Traffic by Number of Ports

Notes: This figure plots the cumulative share of global port traffic (2019–2023) as a function of the number of ports retained in the sample, ranked by traffic volume. The vertical dotted line indicates the $P = 502$ ports retained after filtering. Red dots represent cumulative TEU volume; blue dots represent cumulative port calls.

Wages. Country wages are recovered from the balanced-trade condition $wL = \pi^\top wL$ by iterating a Picard fixed point starting from the ITPD-E production vector $Y_n = \sum_{n'} X_{nn'}$ until $\max_n |(wL)_n^{\text{new}}/(wL)_n^{\text{old}} - 1| < 10^{-12}$. The resulting wL vector is rescaled so that $\sum_n w_n L_n$ matches total ITPD-E production, and wages are obtained as $w_n = (wL)_n / L_n$.

Port capacity. Port capacity K_p is the 99$^{\text{th}}$ percentile of daily PortWatch TEU (imports + exports)/10 at port p over 2019–2023, rescaled by the global maximum. The underlying PortWatch daily series is described in Appendix B.2.

Port traffic (target moment). The calibration target Ξ_p^{data} is the yearly total PortWatch TEU at port p, averaged across 2019–2023. As documented in Appendix F.2, the calibration routine works with $\tilde{\Xi}_p = \Xi_p / \bar{\Xi}$, where $\bar{\Xi}$ is the cross-port mean of Ξ_p^{data}.

F.1.2 Distance matrix assembly

Contiguity masking. In the model calibration, land distances (Appendix B.5) are retained only for contiguous country pairs identified via polygon contiguity (queen adjacency, first-order neighbours).

Sparsification. The raw port-to-port sea-distance block is sparsified using the Global Fishing Watch vessel-voyage transit probabilities documented in Appendix B.5. At each origin port, outbound links are sorted by transit probability and truncated once their cumulative share exceeds 0.90, subject to a hard cap of 2,000 outbound links per origin and a guarantee that the highest-probability destination is always kept. The remaining sea-distance block is trimmed at its 95$^{\text{th}}$ percentile to control the spectral radius of the resistance matrix and keep the fixed-point algorithm of Appendix F.4 feasible.

Distance matrix assembly. The economy-wide distance matrix is built as an $(N + P) \times (N + P)$ block matrix that stacks (i) the contiguity-masked country-to-country land block, (ii) the port-to-country land block, and (iii) the sparsified port-to-port sea block, with zeros on the diagonal. This is the D matrix that enters the resistance matrix Δ in the fixed-point algorithm of Appendix F.2.

F.2 Calibration of transportation cost parameters

The structural trade-cost parameters $\{\kappa_d, \kappa_p, \lambda_1, \lambda_2, \lambda_3, \lambda_w\}$ are calibrated internally by minimizing the distance between model-implied and observed port traffic at baseline. This subsection describes the numerical algorithm.

Inputs. Baseline bilateral trade shares $\{\pi_{nn'}\}$ obtained from ITPD-E (Borchert et al., 2022); pre-balanced country wages $\{w_n\}$ computed from Rossi-Hansberg and Zhang (2025); observed port traffic $\{\Xi_p^{\text{data}}\}_{p\in\mathcal{P}}$ from PortWatch; port capacity $\{K_p\}$ from PortWatch; baseline cyclone risk $\{CycloneRisk_p\}$ from STORM; bilateral distances $\{\epsilon_{ll'}\}$; and population $\{L_n\}$.

Traffic normalization. The absolute level of port traffic is not separately identified from the port-cost shifter κ_p.[78] I work throughout in normalized units: I fix the normalization constant

$$\bar{\Xi} \;\equiv\; \frac{1}{|\mathcal{P}|}\sum_{p\in\mathcal{P}} \Xi_p^{\text{data}}, \tag{F.1}$$

and define the dimensionless traffic vector $\tilde{\Xi}_p \equiv \Xi_p/\bar{\Xi}$. The same scalar $\bar{\Xi}$ is used to rescale both the observed moment $\tilde{\Xi}_p^{\text{data}} \equiv \Xi_p^{\text{data}}/\bar{\Xi}$ and the model-implied moment $\tilde{\Xi}_p^{\text{eq}}(\boldsymbol{\theta})$ entering the calibration objective, and is held fixed across the baseline and the counterfactuals of Appendix F.4.

Target. Let $\boldsymbol{\theta} = (\log\kappa_d, \log\kappa_p, \lambda_1^{\text{land}}, \lambda_1^{\text{sea}}, \lambda_2, \lambda_3, \lambda_w)$.[79] Given $\boldsymbol{\theta}$, the algorithm solves for the equilibrium baseline traffic $\tilde{\Xi}_p^{\text{eq}}(\boldsymbol{\theta})$ and minimizes the mean squared log gap with the observed moment:

$$\mathcal{L}(\boldsymbol{\theta}) \;=\; \frac{1}{|\mathcal{P}|}\sum_{p\in\mathcal{P}} \left[\log\tilde{\Xi}_p^{\text{eq}}(\boldsymbol{\theta}) - \log\tilde{\Xi}_p^{\text{data}}\right]^2. \tag{F.2}$$

Inner loop – baseline traffic fixed point. For a given $\boldsymbol{\theta}$, the algorithm solves for the baseline normalized port traffic as the fixed point of the mapping $\log\tilde{\Xi} \mapsto \log\tilde{\Xi}_{\text{new}}$, where $\tilde{\Xi}_{\text{new}}$ is the traffic implied by Equation (D.33) evaluated at the observed trade volumes $X_{nn'} = \pi_{nn'}\, w_{n'} L_{n'}$ and at the Leontief inverse $\mathbf{B}(\tilde{\Xi}, \boldsymbol{\theta})$:

1. **Build resistance.** Build $\boldsymbol{\Delta}(\tilde{\Xi}, \boldsymbol{\theta})$ from Equations (D.31)–(D.32), replacing the climate term in (D.32) with the empirical form $\bar{t}_p^{-\xi} = \kappa_p\, \tilde{\Xi}_p^{\lambda_2}\, K_p^{\lambda_3}\, (1 + CycloneRisk_p)^{\lambda_w}$ (Equation 21), and verify the feasibility condition $\rho(\boldsymbol{\Delta}) < 0.999$ on the spectral radius.

[78] Substituting $\Xi_p = \bar{\Xi}\tilde{\Xi}_p$ into the port-cost Equation (D.32) gives $\bar{t}_p^{-\xi} = \kappa_p\, (\bar{\Xi}\,\tilde{\Xi}_p)^{\lambda_2}\, K_p^{\lambda_3}\, (1 + CycloneRisk_p)^{\lambda_w} = (\kappa_p\, \bar{\Xi}^{\lambda_2})\, \tilde{\Xi}_p^{\lambda_2}\, K_p^{\lambda_3}\, (1 + CycloneRisk_p)^{\lambda_w}$: any common rescaling of Ξ_p by $\bar{\Xi}$ is absorbed into the redefinition $\kappa_p \to \kappa_p\,\bar{\Xi}^{\lambda_2}$ and leaves every equilibrium object in (D.27)–(D.34) unchanged. Fixing a normalization for Ξ_p is therefore equivalent to pinning the scale of κ_p.

[79] The numerical routine splits the distance elasticity λ_1 of Equation (19) into a land component λ_1^{land} and a sea component λ_1^{sea}, which apply to region-region and port-port links of the resistance matrix, respectively. In the main text, I report a single λ_1 for expositional clarity.

2. **Invert.** Compute the Leontief inverse $\mathbf{B} = (\mathbf{I} - \boldsymbol{\Delta})^{-1}$ and form the implied normalized traffic
$$\tilde{\Xi}_p^{\text{new}} = \frac{1}{\bar{\Xi}} \sum_n \sum_{n' \neq n} \frac{B_{np}\, B_{pn'}}{B_{nn'}}\, X_{nn'},$$
using the normalization constant $\bar{\Xi}$ of Equation (F.1).

3. **Iterate.** Iterate until $\|\Delta \log \tilde{\Xi}\|_\infty < 10^{-4}$.

The inner loop is accelerated using the DAAREM scheme. On invertibility failure, the algorithm falls back to dampened Picard iteration with damping factor 0.3. At convergence, the algorithm stores the baseline objects $\{\boldsymbol{\Delta}^\star, \mathbf{B}^\star, \tilde{\Xi}^\star\}$ together with the normalization constant $\bar{\Xi}$, which is held fixed in the counterfactual routine of Appendix F.4.

Outer loop – phase 1 (grid search). The minimization problem (F.2) is non-convex, so I start with a parallel grid search over $\boldsymbol{\theta}$. The grid for the elasticities spans $\lambda_1^{\text{land}}, \lambda_1^{\text{sea}}, \lambda_2, \lambda_w \in \{-1.5, -1.0, -0.5, -0.1\}$ and $\lambda_3 \in \{0.1, 0.5, 1.0, 1.5\}$. The port-cost shifter κ_p spans $\{0.01, 0.05, 0.1, 0.2, 0.5, 1.0, 2$ For each $(\boldsymbol{\lambda}, \kappa_p)$ combination, the distance shifter κ_d is placed near its spectral-radius feasibility boundary: I compute the largest κ_d such that $\rho(\boldsymbol{\Delta}) < 0.95$ when Ξ is at its observed floor, then evaluate the inner loop at κ_d fractions $\{0.5, 0.75, 0.9, 0.95\}$ of that maximum. The best grid point is retained as the starting value for phase 2.

Outer loop – phase 2 (local refinement). Starting from the best grid point, I run Nelder-Mead on the objective (F.2) until $\|\Delta\boldsymbol{\theta}\|_\infty / \|\boldsymbol{\theta}\| < 10^{-6}$ or 200 iterations. I then run BOBYQA from the Nelder-Mead optimum, with box bounds $\log \kappa_d, \log \kappa_p \in [\log 0.001, \log 5]$ and sign constraints $\lambda_1^{\text{land}}, \lambda_1^{\text{sea}}, \lambda_2, \lambda_w \in [-2, 0]$ and $\lambda_3 \in [0, 5]$. If BOBYQA improves on Nelder-Mead, its optimum is retained. The sign constraints impose the motivating-facts priors of Section 4.2: the elasticities of trade costs to distance, traffic, and windspeed are non-positive, while the elasticity to capacity is non-negative.

Post-convergence. At the optimal $\boldsymbol{\theta}^\star$, I run the inner loop one last time and save the baseline objects $\{\boldsymbol{\Delta}^\star, \mathbf{B}^\star, \tilde{\Xi}^\star, \bar{\Xi}\}$ together with the baseline port-cost vector. These objects constitute the baseline equilibrium consumed by the exact-hat-algebra counterfactual solver of Appendix F.4.

F.3 Exact hat algebra

Counterfactuals in Section 6 are solved in exact hat algebra, taking as inputs the calibrated baseline equilibrium of Appendix F.2. This subsection derives the hatted counterpart of the general-equilibrium system characterized in Appendix D.3. The derivation has the standard advantage that several structural objects – in particular the productivity fundamentals $\{a_n\}$ and the bilateral distance matrix – cancel out in ratios, so the counterfactual equilibrium can be

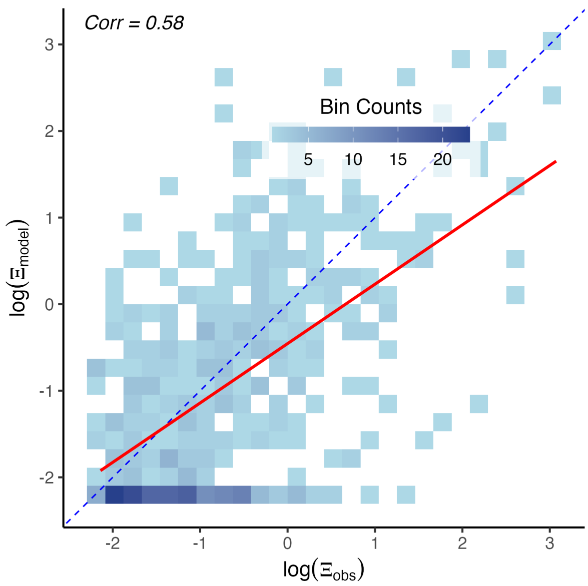

Figure F.2: Calibration fit – targeted port traffic

Notes: This figure plots log-normalized port traffic in the data (x-axis) – measured as average yearly total TEU volume over 2019–2023, normalized by the cross-port mean – against the log-normalized model-implied port traffic at the calibrated θ (y-axis). Port traffic is the targeted moment of the internal calibration of Section 5.3; the scatter is therefore a goodness-of-fit diagnostic rather than an untargeted validation.

characterized using baseline observables together with the calibrated trade-cost parameters.[80]

Let $\{w_n, \bar{c}_n, \tau_{nn'}, \pi_{nn'}, \Xi_p\}$ denote the baseline equilibrium solving Equations (D.27)–(D.34), and $\{w'_n, \bar{c}'_n, \tau'_{nn'}, \pi'_{nn'}, \Xi'_p\}$ the counterfactual equilibrium under perturbed port-cost fundamentals. Taking ratios of Equations (D.27)–(D.34) yields the following hatted system:[81]

$$\hat{\bar{c}}_n^{-\xi} = \hat{w}_n^{(\alpha-1)\xi} \left(\sum_{\tilde{n}} \pi_{\tilde{n}n} \, \hat{\bar{c}}_{\tilde{n}}^{-\xi} \, \hat{\tau}_{\tilde{n}n}^{-\xi} \right)^{\alpha} \qquad \text{(factory-gate cost indices)} \tag{F.3}$$

$$\pi'_{nn'} = \pi_{nn'} \frac{\hat{\bar{c}}_n^{-\xi} \, \hat{\tau}_{nn'}^{-\xi}}{\sum_{\tilde{n}} \pi_{\tilde{n}n'} \, \hat{\bar{c}}_{\tilde{n}}^{-\xi} \, \hat{\tau}_{\tilde{n}n'}^{-\xi}} \qquad \text{(bilateral trade shares)} \tag{F.4}$$

$$\hat{w}_n \, w_n L_n = \sum_{n'} \pi'_{nn'} \, \hat{w}_{n'} \, w_{n'} L_{n'} \qquad \text{(wage bill)} \tag{F.5}$$

$$X'_{nn'} = \frac{\alpha}{1-\alpha} \, \pi'_{nn'} \, \hat{w}_{n'} \, w_{n'} L_{n'} \qquad \text{(bilateral trade volumes)} \tag{F.6}$$

The system (F.3)–(F.6) does not involve the fundamental productivities $\{a_n\}$, which drop out of the ratios. Equation (F.3) shows that the factory-gate cost indices respond to changes in wages and to a sum in which baseline trade shares act as weights on the hatted upstream

[80] I use the convention $\hat{x} = x'/x$ throughout, where x denotes the baseline value and x' the counterfactual value of any variable.

[81] The hatted system preserves the numeraire $\hat{w}_1 = 1$.

cost and trade-cost terms. Equation (F.5) closes the system through labor-market clearing in the counterfactual equilibrium.

Transportation costs. Unlike in standard gravity models, bilateral transportation costs $\tau_{nn'}^{-\xi}$ do not fully cancel out in ratios: the resistance matrix (D.31) is nonlinear in port costs and must be reconstructed at counterfactual values to recover $\hat{\tau}_{nn'}^{-\xi}$. Let $\hat{\tilde{t}}_p^{-\xi}$ denote the hatted port-cost shifter. Following the empirical parametrization of Equation (21), the port-cost hat satisfies

$$\hat{\tilde{t}}_p^{-\xi} = \left(\frac{\Xi_p'}{\Xi_p}\right)^{\lambda_2} \left(\frac{K_p'}{K_p}\right)^{\lambda_3} \left(\frac{1 + CycloneRisk_p'}{1 + CycloneRisk_p}\right)^{\lambda_w}, \tag{F.7}$$

where λ_w denotes the climate elasticity of port-level trade costs.[82] The land and sea distance components of $\mathbf{\Delta}$ are invariant to the counterfactual and cancel out. I therefore construct the counterfactual resistance matrix $\mathbf{\Delta}'$ by rescaling the port columns of the baseline matrix:

$$\delta_{ll'}' = \begin{cases} \delta_{ll'}\, \hat{\tilde{t}}_{l'}^{-\xi} & \text{if } l \sim l',\ l' \in \mathcal{P}, \\ \delta_{ll'} & \text{otherwise.} \end{cases} \tag{F.8}$$

The bilateral transportation cost hats then follow directly from the Leontief inverse:

$$\hat{\tau}_{nn'}^{-\xi} = \frac{\left[(\mathbf{I} - \mathbf{\Delta}')^{-1}\right]_{nn'}}{\left[(\mathbf{I} - \mathbf{\Delta})^{-1}\right]_{nn'}}, \qquad n, n' \in \mathcal{N},\ n \neq n'. \tag{F.9}$$

Port traffic. Equation (D.33) characterizes port traffic in levels. To express counterfactual traffic in objects recovered from the hatted system, I substitute the Leontief representation (D.30) into the conditional routing probability (17). Letting $\mathbf{B} = (\mathbf{I} - \mathbf{\Delta})^{-1}$ and $\mathbf{B}' = (\mathbf{I} - \mathbf{\Delta}')^{-1}$, the counterfactual normalized traffic admits the matrix expression

$$\tilde{\Xi}_p' = \frac{1}{\bar{\Xi}} \sum_n \sum_{n' \neq n} B_{np}' \frac{X_{nn'}'}{B_{nn'}'} B_{pn'}', \tag{F.10}$$

where $\bar{\Xi}$ is the baseline normalization constant of Equation (F.1), held fixed across the baseline and the counterfactual. Fixing $\bar{\Xi}$ (equivalently, fixing the scale of κ_p) is what anchors port-cost shifters across the two equilibria in the same units, and in particular guarantees that a zero-shock counterfactual reproduces $\hat{\Xi}_p = 1$ for every port – a necessary consistency condition for the hat-algebra solver.

Welfare. Taking ratios of the welfare expression in Proposition 2, the counterfactual welfare

[82] Here and throughout the exact hat algebra, primed variables denote general counterfactual values ($x' \equiv \hat{x} \cdot x$). In the RCP8.5 counterfactual of Section 6, $CycloneRisk_p \equiv CycloneRisk_p^{(0)}$ (baseline) and $CycloneRisk_p' \equiv CycloneRisk_p^{(1)}$ (RCP8.5).

change satisfies

$$\hat{V}_n \;=\; \hat{w}_n^{1+(\alpha-1)(\sigma-1)} \left(\sum_{n'} \pi_{n'n}\, \hat{c}_{n'}^{-\xi}\, \hat{\tau}_{n'n}^{-\xi}\right)^{\alpha(\sigma-1)/\xi}. \tag{F.11}$$

Equation (F.11) expresses welfare changes as a function of changes in wages and of a baseline-share-weighted sum of upstream cost and trade-cost hats, both of which are recovered from the inner loop of the numerical algorithm (Appendix F.4).

Counterfactual variants. Section 6 also reports two restricted counterfactuals that decompose the welfare effects of climate change. In the *fixed-routing* counterfactual I replace $\mathbf{B}'$ in Equation (F.10) with its baseline counterpart $\mathbf{B}$, so that the conditional probability that a good passes through port p is held at its baseline value while bilateral trade flows still adjust to the climate shock through Equation (F.4). The *fixed-congestion* counterfactual goes one step further: it removes the feedback from traffic into port costs by setting $\hat{\Xi}_p \equiv 1$ in Equation (F.7), so that the resistance matrix $\mathbf{\Delta}'$ is computed once from the exogenous cyclone-risk (and capacity) shock alone. I use this variant as a decomposition benchmark for the congestion channel.

F.4 Exact hat algebra – numerical algorithm

I solve for the counterfactual equilibrium directly in the hatted system (F.3)–(F.11), taking as inputs the calibrated baseline equilibrium of Appendix F.2, the exogenous shock to cyclone risk (and, where applicable, port capacity), and the structural parameters $\{\sigma, \alpha, \xi, \lambda_1, \lambda_2, \lambda_3, \lambda_w\}$. The algorithm is organized as nested DAAREM-accelerated fixed points.

1. **Shock.** Pre-compute the exogenous port-cost ratio $\left[(1+CycloneRisk_p')/(1+CycloneRisk_p)\right]^{\lambda_w}$ from baseline and counterfactual cyclone risk. Pre-compute the capacity shock ratio $(K_p'/K_p)^{\lambda_3}$, if any. Both ratios are constant across iterations.

2. **Outer loop – port traffic.** Starting from $\log \hat{\Xi}_p^{(0)} = 0$ for all p, iterate on the mapping $\log \hat{\Xi} \mapsto \log \hat{\Xi}_{\text{new}}$:

   (a) **Update resistance.** Form the perturbed port-cost shifter $\hat{t}_p^{-\xi}$ via Equation (F.7), rescale the port columns of $\mathbf{\Delta}$ to obtain the counterfactual resistance matrix $\mathbf{\Delta}'$ (Equation (F.8)), and verify feasibility $\rho(\mathbf{\Delta}') < 0.999$.

   (b) **Invert.** Compute $\mathbf{B}' = (\mathbf{I} - \mathbf{\Delta}')^{-1}$ and the bilateral transportation-cost hats $\hat{\tau}_{nn'}^{-\xi} = B_{nn'}'/B_{nn'}$ on the $\mathcal{N} \times \mathcal{N}$ subblock (Equation (F.9)).

   (c) **Inner loop – wages and cost indices.** Given $\hat{\tau}_{nn'}^{-\xi}$, jointly solve the system (F.3)–(F.5) in the state vector $\left[\log \hat{w}, \log \hat{c}^{-\xi}\right] \in \mathbb{R}^{2|\mathcal{N}|}$:

i. Update $\hat{c}_n^{-\xi}$ by Picard iteration on Equation (F.3) until $\|\Delta \log \hat{c}^{-\xi}\|_\infty < 10^{-12}$.[83]

ii. Update trade shares from Equation (F.4).

iii. Update wages from Equation (F.5), imposing the numeraire $\hat{w}_1 = 1$.

iv. Iterate the joint map $(\hat{w}, \hat{c}^{-\xi})$ until $\left\|\Delta[\log \hat{w}, \log \hat{c}^{-\xi}]\right\|_\infty < 10^{-8}$ or 5,000 iterations. The joint map is DAAREM-accelerated, with a fallback to dampened Picard (damping 0.5) on failure.

(d) **Update traffic.** Recover counterfactual trade volumes $X'_{nn'}$ from Equation (F.6), and update counterfactual normalized traffic $\tilde{\Xi}'_p$ from Equation (F.10), holding the normalization constant $\bar{\Xi}$ fixed at its calibrated value.

Terminate the outer loop when $\|\Delta \log \hat{\Xi}\|_\infty < 10^{-6}$ or after 200 iterations. The outer fixed point is also DAAREM-accelerated. On infeasibility, the algorithm falls back to dampened Picard with damping factor 0.3, halved whenever a feasibility violation is encountered.

3. **Welfare.** Evaluate $\hat{V}_n$ from Equation (F.11) at the converged $\hat{w}_n$ and $\hat{c}_n^{-\xi}$.

Counterfactual variants. The fixed-routing variant replaces $\mathbf{B}'$ with $\mathbf{B}$ in the traffic update at step 2(d), so that the conditional routing probabilities are held at baseline while bilateral trade flows continue to adjust through steps 2(a)–2(c). The fixed-congestion variant skips the outer loop entirely: it computes $\mathbf{\Delta}'$ once from the exogenous cyclone-risk (and capacity) shock alone, runs the inner loop a single time, and reports the resulting welfare change.

F.5 ADDITIONAL QUANTITATIVE RESULTS

This appendix collects the restricted-scenario figures referenced from Section 6. Figure F.3 mirrors the main-text Figure 8 for the two restricted RCP8.5 counterfactuals: regional welfare changes are reported in the left column and port-traffic changes in the right column, with the fixed-routing scenario in the top row and the fixed-congestion scenario in the bottom row. Figure F.4 plots port-level traffic changes against the port-level wind-speed shock across the three scenarios, showing how the traffic–windspeed relationship flattens once firm-level rerouting is held at baseline.

[83]This inner Picard converges since $\alpha < 1$, which makes the cost-index mapping a contraction at fixed $\hat{w}$.

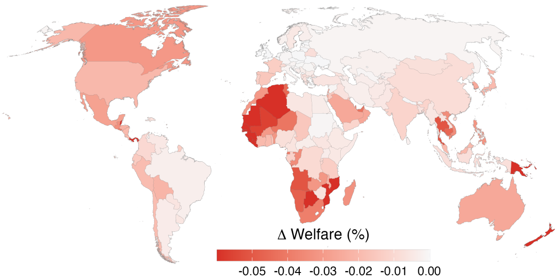

(a) Fixed routing – Δ Welfare (%)

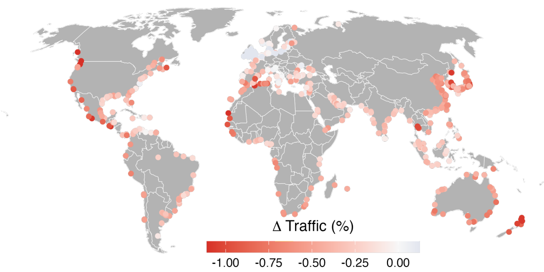

(b) Fixed routing – Δ Port traffic (%)

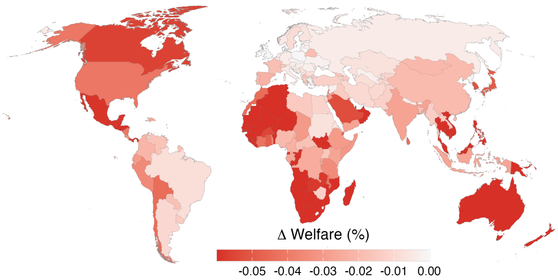

(c) Fixed congestion – Δ Welfare (%)

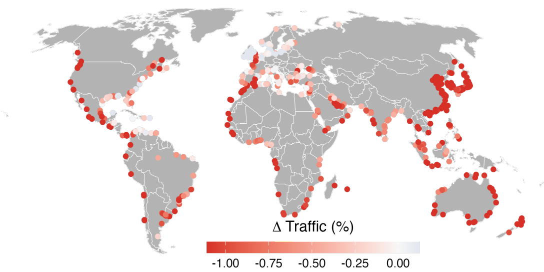

(d) Fixed congestion – Δ Port traffic (%)

Figure F.3: Regional welfare and port traffic – restricted RCP8.5 counterfactuals

Notes: The figure mirrors Figure 8 for the two restricted RCP8.5 counterfactuals defined in Section 6.3. The left column reports the percentage change in region-level welfare (real income, Proposition 2); the right column reports the percentage change in port-level traffic. The top row corresponds to the fixed-routing counterfactual, in which the conditional routing probabilities $\Theta_{p|nn'}$ are held at their baseline values. The bottom row corresponds to the fixed-congestion counterfactual, in which the response of port-level trade costs to traffic is additionally suppressed. Color scales are truncated at the 5th and 95th percentiles.

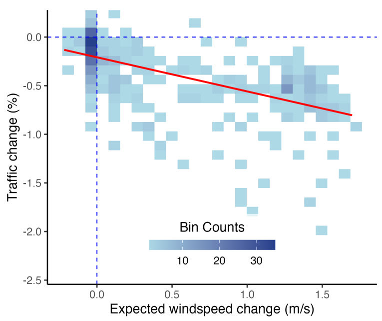

(a) Full model

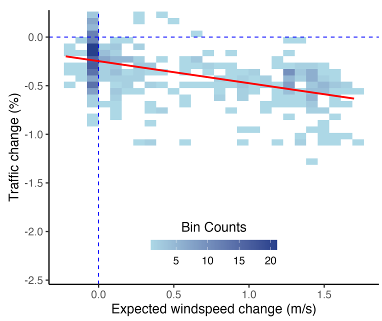

(b) Fixed routing

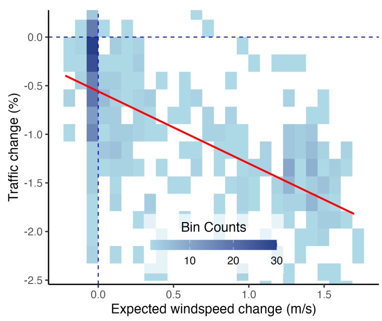

(c) Fixed congestion

Figure F.4: Port traffic change versus the wind-speed shock under the three RCP8.5 counterfactuals

Notes: Each panel is a port-level scatter of the percentage traffic change against the RCP8.5 wind-speed shock at that port, under one of the three scenarios defined in Section 6.3. The fitted OLS line and its slope are overlaid.

G Infrastructure policy

G.1 Investment and port capacity: global-sample robustness

This appendix reports one robustness check on the investment-to-capacity first stage reported in Section 7.2.2: re-estimating Equation (29) on the global port sample instead of restricting attention to control ports located in the treated countries. Figure G.1 plots the event-study coefficients. The dynamic path and the post-treatment average are quantitatively close to the main-text estimate, indicating that the first-stage elasticity is not driven by the choice of comparison group.

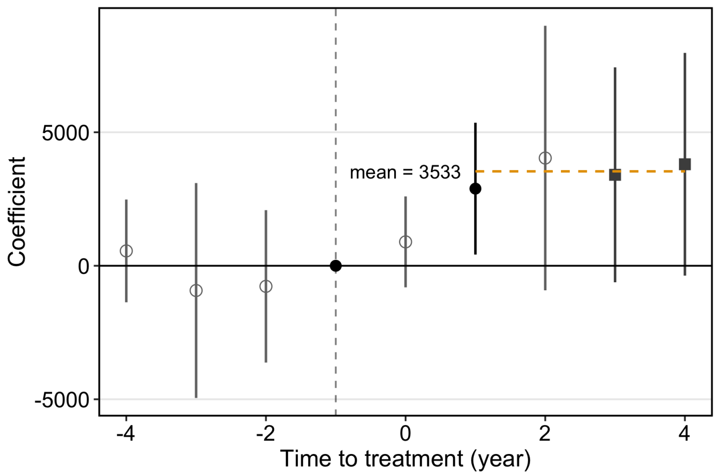

Figure G.1: Port capacity response to a USD 1 billion PPI investment – global port sample

Notes: Event-study coefficients from Equation (29), re-estimated on the full sample of ports in the PortWatch data (rather than only ports located in the treated countries, as in Figure 14). The outcome is the 99th percentile of daily TEU traffic for port p in year t. Bars show 95% confidence intervals clustered at the country level. Black dots indicate point estimates significant at the 5% level, gray squares at the 10% level, and empty dots denote non-significant estimates at the 10% level.

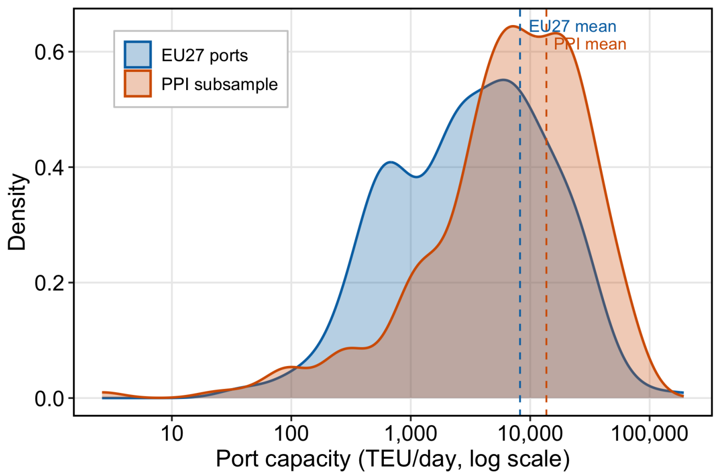

Figure G.2: Port capacity distributions: PPI estimation subsample vs. EU27

Notes: Kernel densities of mean port capacity (TEU/day, log scale) for EU27 ports (blue) and ports located in the 23 PPI-treated countries (orange). Dashed lines mark the sample means. The PPI subsample mean (13668 TEU/day) exceeds the EU27 mean (8222 TEU/day), and 99% of EU27 ports fall within the capacity range of the PPI subsample. Port capacity is defined as the time-averaged 99$^{\text{th}}$ percentile of daily TEU throughput over 2019–2024.

G.2 CHANNEL DECOMPOSITION: CROSS-PORT DISTRIBUTIONS

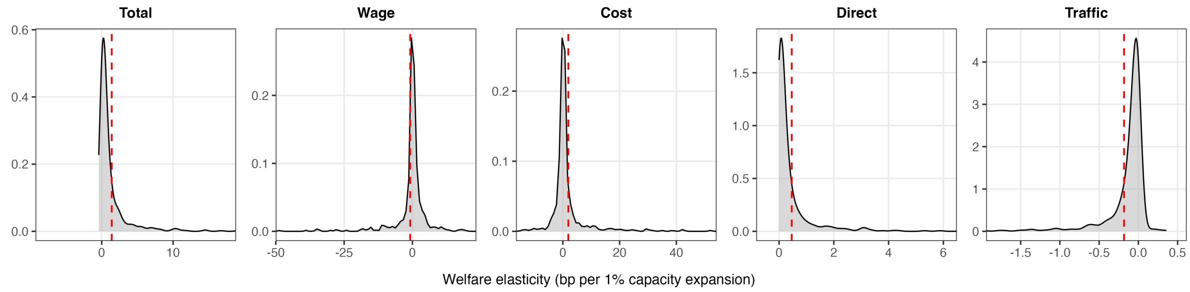

Figure G.3: Cross-port distribution of welfare-elasticity channels

Notes: Each panel plots the kernel density of a welfare-elasticity channel across the 502 ports in the sample. The dashed red line marks the cross-port mean. The wage and cost channels are wide, nearly symmetric, and of opposite sign – large forces that cancel for most ports. The direct routing channel is strictly positive; the traffic-spillover channel is almost entirely negative, reflecting that expanding any port's capacity diverts traffic from neighbouring ports. Densities are computed on the full sample; axis ranges are zoomed to the 2nd–98th percentile range for the wage and cost panels to reveal the shape of the distribution. Welfare elasticities are evaluated at the baseline equilibrium.

G.3 ADDITIONAL RESULTS: INFRASTRUCTURE POLICY

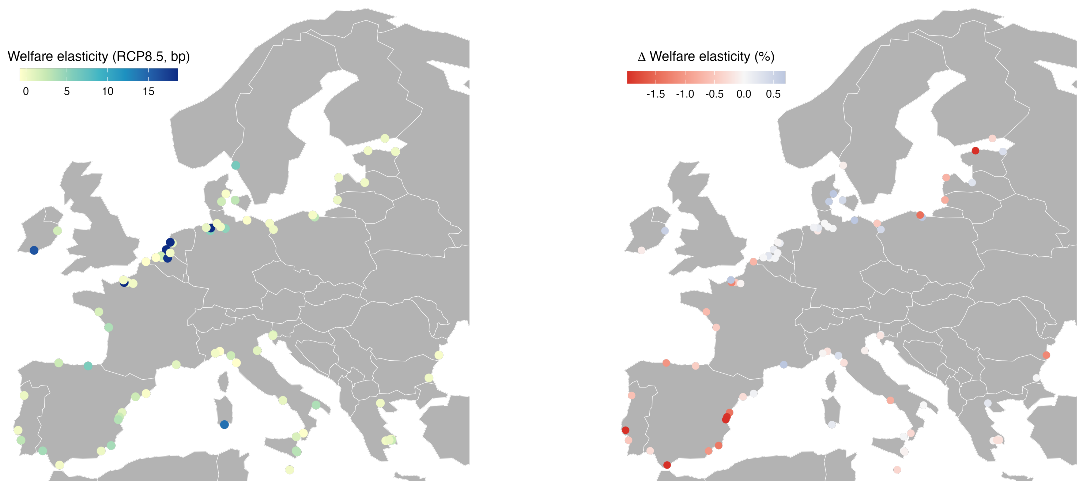

(a) EU27 welfare elasticity, RCP8.5 (b) Δ EU27 welfare elasticity (%)

Figure G.4: EU27 welfare elasticity to port capacity

Notes: Panel (a) plots the port-level elasticity of EU27 welfare to port capacity under RCP8.5. Panel (b) plots the change between the baseline and RCP8.5 elasticities. EU27 welfare elasticities aggregate Equation (25) over EU27 regions using GDP weights. The color scales are truncated at the 5th and 95th percentiles.

Cost-benefit analysis: additional results. Table G.1 reports the full port-level benefit-cost ratios under the EU-planner and national-planner perspectives, both under baseline and under RCP8.5 climates. The remaining figures collect results discussed in Section 7.2.3.

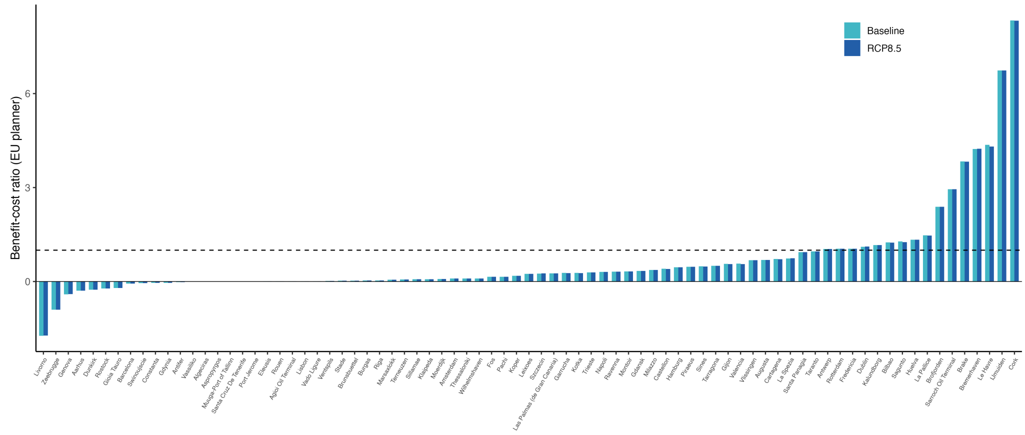

Figure G.5: EU-planner benefit-cost ratio by port

Notes: Port-level EU-planner benefit-cost ratios of a 1% port capacity expansion, baseline and RCP8.5. The benefit is the first-order welfare gain to the EU27 from a 1% capacity increase, priced at current EU27 GDP. Costs are as in Section 7.2.3.

Table G.1: Benefit-cost ratio of a 1% port capacity increase: baseline vs. RCP8.5

		EU Planner			National Planner		
Port	Country	Base	RCP8.5	Δ	Base	RCP8.5	Δ
Cork	IRL	8.339	8.328	-0.011	4.539	4.490	-0.049
Dublin	IRL	1.108	1.114	0.006	-6.197	-6.243	-0.046
IJmuiden	NLD	6.737	6.736	-0.001	4.132	4.132	-0.000
Rotterdam	NLD	1.044	1.046	0.002	0.424	0.424	0.001
Vlissingen	NLD	0.682	0.684	0.002	0.336	0.338	0.001
Amsterdam	NLD	0.094	0.094	0.000	0.041	0.041	0.000
Moerdijk	NLD	0.081	0.081	0.000	0.057	0.057	0.000
Terneuzen	NLD	0.069	0.069	0.000	0.055	0.055	0.000
Le Havre	FRA	4.365	4.312	-0.054	2.678	2.645	-0.032
La Pallice	FRA	1.471	1.465	-0.007	1.065	1.062	-0.002
Montoir	FRA	0.324	0.322	-0.002	0.284	0.283	-0.001
Fos	FRA	0.151	0.154	0.003	0.134	0.136	0.002
Rouen	FRA	0.009	0.009	-0.000	0.003	0.003	-0.000
Port Jerome	FRA	0.007	0.007	-0.000	0.003	0.003	-0.000
Antifer	FRA	-0.017	-0.017	-0.000	-0.017	-0.017	-0.000
Dunkirk	FRA	-0.262	-0.260	0.002	-0.268	-0.266	0.002
Bremerhaven	DEU	4.230	4.238	0.008	3.403	3.410	0.007
Brake	DEU	3.831	3.825	-0.006	2.769	2.761	-0.008

Continued on next page

Table G.1 continued from previous page

		EU Planner			National Planner		
Port	Country	Base	RCP8.5	Δ	Base	RCP8.5	Δ
Hamburg	DEU	0.455	0.455	0.000	0.476	0.477	0.001
Wilhelmshaven	DEU	0.099	0.099	0.000	0.066	0.066	0.000
Brunsbuettel	DEU	0.029	0.029	-0.000	0.013	0.013	-0.000
Stade	DEU	0.027	0.027	-0.000	0.012	0.012	-0.000
Rostock	DEU	-0.222	-0.224	-0.002	-0.232	-0.234	-0.001
Sarroch Oil Terminal	ITA	2.945	2.950	0.006	2.186	2.192	0.006
Taranto	ITA	0.958	0.958	0.000	0.916	0.916	0.001
Santa Panagia	ITA	0.940	0.939	-0.001	0.962	0.963	0.000
La Spezia	ITA	0.739	0.742	0.003	0.839	0.842	0.002
Augusta	ITA	0.688	0.687	-0.000	0.669	0.670	0.001
Milazzo	ITA	0.368	0.368	0.000	0.453	0.453	0.001
Ravenna	ITA	0.318	0.318	-0.000	0.230	0.230	-0.000
Napoli	ITA	0.306	0.303	-0.002	0.171	0.168	-0.002
Trieste	ITA	0.292	0.292	0.000	0.215	0.216	0.000
Vado Ligure	ITA	0.015	0.015	-0.000	0.012	0.012	-0.000
Gioia Tauro	ITA	-0.207	-0.207	0.001	-0.246	-0.245	0.000
Genova	ITA	-0.406	-0.405	0.001	-0.406	-0.405	0.001
Livorno	ITA	-1.732	-1.728	0.004	-1.491	-1.487	0.004
Brofjorden	SWE	2.387	2.384	-0.002	2.080	2.078	-0.002
Huelva	ESP	1.336	1.333	-0.004	0.707	0.704	-0.002
Sagunto	ESP	1.283	1.257	-0.025	0.775	0.760	-0.015
Bilbao	ESP	1.248	1.243	-0.006	0.500	0.498	-0.002
Cartagena	ESP	0.723	0.714	-0.010	0.613	0.605	-0.008
Valencia	ESP	0.571	0.559	-0.013	0.201	0.197	-0.005
Gijon	ESP	0.562	0.556	-0.006	0.291	0.288	-0.003
Tarragona	ESP	0.500	0.499	-0.001	0.434	0.434	-0.001
Castellon	ESP	0.407	0.402	-0.006	0.373	0.368	-0.005
Garrucha	ESP	0.272	0.269	-0.003	0.232	0.230	-0.003
Las Palmas (de Gran Canaria)	ESP	0.261	0.261	0.000	0.422	0.421	-0.001
Santa Cruz De Tenerife	ESP	0.006	0.006	-0.000	0.005	0.005	-0.000
Algeciras	ESP	-0.005	-0.002	0.003	0.052	0.054	0.002
Barcelona	ESP	-0.065	-0.065	-0.000	-0.049	-0.049	0.000

Continued on next page

Table G.1 continued from previous page

Port	Country	EU Planner Base	EU Planner RCP8.5	EU Planner Δ	National Planner Base	National Planner RCP8.5	National Planner Δ
Kalundborg	DNK	1.162	1.167	0.005	1.401	1.405	0.004
Fredericia	DNK	1.044	1.051	0.006	0.958	0.964	0.006
Aarhus	DNK	-0.294	-0.296	-0.002	-0.507	-0.509	-0.003
Antwerp	BEL	1.036	1.036	0.000	0.631	0.631	0.001
Zeebrugge	BEL	-0.897	-0.897	-0.000	-0.193	-0.193	0.000
Sines	PRT	0.483	0.480	-0.002	0.174	0.173	-0.001
Leixoes	PRT	0.248	0.246	-0.001	0.095	0.094	-0.000
Lisbon	PRT	0.011	0.010	-0.001	-0.092	-0.093	-0.001
Piraeus	GRC	0.471	0.470	-0.001	0.335	0.335	0.000
Pachi	GRC	0.154	0.154	-0.000	0.246	0.246	-0.000
Thessaloniki	GRC	0.095	0.095	0.000	-0.031	-0.031	0.000
Agioi Oil Terminal	GRC	0.009	0.009	-0.000	0.016	0.016	-0.000
Eleusis	GRC	0.007	0.007	-0.000	0.012	0.012	-0.000
Aspropyrgos	GRC	0.005	0.005	-0.000	0.007	0.007	-0.000
Gdansk	POL	0.339	0.342	0.003	0.301	0.303	0.002
Szczecin	POL	0.256	0.257	0.001	0.230	0.231	0.001
Gdynia	POL	-0.044	-0.043	0.001	-0.071	-0.071	0.000
Swinoujscie	POL	-0.053	-0.052	0.000	-0.047	-0.047	0.000
Kotka	FIN	0.272	0.271	-0.001	0.510	0.512	0.002
Koper	SVN	0.185	0.185	-0.000	0.003	0.003	-0.000
Klaipeda	LTU	0.077	0.076	-0.001	-0.030	-0.030	-0.000
Sillamae	EST	0.076	0.076	0.000	0.143	0.143	-0.000
Muuga-Port of Tallinn	EST	0.005	0.005	-0.000	0.083	0.083	0.000
Riga	LVA	0.037	0.037	0.000	0.036	0.036	-0.000
Ventspils	LVA	0.018	0.018	-0.000	-0.016	-0.016	-0.000
Burgas	BGR	0.036	0.036	0.000	-0.029	-0.029	0.000
Constanta	ROU	-0.046	-0.045	0.001	-0.048	-0.048	0.000

Notes: BCR = welfare gain / investment cost for a 1% capacity increase at each port. Welfare gain = GDP × elasticity × 0.01. Cost = 0.01 × K_p / 3649 (B USD). EU planner uses EU GDP-weighted welfare; national planner uses own-country GDP-weighted welfare. Δ = RCP8.5 − Baseline.

EU27 counterfactual: country-level results. Figures G.8 and G.9 report the country-level cost of myopia

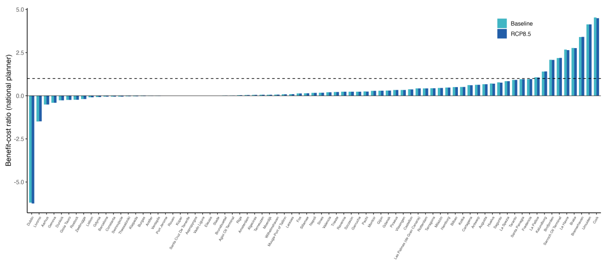

(a) National-planner BCR by port

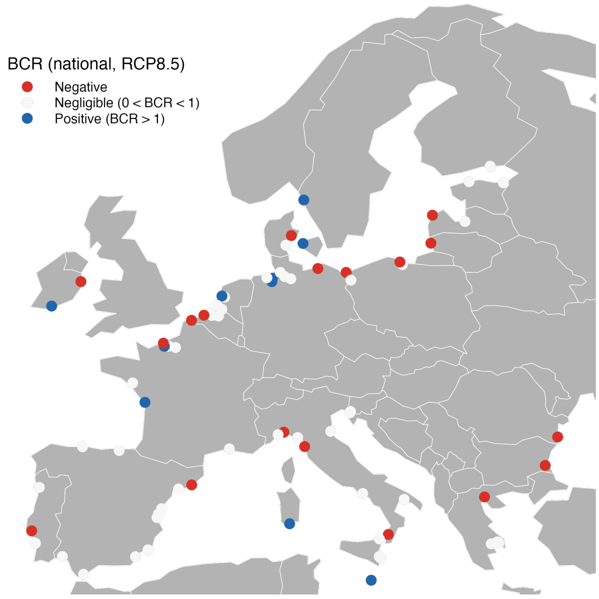

(b) National-planner BCR, RCP8.5

Figure G.6: National-planner benefit-cost ratios

Notes: National-planner benefit-cost ratios of a 1% port capacity expansion. The benefit is the first-order welfare gain to the *port's own country* (not the EU27) from a 1% capacity increase, priced at current national GDP. Costs are as in Section 7.2.3. Panel (a) reports port-level bars, baseline and RCP8.5. Panel (b) maps the ratios under RCP8.5.

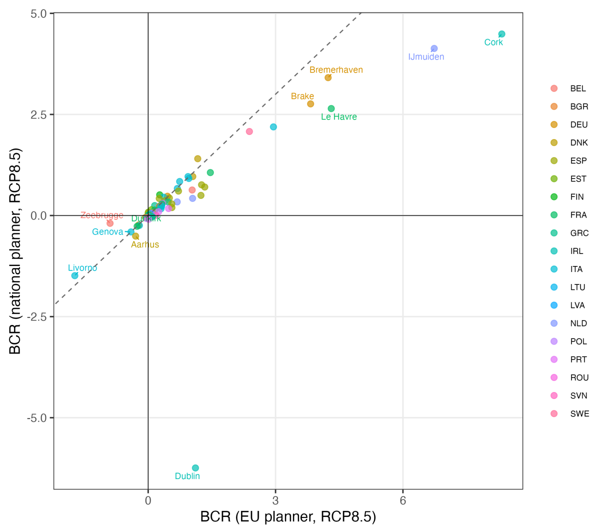

(a) EU vs. national planner, RCP8.5

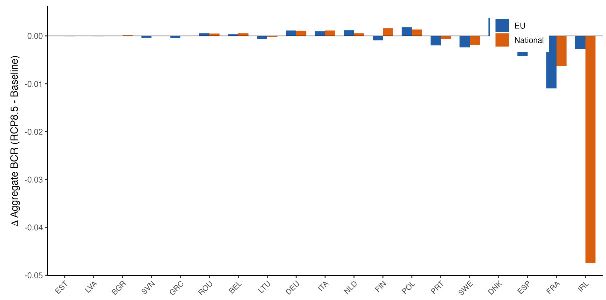

(b) Country-aggregated BCR

Figure G.7: Benefit-cost ratios: EU vs. national and country aggregates

Notes: Panel (a) is a port-level scatter of the EU-planner BCR against the national-planner BCR under RCP8.5. The Spearman rank correlation between the two rankings is 0.90. Panel (b) aggregates port-level BCRs to the country level using current port capacity as weights.

and the welfare gains under the climate-aware allocation, respectively.

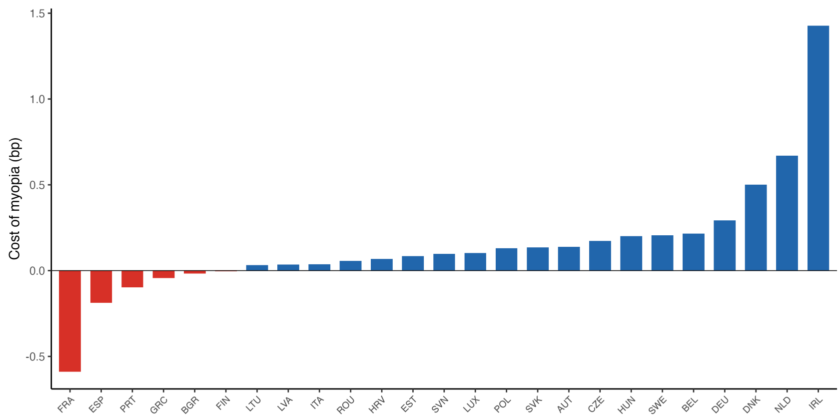

Figure G.8: Country-level cost of myopia (bp)

Notes: This figure reports the country-level cost of myopia: the welfare gap, in basis points, between the myopic and climate-aware allocations of the EUR 84 billion EU27 investment budget. Country-level welfare aggregates regional welfare using GDP weights. Bars are sorted in decreasing order of magnitude. The climate-aware and myopic allocations differ only in the welfare-elasticity vector used to distribute the budget (RCP8.5 vs. baseline); both counterfactuals are evaluated at the RCP8.5 climate.

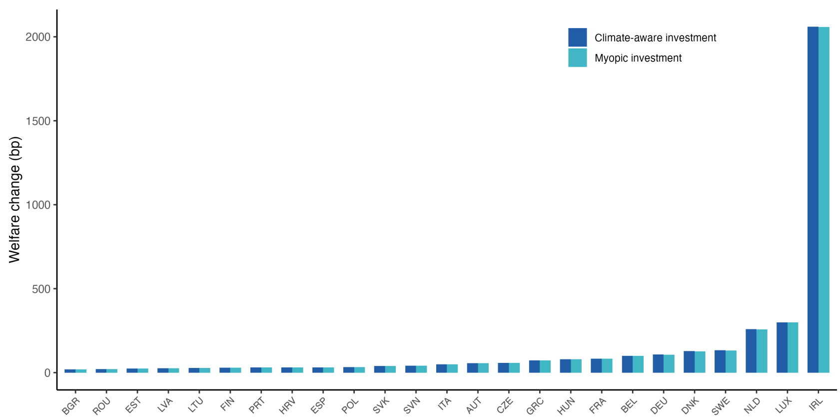

Figure G.9: Welfare gain by country under the climate-aware allocation (bp)

Notes: This figure reports the welfare gain (in basis points) by EU27 country under the climate-aware heuristic allocation of the EUR 84 billion EU27 investment budget. Country-level welfare aggregates regional welfare using GDP weights. Bars are sorted in decreasing order of magnitude.